Nickel Aluminate Reinforced Porous Ceramic Hollow Fibre Membranes

Yi-Lan Elaine Fung

Bachelor of Engineering (Chemical)

Submitted for the degree of Doctor of Philosophy

Department of Chemical Engineering

Monash University

Australia

June, 2014

ADDENDUM

P.135 Section 7.2 para 1

Comment: The selection of reinforcement agents depends on the difference in thermal expansion coefficient between the difference phases. As explained, the general principle to follow is the reinforcement agent must have a higher thermal expansion coefficient than the original pure ceramic. The strengthening effect and suitable loading of the reinforcement agent depend on the thermal expansion coefficients difference between two phases, particle sizes and morphologies of raw materials. For other ceramic membranes such as perovskite based membranes, however, $NiAl_2O_4$ could not be introduced into the membrane matrix by in-situ formation. Mechanical mixing could be attempted.

P.65 Section 3.3.6 line 4

Add: The thermal expansion coefficient of Al_2O_3 is $8 \times 10^{-6}\ ^oC^{-1}$ and that of $NiAl_2O_4$ is $8.41 \times 10^{-6}\ ^oC^{-1}$ (as reported in Reference 93)

P.80 Fig. 4.7

Comment: These samples were sintered at 1500^{o}C for 5 hours. As reported in many studies and shown here Al_2O_3 is well sintered at this duration and temperature, with significant pore closure and grain growth. The sintering behaviour of $NiAl_2O_4$ was studied in more details in Chapter 6. It was proved that sintering of $NiAl_2O_4$ occurred at temperature of 1600^{o}C or above. This explained the difference in sintering behaviour between Al_2O_3 and 22.6 wt% $NiAl_2O_4$ / Al_2O_3 hollow fibre membranes here. The sintering conditions of samples shown here was insufficient for grain growth of $NiAl_2O_4$ and hence pores and lose particles were shown.

P.135 Section 7.2 end of para 1

Add: As reported in many studies, $NiAl_2O_4$ was formed at temperature over 1000^{o}C at the interface of reactants. For $NiAl_2O_4$ to be mechanically mixed into the slurry for ceramic hollow fibre membrane extrusion it has to be grinded into powder. Whether the morphology and strength of $NiAl_2O_4$ / Al_2O_3 hollow fibre membranes with the same composition prepared by in-situ method or mechanical mixing depend on the starting materials for $NiAl_2O_4$ formation and how fine the $NiAl_2O_4$ powder for mechanically mixing is grinded to. If the same raw materials were used for the formation of $NiAl_2O_4$ and it is grinded down to the same particle size as that formed in in-situ introduction, the morphology and strength under the same compositions should remain the same.

However, the particle size range of mechanically grinded powder is usually broad and difficulty to be controlled. For the fabrication of $NiAl_2O_4$ / Al_2O_3 hollow fibre membranes which Al_2O_3 is a reactant for the formation of $NiAl_2O_4$ the reinforcement agent, grinding of $NiAl_2O_4$ into powder followed by mechanical mixing is a more complicated and longer path. If $NiAl_2O_4$ reinforcement is attempted in other ceramic hollow fibre membranes mechanically mixing is an option.

Phase contact between Al_2O_3 and $NiAl_2O_4$ is necessary for the formation of stress field caused by thermal expansion mismatch. Without physical contact between the two phases the strengthening effect could not take place.

Table of Contents

Declaration

I hereby declare that this thesis, except with the Graduate Research Committee's approval, contains no material which has been accepted for the award of any other degree or diploma in any university or other institution and affirms that to the best of my knowledge the thesis contains no material previously published or written by another person, except where due reference is made in the text of this thesis.

Yi-Lan Elaine Fung

Date _____

Acknowledgement

Prof. Huanting Wang and Dr. Jianfeng Yao are hereby acknowledged the supervision, theoretical advice and technical assistance of work presented in this thesis. Monash Centre for Electron Microscopy (MCEM) is acknowledged the use of electron microscopy facilities and Dr Zhaoxiang Zhong of Nanjing University of Technology in China for the use of bubble point tester and mercury porosimetry.

List of Figures

List of Tables

Abstract

Membranes are commonly used in industrial separation processes because of their absence of moving parts, simplicity of separation without phase change, potential of scaling and instantaneous response to system variations. In general, polymeric membranes are of low cost and could be easily prepared, yet they fail at processes that involved high temperatures, extreme pH, corrosive and organic chemicals. Ceramic membranes were therefore introduced to these harsh conditions because of their high thermal and chemical stability, while being insensitive to swelling and could be easily cleaned. Industries that make wide use of ceramic membranes include water treatment, chemical production, petrochemical, metal, automotive, textile, pulp and paper, tannery, biotechnology, cosmetic, pharmaceutical, food and beverage. Among all different membrane geometries, hollow fibre has the highest surface area to volume ratio and highest compactness.

The major limitation of large scale production and application of ceramic hollow fibre membrane is the brittle nature of ceramic. Brittleness is a significant problem when the membrane is of a hollow fibre geometry which is small in size and has thin walls. Apart from cracking under pressure, brittle ceramic hollow fibre membranes are also difficult to be bundled up and to be sealed into equipment as orientated modules.

This thesis presents the fabrication and characteristics of ceramic hollow fibre membranes with enhanced flexural strength, which involves nickel aluminate ($NiAl_2O_4$) as a reinforcement medium and as a pure membrane material. $NiAl_2O_4$ is a non-toxic ceramic material with high melting temperature and strong resistance to acids and bases. The ceramic nature and stability of the strengthened hollow fibre membrane was therefore maintained. $NiAl_2O_4$ was formed by the solid-solid reaction between nickel (II) oxide (NiO) and alumina (Al_2O_3) at high temperature of 1400 ^oC or above. All the ceramic hollow fibre membranes were prepared by the phase-inversion and sintering method. Apart from water the commonly used internal and external coagulant in a phase-inversion process, the use of ethanol-water mixture as internal coagulant was also attempted and its effect on the structure of membrane wall was investigated. Brittleness of the ceramic hollow fibre membranes, which was the main focus of this thesis, was indicated by flexural strength obtained by three-point bending test carried out on individual samples. On top of flexural strength, other characteristics of the ceramic hollow fibre membranes that determine their application, effectiveness and efficiency in separation processes were also studied. These include microstructure, porosity,

active layer porosity and pore size, pure water flux and chemical stability. All the ceramic hollow fibre membranes prepared were porous, with their pore sizes in the microfiltration range, and are suitable for the separation of solid suspensions from liquid.

The study of strength enhancement of porous ceramic hollow fibre membranes started with the reinforcement of porous ceramic materials by the inclusion of external element, which was discrete $NiAl_2O_4$ in the porous alumina matrix formed by the addition of NiO. X-ray diffraction (XRD) pattern proved the formation of $NiAl_2O_4$ without NiO remaining after the sintering process at 1500 ^oC or above for 5 hours. Energy dispersive X-ray spectroscopy (EDS) showed the even distribution of $NiAl_2O_4$ across the alumina matrix through ball-milling mixing of raw materials before sintering. Flexural strength of the porous $NiAl_2O_4/Al_2O_4$ increased with $NiAl_2O_4$ loading up to 146 MPa at 14.7 wt% of $NiAl_2O_4$, which was a result of closure force formed by thermal expansion mismatch between alumina and $NiAl_2O_4$ that deflects crack growth. Flexural strength decreased with further increase in $NiAl_2O_4$ content as densification and shrinkage were hindered by grain growth in random directions which formed agglomerates and loose particles. $NiAl_2O_4/Al_2O_3$ hollow fibre membranes were then fabricated through phase-inversion and sintering method with the same raw materials. A maximum flexural strength of 156 MPa was achieved by the $NiAl_2O_4/Al_2O_3$ hollow fibre membrane containing 16.4 wt% of $NiAl_2O_4$, which was 2.3 times of that of the pure alumina sample prepared under the same conditions. The 16.4 wt% $NiAl_2O_4/Al_2O_3$ hollow fibre membrane had a porosity of 46.8% which could give sufficiently low fluid resistance. It showed a pure water flux of 597 $L/m^2.h.bar$ under a feed pressure of 2 bar and a mean pore size of 330 nm on its active layer. In comparison with ceramic hollow fibre membranes reported in other literatures, $NiAl_2O_4$ reinforced alumina hollow fibre membrane achieved a higher flexural strength than other ceramic reinforcement methods such as the addition of Ni and NiO and a comparable flexural strength as yttria-stablized zirconia (YSZ) a stronger and higher cost ceramic than alumina and as within the porosity range of 47-55%.

Followed by the reinforcement of alumina hollow fibre membrane by discrete $NiAl_2O_4$, nickel nanowire (Ni NW) which has a continuous structure was used as a raw material in the preparation of ceramic hollow fibre membrane precursor. Ni NW was oxidized into NiO in the sintering process in air, resulting in continuous $NiAl_2O_4$ chains in alumina hollow fibre membranes. On top of thermal expansion mismatch between $NiAl_2O_4$ and alumina, crack bridging effect of the $NiAl_2O_4$ chains also led to strengthening effect. Flexural strength was

increased with $NiAl_2O_4$ content up to a loading of 2.00 wt% then decreased with further increase in $NiAl_2O_4$ like the case of discrete $NiAl_2O_4$. The maximum flexural strength achieved was 172 MPa and the corresponding porosity, pure water flux at a feed pressure of 2 bar and mean active layer pore size was 35%, 35 L/m^2.h.bar and 220 nm respectively.

Apart from acting as reinforcement medium in alumina hollow fibre membrane, pure $NiAl_2O_4$ hollow fibre membranes were prepared by mixing alumina and NiO powder in 1 : 1 molar ratio homogeneously, followed by sintering. A sintering time of 10 hours at 1600 ^oC was found to be sufficient for the solid state reaction to complete and sintering of $NiAl_2O_4$. Flexural strength of $NiAl_2O_4$ increased with sintering temperature. The flexural strength achieved at 1630 ^oC the highest sintering temperature attempted was 101 MPa with a porosity of 55% and pure water flux of 862 L/m^2.h.bar at a testing pressure of 2 bar. Its active layer pore size ranged from 50 – 140 nm. In comparison with ceramic hollow fibre membranes with similar porosities, $NiAl_2O_4$ showed an appreciable flexural strength. This proved that $NiAl_2O_4$ was a mechanically strong ceramic and can potentially be used as industrial scale membrane with further studies.

The ceramic hollow fibre membranes presented in this thesis have enhanced flexural strength, which indicates a decrease in their brittleness. The ceramic nature and hence high thermal and chemical stability of the hollow fibre membranes were maintained. These membranes could potentially undergo large scale production for industrial scale microfiltration processes. The strengthening mechanisms presented could also be potentially used in other ceramic materials which brittleness is a hindrance for their wide application.

Chapter 1 Introduction

High quality and efficient separation of different components from mixtures is essential for many industries. Membrane is a popular choice for separation processes due to their lack of moving parts, simplicity of separation processes without phase change, potential of scaling and instantaneous response to system variations, at the same time fulfilling the purpose of contaminant removal or recovery of valuable components in mixtures. Membrane systems are therefore currently applied in a wide range of processes such as water desalination, waste treatment, filtration, distillation, gas separation and catalytic reactions.[1, 2] Polymer flat sheet membranes are the most widely used due to their low cost and ease of fabrication. The major problem of polymer membranes in general is their instability and hence failure under extreme conditions such as high temperature of over 200 ^{o}C, highly acidic or basic feed. [3]

Ceramic membranes were developed to extend the use of membrane system to extreme conditions. The advantages of ceramic materials include high thermal and chemical stability, insensitivity to swelling, ease of cleaning and long service life, which make ceramic membranes suitable in many industrial processes. Apart from water treatment and recycling, in the petrochemical industry ceramic membranes are used in fuel oil and ethanol processing; paper coating and white water recovery in the pulp and paper industry make use of ceramic membranes; in pharmaceutical production and the biotechnology industry ceramic membranes take part in isolation of active agents such as enzymes, proteins and antibiotics; the metal industry uses ceramic membrane to recover heavy metal; in dairy production ceramic membranes are used for microorganisms removal. [2]

In terms of membrane geometry, hollow fibre has the highest surface area to volume ratio and the highest compactness in comparison with flat sheet, capsule and tubular membranes, which potentially gives the most effective performance among membranes of the same volume.[4, 5] Specific applications of ceramic hollow fibre membranes include separation of waste fluid with extreme pH [6], catalytic reactors[7-9], bio-rectors[10] and solid oxide fuel cell (SOFC). [11, 12]

The brittle nature of ceramic materials is the major obstacle for the large scale application of ceramic membrane. Brittleness is a relatively more significant problem with ceramic membranes in hollow fibre geometry because of their small size and thin wall in comparison with other membrane geometries, as most of the separation processes involve high pressure. A hollow fibre membrane module only functions properly with no broken or defective fibre.

[13] Brittle ceramic membranes are also difficult to be sealed into equipment. In most situations, for industrial applications hollow fibre membranes are bundled into modules which are configured and orientated to achieve the best performance. [14]

Strengthening of dense ceramic materials has been widely reported, either through close packing of the ceramic particles or reinforcement, yet study specifically on strengthening porous ceramics is very limited. In the fabrication of ceramic membranes when fluid flux has to be taken into consideration, the extent of close packing has to be well-controlled. Reinforcement is the inclusion of external elements into the ceramic matrix that increases the resistance of crack propagation. Discrete elements and continuous fibres could both act as reinforcement medium in dense and porous ceramics. In porous ceramics, voids and pores decrease the physical contact between reinforcement medium and adjacent particles. The extent of reinforcement required to increase flexural strength of a porous ceramics is expected to be more than that required by a dense ceramic.

In this study, ceramic hollow fibre membranes with high flexural strength and appreciable porosity and pure water fluxes were fabricated for extending the application of ceramic hollow fibre membranes to extreme conditions and for the ease of large scale production. This started with studying the effect of including discrete $NiAl_2O_4$ as reinforcement medium in porous alumina, followed by applying the same reinforcement method in porous alumina hollow fibre membranes. The next approach was the use of continuous fibres as reinforcement medium in ceramic hollow fibre membranes for strength enhancement. Apart from the addition of external reinforcement elements, improvement in strength was also approached through the variation in microstructure of pure ceramic hollow fibre membranes. Brittleness of porous ceramic and ceramic hollow fibre membranes was determined by their flexural strength. The ceramic hollow fibre membranes presented are intended to be used for microfiltration of liquid. The strengthening mechanisms in the ceramic hollow fibre membranes were also investigated for potential application in strengthening other ceramic materials in the future.

This thesis is comprised of seven chapters. Chapter 1 is an introduction to the background of this research study, with the current problem and research aims stated. Chapter 2 is a review of literature that described the work that has been carried out in the area of ceramic reinforcement and ceramic hollow fibre membrane and theories that were used in this research study. Chapters 3 to 6 present the experimental work covered in this research, with

each chapter containing an introduction on background, experimental descriptions, results obtained and discussions on them, followed by a conclusion of overall finding. Specifically, Chapter 3 describes the reinforcement of porous alumina ceramic by the formation of a new phase nickel aluminate spinel ($NiAl_2O_4$) within the alumina matrix; Chapter 4 shows the application of $NiAl_2O_4$ reinforcement in enhancing the flexural strength of alumina hollow fibre membranes; Chapter 5 presents the formation of $NiAl_2O_4$ chains within alumina hollow fibre membranes by using nickel nanowire (Ni NW) as a raw material for strengthening purpose; and Chapter 6 reports the fabrication and characteristics of pure $NiAl_2O_4$ hollow fibre membranes. Chapter 7 sums up all the results obtained, concludes contribution and recommends future work of this study.

Chapter 2 Literature Review

Overview

This chapter presents the basic concepts and theories on membrane in general and specifically on hollow fibre membrane, followed by a detailed review of studies that has been carried out in the area of ceramic material reinforcement and strengthening of ceramic hollow fibre membranes. A review on economic analysis on ceramic membrane production is also included at the end of this chapter.

2.1 Basic concept of membranes

A membrane is defined as a permeable barrier characterized by flux and selectivity properties that provide functional transport across the partition. [15] Materials that have been used to fabricate membrane include polymer, metal, carbon, glass and ceramic. In a membrane filtration process, components in the feed stream that are able to pass through the pores of the membrane are separated out as permeate. The remaining portion of the feed stream, which is the solute, is blocked by the membrane and forms the retentate. Particles are retained either by molecular mass, size or shape based on a sieving mechanism, or by adsorption of retentate on the membrane surface. [1, 2]

Important processing parameters in membrane processes include selectivity, flux and power consumption. Selectivity and flux define the effectiveness and efficiency of a membrane separation process. Power consumption increased with the trans-membrane pressure and the required mass flow rate. Trans-membrane pressure, which is the pressure difference across the membrane, is the driving force for separation processes. The smaller the pores and the lower the porosity of a membrane, the higher the trans-membrane resistance and the osmotic pressure difference between feed and permeate are. Hence a higher applied pressure is required to provide sufficient driving force for the separation process. The energy associated with a pressure-driven separation process is largely dissipated within the fluid as heat. Cooling is required if the temperature of permeate has to be maintained in a small range. [2, 16] Another driving force of separation is the difference in solubilities of permeates in the membrane and the difference in the rate they diffuse through the membrane, which made the solution-diffusion model. The permeates are transported through the membrane by concentration gradient. [17]

Depending on particle packing in the membrane, membrane structure could be dense or porous. Dense membranes are gas-tight because of closely and tightly packed particles. Particle packing in porous membranes are looser in comparison with dense membrane. They are classified into macroporous, mesoporous and microporous based on their pore sizes. Macroporous membranes have pore diameters >50 nm and are used in microfiltration processes which separates solutes of the size 50 nm-10 µm. Mesoporous membranes have their pore size range 2-50 nm and are applied in ultrafiltration processes to separate solutes in the size range 2-100 nm. Microporous membranes have pore diameters <2 nm and take part in nanofiltration process, filtering solutes of the sizes 0.5-5 nm. For solutes smaller than 0.5 nm, a reverse osmosis membrane is required for the separation process. [1, 2, 18, 19] A chart of operative range of these pressure driven filtration processes corresponded to operating pressure and effective particle size is shown in Fig. 2.1.

Pore size of liquid separation membrane ranges down from macroporous to reverse osmosis. Ceramic membranes for microfiltration, ultrafiltration and nanofiltration have successfully been fabricated and are available commercially. [2] Ceramic membranes for gas separation are either dense crystalline materials or have a macroporous ceramic layer acts as a support with a microporous separation film of amorphous silica or zeolite. Membranes achieve gas separation either by acting as a molecular sieve and separate gas by their molecular size, mass or shape, or by gas adsorption on the membrane surface. [1, 20]

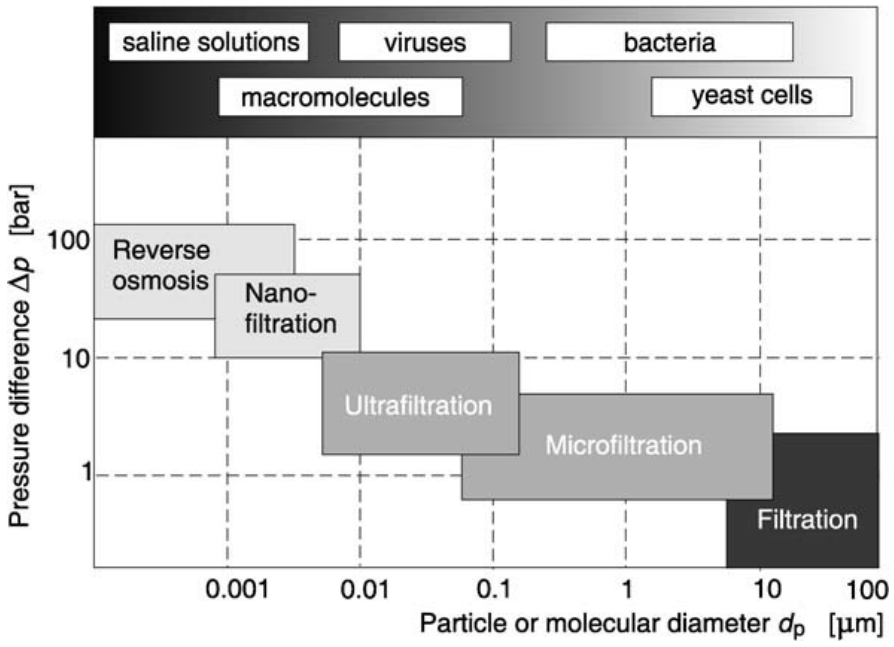

Fig. 2.1 Operative range for pressure driven membrane process and their comparison with some common filtrate.[19]

Apart from pore size, membrane can also be characterized by its chemical nature. A membrane can be hydrophilic or hydrophobic, depends on its material. Without any surface treatment, the common ceramic pure alumina hollow fibre membranes have a hydrophilic nature. [21] Other hydrophilic ceramic membrane materials include titania and zirconia. These metal oxide ceramic links with water easily due to the presence of hydroxyl group (-OH). The hydrophobicity of these ceramic membranes could be increased by surface chemical treatment which attaches other hydrophobic functional group with the hydroxyl group on the membrane surfaces. Hydrophilic ceramic membranes were applied in membrane reactors for the removal of water vapour formed during chemical reactions. Hydrophobic ceramic membranes are suitable for oil emulsion separation such as oily wastewater treatment or when absorption of water into inside layers of membrane is not favoured. [21-24]

2.2 Microfiltration membranes

The ceramic hollow fibre membrane analysed and presented in this thesis are all for solid-liquid separation purpose, with their pore size in the microfiltration range. Microfiltration membranes have been widely used in many separation processes for the removal of large suspended solid particles in liquid. Madaeni et al. presented the use of alumina based ceramic microfiltration membrane in the removal of coke from petrochemical wastewater. A cross-flow filtration set up with seven channel tubular γ-alumina membrane with a nominal pore size of 0.2 μm was used. Their results showed a complete elimination of coke particles from permeate and a 70% decrease in chemical oxygen demand (COD) and biological oxygen demand (BOD) which indicated the rejection of large organic compounds, hydrocarbons and polymeric material. On the other hand, no significant blockage of volatile organic compounds (VOC) was shown by the membrane. Although membrane fouling remained a problem due to the deposition of rejected particles on the membrane surface, an 80% recovery of feed flux was achieved by the use of 0.1 M sodium hydroxide (NaOH) solution as a cleaning agent. [25] Abadi et al. also reported the use of alumina tubular membrane in wastewater treatment, which focused on the separation of oil and grease. Their cross-flow membrane system produced permeate with oil and grease content of 4mg/L that met the National Discharge Standard. The total organic carbon (TOC) removal efficiency was also over 95%. In terms of operating conditions, their results showed an increase in permeate flux up to a trans-membrane pressure of 1.25 bar and fouling occurred with further increasing trans-membrane pressure; increase in cross-flow velocity reduced aggregation of

feed components on the membrane surface, which weakened concentration polarization in the feed and hence increased permeate flux. The increase in operating temperature increased permeation flux and reduced membrane fouling due to a lower fluid viscosity and higher solubility of oil in water respectively. [26] Middlewood et al. who reported the application of cellulose microfiltration membrane in the separation of starch granules from starch milk. The tangential filtration system contained a flat plate membrane. A complete retention of starch granules of >10 μm in size and 67% protein retention was shown. NaOH was also used as a cleaning agent for the flux recovery of membrane. [27, 28] Dong et al. tested the removal of bisphenol A (BPA) from drinking water by microfiltration hollow fibre membrane based on the adsorption mechanism. The polvinylidenefluoride hollow fibre membrane had a pore size of 0.1 μm. Their results showed the initial removal of over 90% BPA, which eventually decreased down to 20% when the membrane was saturated with BPA. Backwashing the membrane using deionized water restored its removal efficiency to 70%. Acidic and neutral condition was also found to be favouring BPA removal, while pH as high as 10.0 to 11.0 lowered the removal efficiency to 30% and 11% respectively. [29]

Apart from acting as filter, microfiltration membrane has also been used as a coalescer. Hlavacek has demonstrated the use of microfiltration membrane as a coalescer for the separation of oil droplets in unwanted industrial oil-in-water emulsion. The hollow fibre membrane module was set up in a cross-flow microfiltration unit. The emulsion used for separation testing contained 2.8-3.2% of oil. The microfiltration membranes tested had pore size of 0.1-0.8 μm. Permeate obtained from the application of microfiltration coalesce contained oil droplets of size over 40 μm, in which their buoyancy was sufficient to float on the top of permeate for the ease of removal. The oil concentration of the lower layer of the permeate was 30 ppm which was significantly lower than the 30000 ppm in the feed. [30]

2.3 Structure of hollow fibre membranes

Membranes are available in different geometries including flat sheet, capsule, tubular and hollow fibre as shown in Fig. 2.2. Flat sheet membranes are the most common and the mostly easily fabricated. Hollow fibre membranes are small circular hollow tubes with thin walls. The diameter of hollow fibre membrane ranges from 50 to 3000 μm. [13] In industrial applications they are present in bundles and are sealed into modules. They made the highest compactness in comparison other membrane systems and the highest surface area to volume ratio. [4, 5]

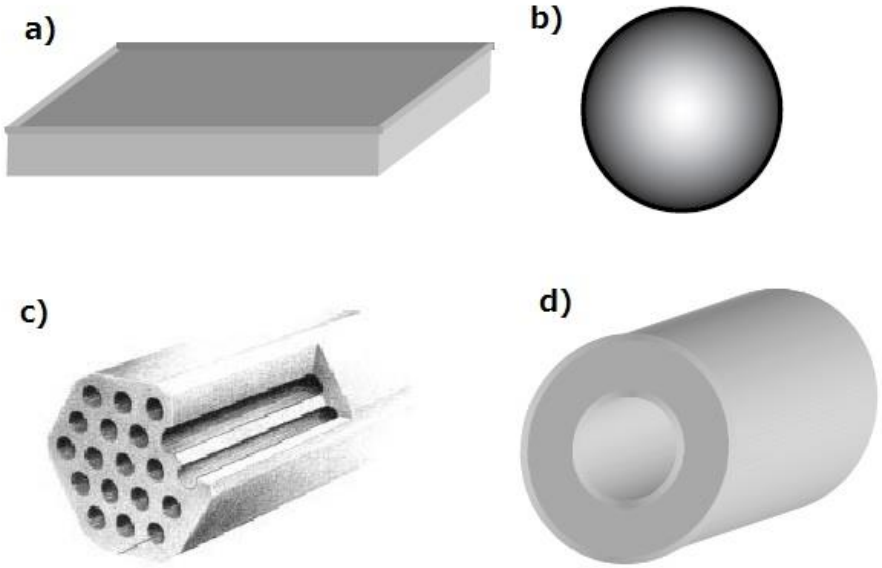

Fig. 2.2 Geometries of membrane (a) flat sheet, (b) capsule, (c) tubular and (d) hollow fibre. [13, 18]

The cross sectional structure of hollow fibre membrane could be symmetric or asymmetric, depending on the fabrication method and materials. [18] To achieve high permeability and appreciable selectivity, most of the ceramic hollow fibre membranes have asymmetric structures consist of dense selective layers forming the outer and inner wall of the membrane and a porous centre. The porous centre is generally formed by a finger-like layer and a sponge-like layer as seen in Fig. 2.3. The thickness of sponge-like and finger-like layer and their porosities are controllable during the fabrication process. The finger-like layer is highly porous, which favours high flux of feed and permeate as well as catalysis depositions. Hollow fibre membranes which are used as reactors preferably have thick or even complete finger-like cross sectional structures. [7, 8, 10, 31, 32] The sponge-like structure which is denser in comparison with the finger-like structure, on the other hand, provides mechanical strength and hence acts as a strong support layer of the hollow fibre membrane. [9, 33-35] In general, the porosity of ceramic membranes is kept at 35% or above to provide sufficiently low fluid resistance [32, 36] and hence an appreciable efficiency when performing separations.

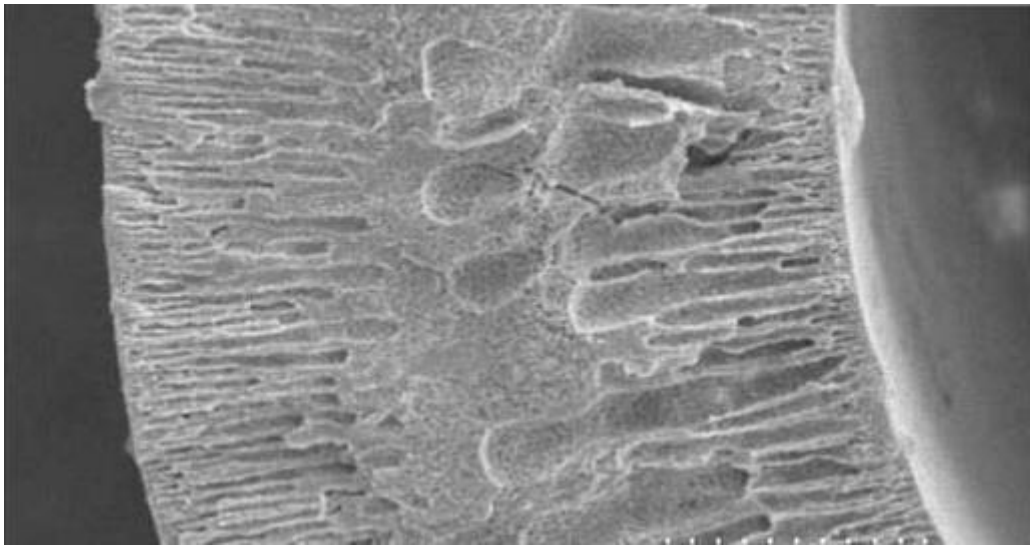

Fig. 2.3 Asymmetric cross sectional structure of a ceramic hollow fibre membrane. [35]

2.4 Mass transport and fouling in hollow fibre membranes

As mentioned, the mass transport through a membrane is either pressure driven which leads to the flow of permeates through pores, or concentration gradient driven which leads to solution diffusion. There are three mass transport mechanisms in asymmetric hollow fibre membranes that have a dense selective layer, poiseuille flow, knudsen flow and solution diffusion as presented schematically in Fig. 2.4, were reported by Wang and Chung. [37] Poiseuille flow occurs in the pores of the selective layer, where the pore is relatively large for the transporting molecule. Knudsen flow occurs when the free mean path of the transporting molecules is large compared to the passage in the membrane. Solution diffusion occurs through non-porous dense region of the active layer.

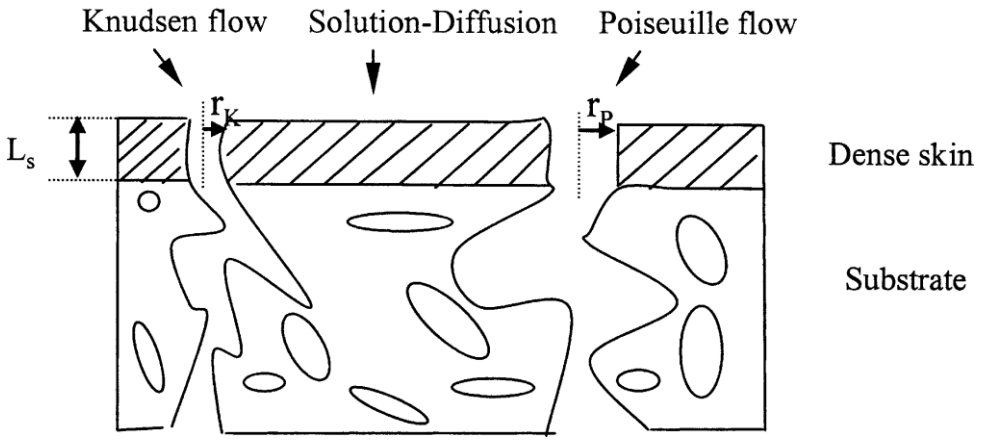

Fig. 2.4 Schematic presentation of mass transport mechanisms in asymmetric hollow fibre membranes that have a dense selective layer. L_s is the thickness of dense selective layer. r_K is the pore radius for knudsen flow. r_P is the pore radius for poiseuille flow. [37]

Baker explained the relative size and permanence of pores identify the mass transport mechanism in a membrane. Membranes which solution-diffusion is the major mass transport mechanism have tiny pores which are spaces between molecules with thermal motions. These small spaces appear and disappear on about the same time scale as the motion of permeants traversing the membrane. For membranes which mass transport is performed mainly through pore-flow, the pores are relatively large, permanent and fixed in size and position regardless of permeant motion. As the thumb rule, pore flow occurs in membranes that contain pores of over 1 nm in diameter, which include all microfiltration and ultrafiltration membranes. [17] Poiseuille flow through pores driven by pressure difference was the dominating mass transport mechanism in the microfiltration ceramic hollow fibre membranes prepared in this study.

Apart from mass transport mechanism, the filter mechanism of porous membranes can also be identified as screen filtration or depth filtration, which is shown in the schematic diagram in Fig. 2.5. Screen filtration membranes reject solutes as retentate on the membrane surface. Depth filtration membranes allow all particles to get into the interior of the membrane and separate out permeate by capturing solute in the small constrictions in the membrane capillaries or adsorption of solute in the tortuous path through the membrane. [17] As described in the previous section, most of the ceramic hollow fibre membranes reported have their surface layer denser than centre layer, which demonstrated screen filtration by having the selective layer on the membrane surface.

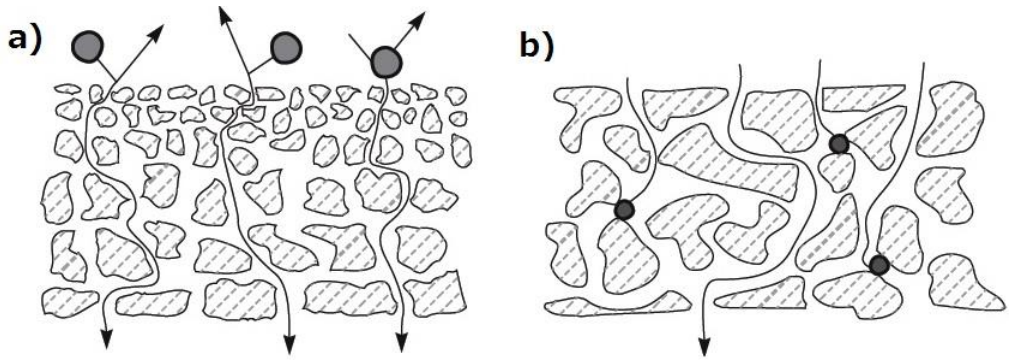

Fig. 2.5 Schematic presentation of (a) screen filtration mechanism and (b) depth filtration mechanism. [17]

The flux of permeates through pore-flow in a membrane is described by Darcy's law $v_{\beta,a_v} = -\frac{K_\beta \Delta P}{\mu_\beta L}$, which v_{β,a_v} is the average velocity of fluid flow, K_β is the permeability of membrane, ΔP is the pressure drop, μ_β is the fluid viscosity and L is the membrane thickness.

The Darcy's Law relates the flux with the pressure gradient across the membrane, concentration of permeate in the membrane and the membrane nature. Membrane nature, including membrane material, tortuosity and thickness, is determined at the membrane production stage and all contributed to the overall membrane resistance. Carman has proposed the Carman-Kozeny equation (C-K equation) $K_\beta = \frac{{L_{CK}}^2 {\varepsilon_\beta}^3}{C_{CK}}$ which K_β is the permeability of membrane, L_{CK} is an appropriate length scale, ε_β is the porosity and C_{CK} is the Carman-Kozeny constant. It related the resistance of a filtration cake formed by rigid particles and the mean particle size, thickness and voidage. [38] In the case of ceramic membrane, although the selective layer could be modelled as a filtration cake, because of the change in microstructure and grain deformation during the sintering process, the pores are not perfectly cylindrical. The C-K equation has been modified to encounter the more complex porous structure of ceramic membranes. Li et al. introduced two parameters that implied the effect of grain shape and aggregate style of particles into the C-K equation for modelling the water permeability of ceramic membrane and compared the model with experimental results. The tubular ceramic membrane they tested all had a porosity of 30% with pore sizes ranging from 100 – 800 nm and thickness of 10 – 80 μm. Within the corresponding pore size and thickness range, as well as the porosity of 30%, the results obtained by the modified C-K equation agreed well with the experimental results. [39] Xu and Yu developed an analytical expression based on the fractal dimension of the homogeneous porous media, which took over the empirical Carman-Kozeny constant. Their proposed model was expressed as a function of microstructure parameters fractal dimension, porosity and maximum pores size. Fractal geometry theory was applied to calculate the pore area and tortuosity. The C-K equation with analytical constant was hence more closely related to the microstructures in porous materials. [40]

Another way of calculating the flux across a ceramic membrane was taking the membrane as a bundle of capillaries and applied the Hagen-Poiseuille equation (H-P equation) $j = \frac{\Delta P {d_m}^2 \varepsilon}{32 \mu L \tau}$ which j is the fluid flux, ΔP is the pressure drop, d_m is the mean pore size of membrane, ε is the porosity, μ is the fluid viscosity, L is the membrane thickness and τ is the tortuosity. It describes the relationship between pressure drop and fluid velocity in a capillary. An assumption of the H-P equation was absolutely round particles in the membrane, which is not valid for ceramic membrane. Same as the C-K equation, a lot of modified forms of the H-P equation has been presented. As a comparison with their modified C-K equation, Li et al. has

also developed an improved H-P equation that included an extra parameter to encounter the increased tortuosity in ceramic membrane due to the wide distribution of particle size. For the ceramic membrane Li et al. tested, H-P equation corresponded to the experimental pure water flux when the pore size was 0.8 μm or less with a fixed thickness, while it could not accurately model the effect of membrane thickness or porosity on pure water flux. [39] Many other modifications of the H-P equation, on the other hand, were not membrane structure focus. For example, Marchetti et al. considered surface-membrane interaction during the permeation process, which was shown to be different with various solvent mixture permeating through the membrane, and introduced several correction factors into the H-P equation. The correction factors were in terms of pore size and hence the modified H-P equation were applicable in both ultrafiltration and nanofiltration membranes, while a more significant correction was made on the prediction of permeation through nanodimension pores. [41] Microfiltration membranes have pores a lot larger than most solvent. The effect of solvent-membrane interaction in predicting permeation rate through microfiltration ceramic membrane is therefore less significant in comparison with microstructure of membrane.

Hollow fibre membranes are bundled up and sealed into modules for all applications instead of being used as individuals. The two basic geometries of hollow fibre membrane modules are shell side feed and bore-side feed as shown in Fig. 2.6. A shell-side feed module has a loop or closed bundle of hollow fibres in a pressure vessel which is the shell. Pressure is applied from the shell and permeate is driven through the membrane and collected at the open end of the fibre bundle. This module is simple to be manufactured and allows very large membrane area. On the other hand the hollow fibre wall must be able to support considerable hydrostatic pressure, hence the hollow fibres involved must be strong and generally have small diameter. A bore-side feed hollow fibre membrane module has fibres opened at both ends and the feed is circulated through the bore of the fibre bundle. Concentration gradient and fouling due to trapped particulate matter from the feed stream is significant in the stagnant areas between fibres. The large pressure drop develops along the length of the hollow fibre is also a problem that lowers the driving force for permeation. The hollow fibres used in a bore-side feed module have larger diameter than those used in a shell-side feed module for minimizing pressure drop inside the hollow fibres. Because of the direct flow of feed stream across the active surface of the hollow fibre membranes, there is no stagnant dead space. [13]

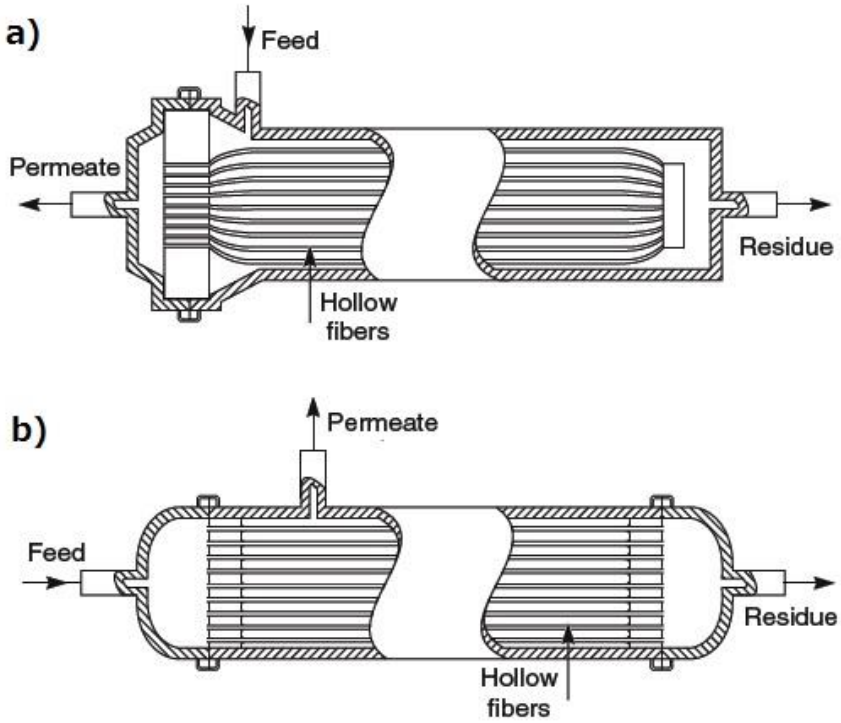

Fig. 2.6 Basic geometries of hollow fibre membrane modules (a) shell side feed and (b) bore-side feed. [13]

Initially the large pores of microfiltration membranes allow very high permeate fluxes. As time goes by, retentate accumulates on the selective layer surface of membrane and cause fouling in the form of adsorption, pore blockage, deposition or gel formation. The total membrane resistance at a specific time over a filtration process is therefore the sum of the membrane resistance itself and the fouling resistance. [42] Cross flow filtration mode has a benefit of maintaining high filtration rate due to the continuous flow of shell stream parallel to the selective layer surface. The turbulence created by the flow of shell stream creates a sheering action that continuously sweeps away particles and retentate on the membrane surface. [43] This minimizes the chance of retentate building up on the selective layer. Le-Clech et al. summarizes the factors that affect the total membrane resistance include the operation mode of the filtration process, type of feed and permeate streams and membrane morphology and surface chemistry. [44] Backflushing, which involves forcing a quantity of permeate back through the membrane, is also a practical solution to remove deposited particles on the membrane surface. An alternative to permeate backflushing is blowing compressed gas through membrane for cleaning up of deposited layer on membrane surface. The application of electric field has also been shown to be effective as a cleaning technique of the membrane surface. [43, 45] Bai and Leow introduced a module that combines dead-end and cross-flow filtration for solving fouling problem and enhance flux through the

membrane. The module was formed by placing a bundle of hollow fibre membranes of a nominal pore size of 0.1μm within a cylindrical membrane of a nominal pore size of 5μm. Large particles in the permeating flow were rejected by the cylindrical membrane of cross flow mode and hence did not deposit on the hollow fibre membranes where dead-end filtration was carried out. Under different influent concentrations and cross flow velocity, the combined dead-end and cross-flow filtration module always showed higher permeation flux than the dead-end hollow fibre filtration control module. [46, 47]

2.5 Ceramic properties and applications

Ceramic materials are well-known for their extraordinary insensitivity for swelling in any solvent and chemical stability. They are generally hydrophilic. [48] Alumina (Al_2O_3) which is an economical and widely used ceramic was proved to be far more stable than stainless steel 316 in hydrochloric acid (H_2SO_4) of pH 1, although slight corrosion was still shown. [49] A porous structure of alumina was also proved to demonstrate low variation in mass, flexural strength, porosity, pore size distribution and microstructure after long submerge in 20 wt% sulphuric acid aqueous solution. [50] Krasnyi et al. has tested the chemical stability of two porous ceramics in sulphuric acid (H_2SO_4), hydrochloric acid (HCl), sodium hydroxide (NaOH) and soda ash (Na_2CO_3) solutions in multiple concentrations. They showed porous ceramic mixture with alumina and SiO_2 dominated had acidic resistance, alkali resistance and chemical resistance of over 80%. A highest and lowest chemical stability of the porous ceramic was shown in soda ash solution with any concentration and concentrated sodium hydroxide solution respectively. [51] Van Gestel's group reported the stronger acidic and alkali resistance of crystalline ceramics in comparison with amorphous ceramics by performing corrosion test on Al_2O_3, TiO_2 and mixed Al_2O_3-TiO_2 membranes. [52] These properties made ceramics a suitable material for porous membranes for industrial waste treatment. Individual ceramic material or ceramic at a particular phase, on the other hand, show corrosion in some chemical attack. For example, γ-Al_2O_3 which has a lower crystallinity than α-Al_2O_3 is less inert than α-Al_2O_3 in strong acid; TiO_2 in amorphous phase is also less stable than its anatase phase. [53] SiO_2 is inert in organic solvents but has a low resistance in alkaline solution and the alkaline attack is even more effective at higher temperatures. [49] Jana et al. prepared ceramic microfiltration disc membranes with various compositions of clay and kaolin and sintering temperature, then tested their change in weight, porosity, pore size, water permeability and flexural strength after acid and base treatment. 2-10% of weight loss was shown by the samples. The chemical corrosion led to a minor

increase in porosity, mean pore size and water permeability and a slight decrease in flexural strength. The sample that contained corundum showed the best acidic and basic stability. High sintering temperature also increased the chemical stability of the clay-kaolin membrane by the formation of mullite and nephiline. [54]

Ceramics also have extraordinary thermal stability, which made it an alternative material for membrane used at high temperature conditions such as capturing carbon dioxide in flue gas released from power plant. Flue gas from power plant is of a temperature over 200^{o}C which is over the limit for most polymer membrane. [1] The melting temperature of some widely used ceramics such as alumina, beryllia (BeO), zirconia (ZrO_2) and silicon carbide are all over 2000^{o}C when the material is fully dense. [55] In the preparation and application of porous ceramic membrane, considerations other than the melting temperature of the ceramic material has to be taken into consideration since many characteristics of the porous membrane varies with temperature, for example, pore size and its distribution, grain size and crystallographic phases. [49] When determining of the thermal stability of ceramic hollow fibre membranes with the selective layer and support layer of the same material, the sinter activity and phase transformation of the membrane material have to be taken into account. Porous ceramics with high thermal stability have negligible sintering activity, phase transformation, change in mechanical strength and pore structure at their working temperatures for a period of time comparable to the practical application time. The work of Lin et al. showed that pure γ-Al_2O_3, TiO_2 and ZrO_2 showed phase transformation from 900 ^{o}C, 450 ^{o}C and 600 ^{o}C respectively. [56] α-Al_2O_3 which is the ceramic mainly used in the experimental work described in this thesis is the thermodynamically most stable phase of alumina and does not undergo further phase transformation in heat treatment. [56-58] γ-Al_2O_3 was converted and stayed as α-Al_2O_3 when the annealing temperature reached 1228 ^{o}C. Significant densification through sintering could be observed in α-Al_2O_3 at a temperature of 1300 ^{o}C or above. [58, 59]

2.6 Sintering and densification of ceramics

Sintering, or calcination, is the densification process for a particulate ceramic compact through bond formation and grain growth. It is therefore an essential and critical step for any ceramic production. Sintering commonly occurs when the temperature reaches half to two-third of the melting temperature of the ceramic. [4] The melting temperature of some widely used ceramics such as alumina, beryllia (BeO), zirconia (ZrO_2) and silicon carbide are all over 2000 ^{o}C. [55] Apart from the melting point of individual ceramic, particle size also

affects the sintering temperature. Ceramic powder of finer particle size can be sintered more rapidly at a lower temperature than powder with coarse particles. Finer particles demonstrated stronger adhesive effect on the other hand. [60] The tendency of fine particles to agglomerate increases the difficulty for the formation of a homogeneous organic-inorganic mixture for the extrusion of ceramic hollow fibre membrane precursor. As stated by Greil, environmental effect of sintering such as reaction with CO_2, SO_3, oxidation or hydrolysis could lead to the formation of a new glassy phase which enhances bonding of grains. In this case strengthening of a ceramic could occur at a much lower temperature. [61]

As explained by Binner and Rahaman, sintering is a mass transport mechanism motivated by differential surface curvature. The grain boundaries move towards their centres of curvature when the temperature is sufficiently high for sintering to occur. Grain growth which is the increase in average grain size during sintering was a result of the powder compact lowering its free energy to reach its equilibrium state through mass transport to larger particles and contact regions between particles. As atoms in the grain boundaries have higher energy than those in the bulk grain, the driving force for grain growth is the reduction in grain boundary energy by a decrease in grain boundary areas. The reduction in total free energy is the sum of change in free energy associated with volume, grain boundaries and grain surfaces. Before grain growth occurs, neck growth which occurs at a significantly lower free energy drop takes place when centres of individual particles approach that of another touching particle. Pore closure, although is not directly a consequence of grain growth phenomenon, its interparticle mass transport and kinetics do lead to pore shrinkage and hence closure. Pores are empty space formed by grains mismatch. The number of grain forming a pore varies across the particle network. Once grain growth occurs, the adjacent particles would in general be smaller. The mass transport to larger particles for grain growth continuously decreases the number of grains the pore is formed by, until the pore is closed. [62-65]

As temperature gradually rises up to the sintering temperature, the sintering process could be divided into three stages. In the initial stage when the temperature is still low for sintering, particle rearrangement for increasing inter-particle contact and neck formation at contact points of particles occurs. The intermediate stage involves neck growth, limited grain growth and high volume shrinkage. When temperature is high enough the final sintering stage would be reached, when grain growth is much faster while volume shrinkage is limited. [64]

In the sintering process of dry solid ceramic with no mechanical pressure applied, the mass transport mechanisms are surface diffusion, grain boundary diffusion and lattice diffusion. Surface diffusion results in particles joining, surface smoothing and rounding of pores. The diffusion along grain boundaries and through grain lattices lead to neck growth and volume shrinkage which result as densification. [63] The qualitative sintering mechanism between two particles is modelled in Fig. 2.7.

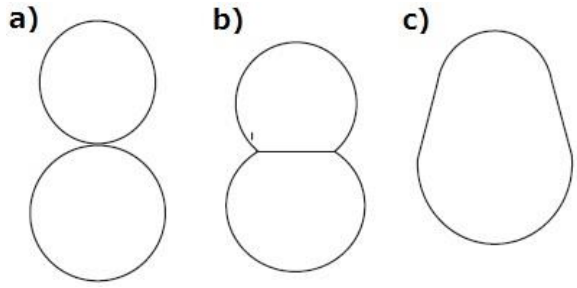

Fig. 2.7 Modelling of sintering mechanism between two particles at different sintering stage (a) increasing inter-particle contact as a result of particle rearrangement, (b) neck growth by surface diffusion between particles and (c) grain growth. [4]

Apart from conventional sintering which has been used in most of the ceramic hollow fibre membrane productions, microwave (MW) sintering and spark plasma sintering (SPS) have been developed to achieve densification and bonding purposes of ceramics within a shorter period of time. Conventional sintering takes several hours in general for the formation of bonds among ceramic powder, while these alternative sintering methods minimize the sintering time down to minutes, at the same time achieving sintering effect at a lower temperature, hence are more energy and cost effective. The major difference between MW sintering and conventional sintering is the generation of heat in the sample. Heat is generated by heating elements then transferred to the sample through radiation in conventional sintering, while in MW sintering microwave energy is absorbed by the sample then was transformed into heat within the sample. Liu et al. showed the results of both conventional sintering and MW sintering on a mixture of 0.6 - 0.9 μm coarse grain alumina powder and 40 – 80 nm nanosized alumina powder. They proved a relative density of alumina as high as 98.5% was achieved by MW sintering at 1500 ^{o}C in 30 minutes, while the highest relative density reached by conventional sintering at 1550 ^{o}C for 2 hours was 96.1%. [66] Bian et al. also reported the comparison of conventional sintering and MW sintering on nanostructured alumina-titania composite ceramic powder. The tested composite contained 87 wt% alumina of grain size 20 – 45 nm and 13 wt% titania of grain size 20 – 50 nm. The relative density of the Al_2O_3-TiO_2 composite reached 98.1% after 10 minutes of MW sintering at 1250 ^{o}C, while

conventional sintering of temperature as high as 1450 ^{o}C gave the composite a relative density of 91.5% after 1 hour. [67] SPS, on the other hand, is a sintering method that involves external pressure and electric current. The sintering effect in SPS is a contribution of joule heating created by the thermal effect of current. In an SPS process pulsed direct current is utilized through the sample along with uniaxial pressure to consolidate the ceramic powder. The current also produces plasma that causes cleansing effect on particle surfaces, which enhances sintering. [68] Shen et al. has applied SPS on SiN_4 based ceramics and observed a rapid full densification at the temperature range of 1450 – 1550 ^{o}C under a uniaxial pressure of 50 MPa. Increasing the sintering time from 2 minutes to 4 minutes changed the average grain size from 210 nm to 350 nm. [69] Apart from ceramic materials, SPS has also been applied in ceramic-metal composite, as the $NiAl_2O_4$-Cu-Ni prepared by Sun et al. Due to its high melting point of 2110 ^{o}C, $NiAl_2O_4$ could hardly be sintered to high density by conventional sintering. SPS as a technique that enhances sintering at lower temperature and in shorter period of time was therefore used for preparing $NiAl_2O_4$-metal composite material. The sample sintered at 1300 ^{o}C for 10 minutes with a heating-up time of 5 minutes gave the $NiAl_2O_4$-Cu-Ni composite a relative density of 86.0%. [70] These alternate sintering methods, although are more time and energy effective, are not suitable for sintering porous membrane. The limited grain growth and close to full densification properties of ceramics prepared by MW sintering and SPS hinder the flow of liquid through them. The addition of external pressure on polymer binded ceramic hollow fibre membrane also causes deformation of the hollow fibre before sintering occurs.

In additional to surface curvature, the driving force for sintering in these processes also involves externally applied pressure or chemical reactions. [65] Some of the ceramic densification and bonding methods include pressurized sintering, hot pressing, pyrolysis, melting, chemical vapour deposition (CVD) and physical vapour deposition (PVD) etc. [64]

2.7 Grain growth in porous ceramics

In porous ceramics, the increase in average grain size generally comes with the increase of pore size. The number of grain and the number of pores on the other hand both decrease. Grain growth can be divided into normal growth and abnormal growth. The normal grain growth of porous ceramics shows a fairly narrow range of grain size and shapes and a close to constant grain size distribution through the whole grain growth process, while pores are remained in grain boundaries. In an abnormal grain growth, random large grains are

developed and grow fairly rapidly which significantly change the grain size distribution throughout the grain growth process. Pores in an abnormal grain growth are broken away from grain boundaries and left inside the large abnormal grains. These pores are difficult to be removed. Prolonged sintering increases the possibility of abnormal grain growth. [65]

Grain size and grain size distribution have significant effects on the fracture strength and density of ceramics, which makes grain size and grain growth critical control factors for the fabrication of ceramic membrane. Wang et al. specifically studied the effect of annealing treatment on the mechanical properties of ZrB_2-SiC-graphite (ZSG) ceramics. The little grain coarsening shown in the ZSG ceramic was attributed to oxide impurities removal through the reaction with graphite. This favoured densification of the ceramic and hence increased the flexural strength and Vickers' hardness. The fracture toughness on the other hand was decreased with increasing annealing time mainly due to the decrease in crack propagation extent and residual stress in the ceramic. [71] Zou's group sintered TiB_2-TiC + 8wt% nano-Ni composite ceramic at various processes with different temperature holding stages and time and investigated the effect of sintering process on the mechanical properties and microstructure on this ceramic composite. They found out longer holding time and multiple holding stages led to obvious grain growth of TiB_2 and TiC as well as formation of pores and relatively low flexural strength. [72] The sintering time for the fabrication of high flexural strength ceramic hollow fibre membrane is therefore ideally being long enough for densification and formation of bond between particles while limiting grain growth. Yu et al. presented how grain size distribution reported the effect of grain size distribution on creep damage evolution of polycrystalline materials. Their results show a slower void growth rate along grain boundaries with a wider grain size distribution, which was explained by the increase in disorder in directions of all grain boundaries that lower the probability of individual grain boundary to be perpendicular to the direction of external stress. [73] Despite this, abnormal grain growth should also be avoided in the fabrication of mechanically strong ceramic membrane because of the difficulty in removing pores that are trapped inside large grains associated with abnormal grain growth.

2.8 Ceramic hollow fibre membranes fabrication

Fabrication method of ceramic hollow fibre membrane includes dry spinning and combined phase-inversion and sintering. Dry spinning started with ceramic powder and polymer binder being mixed to form a paste. The paste was then extruded through a spinneret and formed

ceramic hollow fibre precursors. High temperature heat treatment on the hollow fibre precursors removed the polymer binder. Hollow fibre membranes produced by this method have symmetric structures. [3, 74] Combined phase-inversion and sintering involves the preparation of spinning suspension with solvent, followed by the spinning of hollow fibre precursor and final sintering. [4, 75] This is by far the most common fabrication method for ceramic hollow fibre membrane. Both dense and porous ceramic hollow fibre membrane could be obtained by phase-inversion and sintering through adjustment of particle size, content of spinning suspension, sintering condition and coagulant used for phase-inversion. [5, 76] The asymmetric structure of hollow fibre membranes produced by phase-inversion and sintering has a relatively dense layer on the outer surface and a porous supporting inner layer, which makes it ideal for separation purpose with low resistance to the flow of feed and permeate. [9]

The particle size of raw material significantly affects the mechanical strength, pore size and porosity of the final hollow fibre membrane by particle packing. As reported in several studies, the smaller the particle size, the higher the particle packing density is. Including small particles in the configuration of large particles could increase the packing density by having the smaller particles filling the gabs in between larger particles. The packing density therefore depends on the ratio of particle size and mixture, which is presented graphically in Fig. 2.8. An optimal packing density is reached when the gabs in the large particles matrix is completely filled up by the smaller particles. [77-79] Tan et al. and Liu et al. have prepared alumina hollow fibre membranes of different strength and porosity by mixing micron size and nano size alumina particles. [35, 75] Results obtained by Tan et al. shows that with alumina particles of size 1μm, 0.3μm and 0.01μm, mixing them in a ratio of 46.5/46.5/7 gave the hollow fibre membrane with the lowest porosity and highest mechanical strength. Liu et al. mixed 0.01μm alumina particles into 1μm alumina particles in the preparation of alumina hollow fibre membranes and proved the increase of 0.01μm content led to the decrease in pore size in the final product.

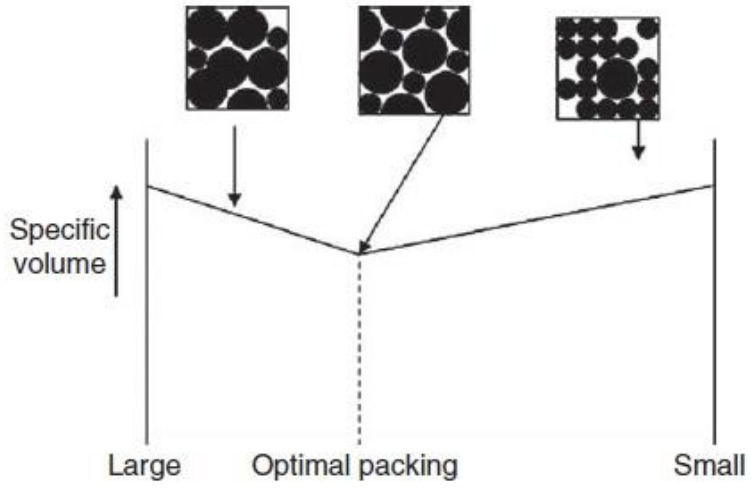

Fig. 2.8 The change in specific volume with different ratios of large and small particles in a powder mixture. [5]

Sintering temperature is another critical factor that determines the mechanical strength, pore size and porosity of ceramic hollow fibre membranes, by controlling the grain growth, shrinkage and closure of pores. [4] Many studies on ceramic materials and ceramic hollow fibre membrane show that higher sintering temperature enhances shrinkage and closure of pores, which lead to densification of the hollow fibre membrane and hence favours mechanical strength. [3, 9, 35, 75] A significant decrease in porosity occurs if the sintering temperature reaches a critical, where the ceramic membrane becomes fully dense and gas tight. This critical sintering temperature varies for different ceramics. Liu et al. showed a great drop in porosity occurred in alumina hollow fibre when the sintering temperature went over 1500 ^{o}C. [35] Kingsbury et al. also sintered alumina hollow fibre at different temperatures and showed an increase in the pore size of the sponge-like layer under a sintering temperature of over 1400 ^{o}C. [33] Another widely used ceramic yttria-stabilized zirconia (YSZ) on the other hand showed a significant drop in porosity when the sintering temperature exceeded 1350 ^{o}C according to the work of Zhang et al. [32] Addition of sintering additive such as magnesium oxide (MgO) could lower the sintering temperature, which led to a fully dense structure at a lower temperature. [80]

Considering the long and thin shape of hollow fibre membrane and the use of organic binder in extrusion, the possible problem at the sintering stage include warpage, excess grain growth, incomplete decomposition of binder and incomplete reaction of starting materials. [64] Warpage is a result of inappropriate support during sintering or inhomogeneity in the hollow fibre membrane precursor, which causes deformation of the hollow fibre. Excessive grain growth occurs if the set temperature was too high and the grain boundaries move faster than

pores, leaving pores isolated inside grains and hence limiting pore shrinkage. Insufficient sintering time and high heating rate leads to insufficient time for the burn off of organic binder and the complete formation of ceramic if a starting material such as carbonates, sulphates and nitrates is used to give a different final composition. This leaves impurities such as carbon in the final membrane. The control on sintering temperature, time and heating rate is therefore important to prevent these.

Cross sectional morphology of hollow fibre membranes also have a great impact on their mechanical strength, porosity and mass transport resistance. In preparation of ceramic powder spinning suspension for phase-inversion, addition of non-solvent increases the suspension viscosity and slowed down the rate of phase inversion, hence lead to a thicker sponge-like layer. [33, 34, 80] At the extrusion stage for hollow fibre precursor, parameters that controls the cross sectional morphology include internal and external coagulant used, flowrates of coagulants and the size of air gap. Kingsbury et al. reported the increase in internal coagulant flowrate and the size of air gap favoured the formation of highly porous finger-like voids in the hollow fibre membrane. [9, 33] Zhang's group compared the use of water and ethanol as external coagulant and found that the later led to long finger-like voids across the centre of the hollow fibre membranes without any sponge-like structure. [32] Yin et al. tried using a mixture of NMP a solvent and water a non-solvent as an internal coagulant, while keeping water as an external coagulant same as the general phase-inversion process. Their results showed that mixing a solvent into internal coagulant created a different exterior and interior precipitation rate in the hollow fibre and formed long finger-like pores which extended from the inner wall to the dense layer near the outer wall. [31] Liu et al. used a mixture of 75 wt% NMP and 25 wt% water as internal coagulant for the preparation of YSZ hollow fibre membranes from nanosize YSZ powder. The resulting YSZ hollow fibre membranes were gas tight, with two-third of the cross-sectional area from the internal wall being dense. [81]

2.9 Ceramic reinforcement mechanism

Reinforcement of ceramic is referred as the introduction of external elements that increase the resistance of crack propagation in the monolithic ceramic matrix. These elements could be discrete or continuous. Discrete elements include particles, whiskers and short fibres. All long continuous fibres are classified as continuous elements. [82]

Discrete elements strengthen a monolithic ceramic mainly through microcracking and crack deflection. Fig. 2.9 shows a schematic diagram of these two mechanisms. When the discrete element has a higher thermal expansion coefficient than the ceramic matrix, it contracts more than the matrix at the post-sintering cooling stage and creates a stress field. When a macrocrack hit this stress field, it is dispersed into microcracks. The formation of microcracks created new surfaces, hence dissipates energy and reduces the stress intensity at the tip of the macrocrack. The presence of microcracks also deflects or branches the growth of macrocrack and hence further reduce the stress intensity when the travelling path of the crack is increased and the cracking plane is no longer perpendicular to the tensile stress. [83] Evans reported that macrocracking in ceramic materials is accompanied by microcracking, while how significantly these microcracks contribute to ceramic toughening depends on the stress intensity associate with these microfractures. [84]

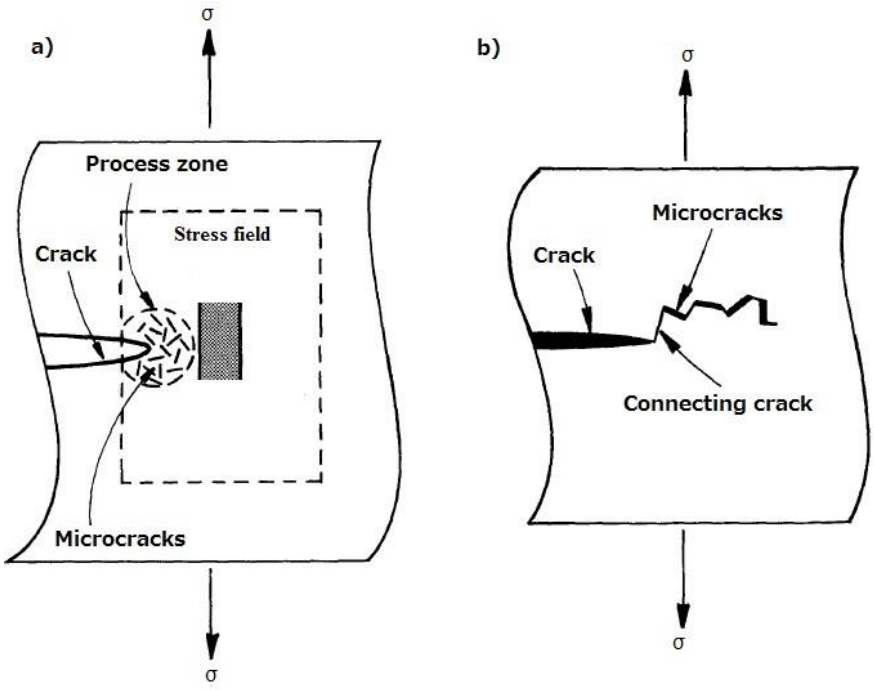

Fig. 2.9 Strengthening mechanism by discrete reinforcement elements in monolithic ceramic (a) microcking and (b) crack deflection. σ refers to applied stress. [83]

Continuous fibres enhance the mechanical properties of ceramics by both crack deflection and crack bridging mechanism, which are shown schematically in Fig. 2.10. Fibres in a ceramic matrix carry out crack deflection by bypassing the crack initiated in the matrix into fibre-matrix debonding cracks, hence resisting the propagation of crack into the fibres. [82] The shear stress along the matrix-fibre interface also leads to fibre pull-out which also increased the required energy for the crack to develop. Crack bridging takes place when the

fibres are supporting part or full load and are pulled-out during or after the ceramic matrix fails. The bridging material was a tougher inclusion than the ceramic matrix that exerted a closing force on crack faces and increased the driving force required for crack propagation. In the wake of the crack, with the presence of fibres, the fractured surfaces remained bridged until the load applied is sufficient for complete fibre failure. Curtin has presented a continuum model of crack bridging toughened ceramic, which represented the effect of bridging medium by an average closure force as a function of crack opening. The modelling result showed that the material strengthening effect highly depended on the randomness of bridge locations, as cracks avoid highly ordered and efficiently bridged regions. [85] Paar et al. studied the failure process in crack-bridged ceramic by modelling the three damaging mechanisms involved, which were matrix cracking, fibre-matrix interfacial debonding and slipping and fibre failure, in the order of happening as a crack grows. The strength of matrix material was assumed to follow a Weibull distribution and that of fibres was assumed to follow a two-parameter weibull distribution in their simulation. Their comprehensive model simulated the stress-strain curve of 1-dimensional unidirectionally reinforced ceramic matrix composites, which was compatible with experimental results up to the onset of massive fibre failure while the ultimate strength of the composite was over-estimated. [86]

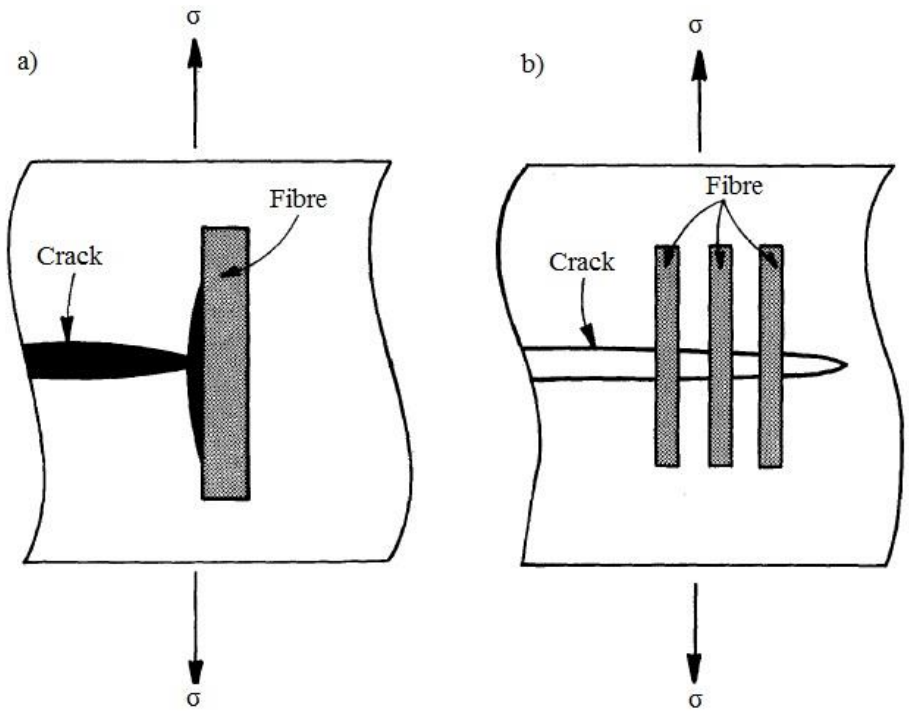

Fig. 2.10 Strengthening mechanism by continuous fibres in monolithic ceramic (a) crack deflection along fibre interface and (b) crack bridging. σ refers to applied stress. [83]

Crack pinning is another reinforcement mechanism in ceramic and could be achieved by both discrete and continuous elements. Instead of bypassing crack propagation, crack pinning toughens the ceramic matrix by stopping crack propagation at the point where the crack hit the reinforcement element, as shown in Fig. 2.11. Elements that carry out crack pinning could therefore be referred as crack bridges without debonding. The spacing between the reinforcement element dispersed across the matrix must be small in comparison with the crack size for crack pinning to be effective. [83] Funfschilling et al. has reported the effect of crack pinning in the toughening of silicon nitrides, which was responsible for the significantly enhancement in mechanical properties before debonding between reinforcement element and the ceramic matrix occurred. It was after the crack pinning failed and debonding occurred then crack bridging dominated the reinforcement. [87]

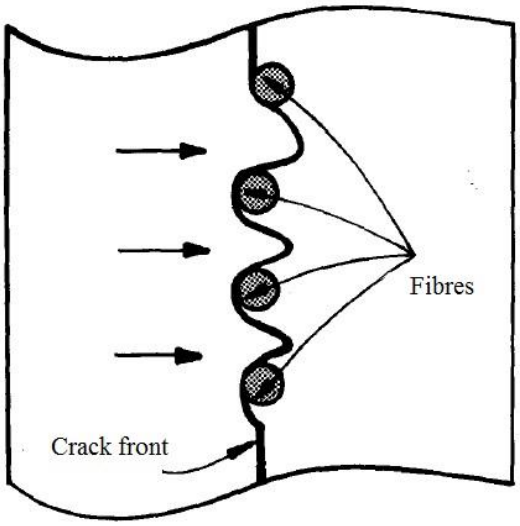

Fig. 2.11 Crack pinning reinforcement mechanism of continuous fibres in monolithic ceramic. [83]

Without external reinforcement elements, some ceramics undergo phase transformation during fracture and such phase transformation could lead to material toughening. Zirconia is an example which undergoes two transformations, from cubic to tetragonal then to monoclinic phase, between its melting temperature and room temperature. Cubic zirconia is the most stable form, yet has the lowest toughness and strength. Enhancement in mechanical properties including strength and fracture toughness was shown through its transformation to monoclinic phase. The energy for phase transformation to occur is transferred from the stress field associate with crack growth, hence the stress intensity at the crack tip. [88]

2.10 Dense ceramic reinforcement

A lot of studies have been carried out on the reinforcement of dense ceramic materials to overcome the brittleness nature of ceramics. The inclusion of silicon carbide SiC in ceramic materials for the formation of ceramic-ceramic nanocomposites has been widely used and reported in many studies. Silicon carbide (SiC) is a ceramic that processes high mechanical strength and thermal resistance. It can be synthesized by a pre-ceramic polymer polycarbosilane (PCS). The advantages of using pre-ceramic polymer are fine grain sizes of the final product and well dispersion of the ceramic powder when a mixture or composite is being prepared. SiC fibre has been manufactured in laboratory and industrial scale. The major steps involved in SiC fibre production included melt-spinning in a nitrogen environment and air curing, followed by a heat treatment in nitrogen. [89, 90] Some studies had been done to improve the tensile strength of SiC fibres. Yang's group proposed the mixture of PCS and hydroxyl-terminated polybutadiene (HTPB) as a SiC fibre precursor. During the mixing PCS reacted with HTPB and formed cross-lined polymers, which minimize the oxygen needed for the air-curing process. With 3wt% of HTPB added, the SiC fibres with low oxygen content showed a 26% increase in tensile strength and an oxidation resistance up to 1200 ^{o}C. [91] Shi's group used PCS as a precursor and doped nano-SiC into alumina to form a fully dense composite by hot pressing. The results showed that a flexural strength as high as 516 MPa was achieved by 1 wt% of nano-SiC. [92]

Apart from SiC, other materials have been added into ceramic matrix for reinforcement purpose. Nickel reinforcement was tried and proved to successfully strengthen fully dense alumina by creating a stress field within the alumina matrix [93], while the toxicity of nickel makes this particle reinforcement method unfriendly to human and the environment. [94] The formation of eutectic mixture with gadolinium aluminium perovskite ($GdAlO_3$) in the alumina matrix changed brittle fracture of pure alumina to plastic deformation like metals [95] but its raw material gadolinium oxide is of a very high cost. Similarly, the high cost of raw material was also an obligation for the reinforcement of ceramic by gold particles, as reported by Yi et al. Gold particles are ductile and elongated which made it suitable for ceramic toughening. Due to the limited pull-out and frictional sliding, it was applied in the toughening of dental ceramics. [96] The high cost of raw materials made gadolinium oxide and gold particles impractical for large scale application in reinforcement of industrial ceramic membranes. Fibre reinforcement in ceramic matrix was reported in many studies. Some of the fibres used as a bridging material in ceramic matrices included nano-SiC fibres

and carbon nanotube (CNT). Ceramic materials of high flexural strength were produced. The preparation processes were complicated in general, because of the difficulty in dispersing fibres and oxidation of fibres when sintered in air. [86, 92, 97] Extra preparation such as vacuum or noble gas sintering environment was required to keep the properties of the bridging materials. Boccaccini's group reviewed the incorporation of carbon nanotube in ceramics through electrophoretic deposition (EPD). The carbon nanotube-ceramic nanocomposite systems reviewed includes SiO_2/ CNT, TiO_2/ CNT/, MnO_2/ CNT and Fe_3O_4/CNT. These were done by preparing a stable CNT suspension in polar solvent using acid-treated CNT, then obtained a porous CNT film and deposit ceramic nanoparticles through EPD. The ceramic nanoparticles either infiltrated the porous CNT structure or formed a layered composite structure. [98] In general, a weak bond between the reinforcement fibre and the ceramic matrix results in a toughened composite by fibre pull-out mechanism, while a strongly bonded fibre-matrix interface forms a brittle fibre-ceramic composite. Singh and Sutcu performed a fibre push-out test on zircon-SiC composite. Their results showed that the composites reinforced by boron nitride (BN) coated SiC fibres produced and uncoated SiC fibres both had very small interface debond energy. [99] Both BN-coated and uncoated SiC fibres are therefore suitable for toughening ceramics. Du et al. incorporated boron nitride nanotube in silica (SiO_2) ceramic and achieved a relative density of 92% after a hot-pressing of the composite at 1400 ^oC with a flexural strength of 120.5 MPa which was 230.8% of SiO_2 ceramic. [100] In the work of Shi and Wang, the densification of zirconium diboride (ZrB_2) by SiC and ZrC for enhanced mechanical strength was followed by a surface treatment. [101] Surface oxidation of the ZrB2-SiC-ZrC ceramic formed a glass layer that led to a flaw healing effect and hence raised its flexural strength by about 15%.

2.11 Porous ceramic reinforcement

Porosity which is an important factor for the performance of a membrane could hardly be demonstrated by dense ceramic materials due to their high trans-membrane resistance and hence inefficient flow of feed and permeate. The use of ceramic membrane as soild-oxde fuel cells and membrane reactors also require the membrane to be sufficiently porous. Strengthening of porous ceramics has also been mentioned in some studies. The porosities of these materials range from 20% to 50%. SiO_2 reinforcement [102] was tried and successfully for a strong alumina matrix which had a bending strength of over 95 MPa with an addition of 20 wt% SiO_2. The bending strength was raised up to double of the original at the same time however porosity was sacrificed and down to below 25%. The same densification effect

occurred in porous SiC ceramic bonded by mullite, in which an increase in mechanical strength came with a drop in porosity with the addition of mullite. [103] The addition of TiO_2 also led to an 18% increase in flexural strength but also lowered the porosity by 8%, although in the study of Monash and Pugazhenthi the resulted 36% porosity of clay ceramic containing 6 wt% of TiO_2 still make this ceramic a choice for membrane fabrication [104]. Another attempt to increase the bending strength of alumina by the addition of nano-sized alumina particles into micron-sized alumina matrix, in the form of nano powder and sol-gel derived nanoalumina. [105] It was proved that a 4-6 wt% of nanoalumina presence in the micron alumina matrix could gave a 100% and 500% increase in bending strength by powder mixing and sol-gel derivery respectively. The bending strength of porous alumina fabricated by Kritikaki and Tsetsekou reached about 85 MPa with porosity being kept above 35% and potentially more work could be done to improve it even futher. Whiskers or fibres reinforcement of porous ceramic, based on the same bridging mechanism as dense ceramic strengthening, has also been studied. Before this, Li and Narita presented a porous aluminium borate ($9Al_2O_3 \cdot 2B_2O_3$) ceramic structure solely formed by whisker. [106] Although the micron scale pore size and relatively low bending strength of 2.2-56.1 MPa of this aluminium borate ceramic made it unsuitable to be used as a membrane for seperation purpose directly, its high porosity up to 85% gave it a potential to be combined with other ceramic particles, in which the whisker network would provide an ultra strong reinforcement.

Besides reinforcement from external materials, some studies focused on the fabrication method of porous ceramic to maximize its flexural strength. Li and Zhang has investigated the mechanical strength and microstructure of porous Si_3N_4 fabricated by three different methods, including oxidation-bonding with sol-gel infiltration sintering, cold-pressing with pressureless sintering and 3D-printing with pressureless sintering. [107] Cold-pressing with pressurelss sintering was found to achineve the highest flexural strength of 143-207 MPa with porosity kept above 46%. Its average pore size of micron scale however is relatively large for many seperation processes. Jayaseelan's group made use of the preferential neck growth of grains before densification and sintered porous alumina with pulse electric current, forming alumina with controllable porosity between 30% to 50%. The porous alumina undergone pulse electric current sintering showed a flexural strength more than double of alumina with the same porosity undergone hot pressing or pressureless sintering. [108]

Surface modification is another strategy of flexural strength enhancement in porous ceramic. A layer of alumina coating by supersonic plasma spraying was proved to give a slight

increase of 4% in the flexural strength of Si_3N_4. [109] Spray coating is not suitable for strengthening membranes used for liquid seperations as the coating resulted as a dense layer on the outer surface, which siginificantly decreased liquid diffusion into and out of the membrane.

2.12 High porosity ceramic hollow fibre membranes

Rather than mechanical properties, many studies on ceramic hollow fibre membranes were mainly focusing on enhancing porosity and controlling pore size distributions. These high porosity ceramic hollow fibre membranes were used as membrane reactors, catalytic reactors, solid oxide fuel cells (SOFC) and supports for the deposition of an active layer made of other materials. Apart from the high surface area to volume ratio, the channels in the finger-like region of the high porosity ceramic hollow fibre membranes also enhance heat and mass transfer and mixing of particles during reactions. Gbenedio's group made use of the high surface area to volume ratio of hollow fibre membrane and formed a Pd/alumina membrane reactor for propane dehydrogenation purpose. The alumina hollow fibre substrate used contained 80% finger-like porous structure from the cross-section, which is where catalyst was deposited. [8] Pd/alumina hollow fibre membrane with deposited catalyst was developed into different membrane reactor designs, including catalytic hollow fibre membrane micro-reactor (CHFMMR) which was found to show a performance two and a half times higher than traditional fix-bed reactors. [7] Tan and Li introduced catalytic combustion of methane in ceramic hollow fibre membrane. In their study the perovskite hollow fibre membrane produced were highly porous, with about 70% of the cross-sectional area formed by porous finger like structure. The high porosity provided high area per unit volume for the deposition of methane combustion catalyst and achieved sufficient oxygen permeation rate for the combustion to occur. [110] Garcia-Garcia et al. prepared highly porous asymmetric alumina hollow fibres for depositing 10% CuO/CeO_2 catalyst for the conversion of CO and water into CO_2 and H_2. The finger-like structure in these hollow fibre membranes act as multiple channels with lengths of 400 μm and hence provided a large surface area for catalyst deposition. The conversion of CO-water mixture to CO_2 and H_2 was 20% higher than that in a fixed-bed reactor [7]. Liu's group introduced the use of ceramic hollow fibre membrane as a micro-bioreactor. The hollow fibre membranes produced were also of a high porosity with thick finger-like fringes layer for maximizing space for microbe immobilization and growth. [10] Yin et al. has presented a highly asymmetric YSZ hollow fibre membrane to be used in micro-tubular solid oxide fuel cells (MT-SOFCs). This YSZ hollow fibre membrane had a

thin dense layer of only 3-5 μm that act as an electrolyte film while the porous layer serve as an electrode of the SOFC for catalyst deposition. [31] Kilgus and Gepert et al. produced alumina hollow fibre membranes with porosity as high as 70% for the deposition of Palladium layer for the purpose of hydrogen separation. [111] To make full use of the high porosity in alumina hollow fibre membranes, some surface modification methods have been presented. Liu and tan et al. reported a facile acid etching method that turned the inner and outer layer of asymmetric ceramic hollow fibre produced by phase-inversion and sintering method into highly porous. [112] Koonaphadeelert and Li carried out surface modification to turn the fibre surface hydrophobic through the formation of fluroalkylsilane (FAS) films, which minimize the resistance during separation processes. [113]

2.13 Strengthening of ceramic hollow fibre membranes

Hollow fibre membranes fabricated to favour porosity had poor flexural strength in general. Studies specifically focusing on improving mechanical strengths of ceramic hollow fibre membranes are limited. Most of the attempts on strengthening ceramic hollow fibre led to densification in the ceramic matrix and therefore a scarification in porosity. Liu's group tried mixing nano-sized alumina with micro-sized alumina powder in different ratios. By mixing alumina powder of 1 μm, 0.3 μm and 0.01 μm at a ratio of 46.5/46.5/7 by weight precentage came up with fibres of bending strength double of that prepared by 1 micron powder, at the same time turned the fibres nearly gas tight. [35] The same strengthening effect by mixing nanosize particles was demonstrated by the gas tight YSZ hollow fibre membranes prepared by Liu et al. [81] Kingsbury et al. prepared alumina hollow fibre of a large region of finger-like void which provided a large surface for catalyst deposition, while an increase in sintering temperature which favoured the mechanical strength of the membrane traded off its porosity. [33] Yang's group obtained Ni/YSZ hollow fibre membranes with a finger-like porous layer as well, which was suitable as anode support for solid-oxide fuel cells. Mechanical strength was again increased by raising the sintering temperature and resulted as a 27% drop in porosity. [114] The same densification effect occurred in the Ni/YSZ preparted by Meng and Yang et al. who proved the enhancement in flexural strength by increasing content of ethanol in the spinning suspension for phase-inversion hollow fibre production. A flexural strength of over 200 MPa was achieved by having 35wt% of ethanol in the spinning suspension, while the porosity of this Ni/YSZ hollow fibre membrane was reduced to below 25%. [34] Han's group included SiO_2 and kaolin in alumina hollow fibre membranes. The flexural strengths to of both SiO_2-Al_2O_3 and kaolin-Al_2O_3 hollow fibre membranes were increased but only up to

a maximum of 46.6 MPa and 36.7 MPa, with a porosity of 35.2% and 30.7% respectively. [115] Zhang et al. has prepared silicon nitride (Si_3N_4) hollow fibre membrane with a bending strength of 290 MPa and porosity remained at 50%. The high bending strength was a consequence of the three dimensional network formed by the rod-like Si_3N_4 grains after sintering at 1700 ^oC. The rod-like grains could be interpreted by anisotropic growth of the β-Si_3N_4. The lower boundary energy in length direction than width direction favoured nucleation towards a single direction. [116] In most cases, a balance has to be taken between porosity and mechanical strength, depends on the function of the ceramic hollow fibre membrane.

Some studies focused on modifying the formation of hollow fibre precursor have produced ceramic hollow fibre membranes with outstanding properties. Choi and Kim et al. included 1,4-dioxane a non-solvent additive into the spinning suspension for a closely packed sponge structure in the alumina hollow fibre precursor then use a sintering additive magnesium oxide (MgO) to lower the sintering temperature. A densely packed and strong alumina hollow fibre membrane was formed, with its porosity kept at 40% and a narrow pore size distribution. [80] YSZ hollow fibre membranes with porosity over 40% and flexural strength as high as 154.5 MPa was successfully fabricated by Zhang et al. by a modified phase-inversion method. Ethanol, which was a non-solvent of NMP was used as the external coagulant for phase inversion during fibre extrusion. This created a difference in phase exchange to the inner and outer wall direction and hence formed long finger like structure extent from the inner fibre wall. This strong and highly porous hollow fibre membrane was only applicable in microfiltration due to its relatively large pore size of 180-300 nm. [32]

Apart from reinforcement inside ceramic hollow fibre membranes, some literature reported the preparation of dual-layer hollow fibre membranes, in which different materials can be used for the selective layer and support layer. Inclusion of high strength materials in the support layer of dual-layer hollow fibre membranes is also a method for reducing brittleness of ceramic hollow fibre membranes. [117] Dual-layer hollow fibre membrane was fabricated by co-extruding two spinning suspension through a spinneret into a coagulant, followed by sintering. [118]

2.14 Formation of nickel aluminate and its applications

Nickel aluminate spinel ($NiAl_2O_4$) is a non-toxic ceramic materials with high thermal stability up to 2110 ^oC [119] and strong resistance to acids and basics. [120] It is formed by the reaction of alumina and a source of nickel ion.

The formation of $NiAl_2O_4$ via various raw materials has been reported in many literatures. De Korte's group created $NiAl_2O_4$ by the calcination of nickel and aluminium nitrate in air at 900 ^oC, where three phases $NiAl_2O_4$, nickel (II) oxide (NiO) and alumina was formed. The ratio of the three phases depends on the content of nickel. [121] Kotula's group performed a solid-state reaction between NiO film and alumina substrate and a layer of $NiAl_2O_4$ was formed in the NiO-alumina boundary after a heat treatment of 1100 ^oC. [122] Peelamedu et al. performed the same reaction using NiO-alumina powder mixture and synthesised $NiAl_2O_4$ in a short period of time in a microwave field. The shorten reaction time was a result of different microwave absorbing ability of NiO and alumina. A higher phase mobility and reaction kinetics was created by this anisothermal heating. [123] Loginova et al. introduced the formation of $NiAl_2O_4$ by oxidizing of nickel aluminide (NiAl) single crystal with (1 1 1) orientation. NiAl(1 1 1) was oxidized by exposure to oxygen in room temperature and $NiAl_2O_4$ was formed in the interface of alumina and nickel in the presence of oxygen at a temperature of 1127 ^oC. [124] Han's group compared the use of Ni_2O_3 and γ-alumina as starting materials with NiO and α-alumina for the formation of $NiAl_2O_4$ through a solid state reaction. They showed that a complete transformation to $NiAl_2O_4$ was demonstrated by the mixture of NiO and α-alumina but not that of Ni_2O_3 and γ-alumina. [125] Hasin et al. reported the formation of highly pure $NiAl_2O_4$ powder through the reaction between aluminium hydroxide, nickel nitrate and triethanolamine in ethylene glycol and calcination at 1000 ^oC. [126]

Studies on the formation of $NiAl_2O_4$ all showed $NiAl_2O_4$ obtained through solid state reaction exist in a multi-phase rather than as a single phase by itself. Some studies on the other hand focused on the phase equilibrium of $NiAl_2O_4$. Phillips et al. presented the equilibrium diagram of the NiO-Al_2O_3- $NiAl_2O_4$ system. Their results showed that NiO-alumina mixture would give a single $NiAl_2O_4$ phase if the content of NiO was between 50 – 62 mol% with a sintering temperature of 1650 ^oC. [119] Han's group prepared $NiAl_2O_4$ by solid state reaction between NiO and alumina powder and studied the effect of sintering temperature on phase changes. At a sintering temperature below 1200 ^oC, all three phases, alumina, NiO and

$NiAl_2O_4$ were shown. When sintered at a temperature 1200 ^oC or over, only NiO and $NiAl_2O_4$ were present. [127] They also found that a sufficiently long ball-milling time would create a homogeneous mixture, hence resulted in a complete transformation of alumina to $NiAl_2O_4$.

Nickel oxide, a reactant for the formation of nickel aluminate through solid state reaction with aluminium oxide, could be synthesized by multiple methods. The nickel oxide synthesized could be in the form of particle or fibre. Xiang's group prepared fine nano-sized NiO particles of 10-15 nm through the calcination of $Ni(OH)_2{\cdot}NiCO_3{\cdot}xH_2O$, a precipitation obtained from aqueous nickel (II) chloride ($NiCl_2$) and ammonium bicarbonate (NH_4HCO_3) in air. [128] Lai et al used $Ni(NO_3)_2$ solution as a source of nickel and sodium hydroxide (NaOH) solution to form nickel hydroxide ($Ni(OH)_2$) under microwave heating. The $Ni(OH)_2$ then undergo liquid oxidation with the addition of sodium hypochlorite (NaClO) solution, followed by calcination in air, forming NiO particles of 5 – 35 nm. Under the report calcination temperature of 300-700 ^oC, the lower the calcination temperature, the finer the NiO particles were. [129] Salavati-Niasari et al. synthesized NiO particles of 24 – 36 nm through heat treatment of nickel octanoate in 400 – 900 ^oC in air. They also reported heating nickel octanoate at above 400 ^oC in argon converted nickel octanoate into pure nickel [130]. Gandhi's group stated the one pot sonochemical method for the formation of NiO, which used nickel acetate monohydrate as a source of nickel and reacted with concentrated hydrochloric acid (HCl), followed by multiple ultrasonication in different temperatures. The NiO particles formed were 50 – 60 nm in size. [131] Nickel octanoate was also used by Fereshteh et al. as a starting material, which was decomposed in oleylamine ($C_{18}H_{37}N$) and triphenylphosphine ($C_{18}H_{15}P$) and formed NiO particles of 20 – 30 nm. [132]

$NiAl_2O_4$ reinforcement has been applied in strengthening dense alumina ceramic. The boundary strengthening effect in the ceramic materials was a result of the stress field created by the difference in thermal expansion between alumina and $NiAl_2O_4$. $NiAl_2O_4$ has a higher thermal expansion coefficient than alumina. During the sintering stage, both $NiAl_2O_4$ and alumina expanded and touched the adjacent particles. In the post-sintering cooling, $NiAl_2O_4$ contracted more than alumina and created a stress field and hence a closure force along the alumina grain boundary where crack growth would be deflected. Lieberthal and Kaplan compared the strengthening effect of $NiAl_2O_4$ and nickel particles in dense alumina ceramic and proved that $NiAl_2O_4$ showed an even stronger reinforcement than nickel particles. [93] In the waste treatment industry, $NiAl_2O_4$ has been formed as a by-product for the removal of

nickel. Because of the stability of $NiAl_2O_4$, the toxic metal nickel is transformed into the non-toxic $NiAl_2O_4$ by its reaction with alumina for disposal or storage. [133, 134]

2.15 Economic analysis

Apart from selectivity and productivity, total production cost is also an important factor for the selection of suitable membrane system for industrial separation processes. Total production cost is the sum of capital cost and operating cost of the membrane system. Capital cost could be minimized by choosing low cost materials for membrane production and high permeate flux which lowers the required membrane area. Mechanical integrity, durability and permeate flux through the membrane which determines the driving force required contributed to the operating cost of the membrane system. [135] The use of ceramic as a membrane material reduces operating cost because of its resistance to high temperature and aggressive feeds. Strengthening of ceramic membrane, which is the focus of this study, also contributes in lowering operating cost by extending the service life and hence reducing the replacement frequency of the membrane system.

Some economic assessments have been carried out specifically on water separation to analyse the cost-effectiveness of using membrane as an alternative to conventional water treatment methods. Owen et al. stated the most significant factors in a membrane system that affected the total cost were membrane cost, membrane replacement frequency and power consumption. Membrane cost was taken as the sum of membrane unit and non-membrane plant which is independent of membrane material. Membrane replacement frequency is dependent on its lifetime, which in general was three to five years for polymeric membranes and up to ten years for ceramic membranes. Power consumption depended on trans-membrane pressure required and the cross-flow velocity in hollow fibre or tubular membrane modules. [136] The total production cost of ceramic an inorganic membrane, in general, falls within the range of USD \$500 – 1000 / m^2. α-alumina cost around USD \$500 / m^2 which is considered as a low cost ceramic material for membrane production [135, 137]. Singh et al. has carried out an economic analysis on a ceramic microfiltration membrane system in which α-alumina tubular membrane with a nominal pore size of 200 nm was used to separate suspended solids, protein and fat impurities in corn starch hydrolysate. The α-alumina multi-channel tubular membrane was USD \$1600 / m^2. The minimum operating cost was determined by testing for the optimal trans-membrane pressure and cross-flow velocity. Taken account of all the operating cost including power consumption, membrane cleaning, maintenance and disposal

cost, in comparison with the conventional rotary vacuum precoat filter, the total production cost of using a ceramic microfiltration system was more than USD $1.3 million less per year. The ceramic membrane modules accounted for 85% of the total cost [138], which further supported the importance of membrane strengthening and extension of membrane service life in overall cost reduction.

In comparison with polymeric membrane, Guerra et al. has developed a model that took membrane material cost, lifespan and labour requirement into account to identify the competiveness of ceramic membranes for microfiltration and ultrafiltration. The model was based on the total water production cost of polymeric PES membrane and alumina ceramic membrane under the same operating condition. The material cost of alumina membrane was USD $500 / m^3 which was ten times of that of PES membrane. The long service life of alumina membrane at the same time made the annual membrane replacement cost only 39% higher than that of PES membranes. Their result showed a 12% higher full-scale implementation cost for ceramic membranes than polymeric membranes, while at more aggressive filtration conditions where ceramic membranes experience less fouling than polymeric membranes, ceramic membrane was more cost competitive. [139]

Alumina powder and nano-size nickel oxide powder were the starting materials for the ceramic materials and hollow fibre membranes covered in this thesis. The alumina powder used were commercially available at USD $235 / kg. [140] Nano-size nickel oxide powder were synthesized from nickel carbonate, basic hydrate (BNC) which was purchased at USD $111 / kg. [141]

2.16 Knowledge gap

Many studies on ceramic hollow fibre membranes focus on their microstructure and aim at high porosity to favour fluid flux, yet studies specifically on their mechanical strength is limited. Reinforcement of ceramic materials which reduces their brittleness has mostly been applied in dense ceramics rather than porous ceramics. In using ceramic materials as membrane, however, both fluid flux and mechanical strength are equally important for the efficiency of a separation process and service life of the membrane respectively.

Despite being a non-toxic ceramic with high thermal and chemical stability, $NiAl_2O_4$ has never been reported as a membrane material, neither by itself nor as a membrane component. As a reinforcement medium, $NiAl_2O_4$ has been included in dense Al_2O_3 and the dense

$NiAl_2O_4/Al_2O_3$ showed improved flexural strength. $NiAl_2O_4$ reinforcement has never been applied in porous ceramics or ceramic membranes.

The aim of this study is to fabricate ceramic membranes with enhanced flexural strength, at the same time minimizing the trade-off on the efficiency and effectiveness of the membrane separation process for the strengthening effect. $NiAl_2O_4$ is included in porous Al_2O_3 hollow fibre membrane for reinforcement purpose. The boundary strengthening effect of thermal expansion mismatch is expected to exist in porous ceramics along interfaces of $NiAl_2O_4$ and alumina, yet not as significant and in every single direction around the $NiAl_2O_4$ particle as demonstrated in dense $NiAl_2O_4$ reinforced alumina because of the presence of pores where $NiAl_2O_4$ is not in physical contact with adjacent alumina. Pure $NiAl_2O_4$ hollow fibre membrane is also fabricated and its properties and feasibility as a strong ceramic membrane material are reported. These high flexural strength ceramic hollow fibre membranes could potentially be produced in industrial scale and as membrane modules for microfiltration processes. The improved flexural strength also increases the service lives of membranes and hence reducing operating cost of separation processes in long term.

Chapter 3 Investigation of reinforcement of porous alumina by nickel aluminate spinel for its use as ceramic membrane

Overview

As a preliminary study for the strength enhancement of porous ceramic hollow fibre membranes, the reinforcement of porous ceramic materials by the inclusion of external element was investigated. This chapter reports the reinforcement of porous alumina ceramics by forming nickel aluminate spinel ($NiAl_2O_4$) phase in alumina matrix via the reaction between nickel (II) oxide (NiO) and alumina (Al_2O_3). X-ray diffraction (XRD), scanning electron microscopy (SEM), energy dispersive X-ray spectroscopy (EDS), three-point bending test, mercury porosimetry and gas permeation were used to characterize the porous ceramic samples. The highest flexural strength of 146 MPa was achieved in the porous alumina with 14.7 wt% $NiAl_2O_4$, with a porosity of 30.5%. A decrease in flexural strength and increase in porosity was observed in porous alumina with over 14.7 wt% $NiAl_2O_4$. The appreciable flexural strength and porosity made $NiAl_2O_4$ reinforcement a promising method for fabricating ceramic membranes with improved toughness in different geometries including hollow fibre membranes.

3.1 Introduction

Porous ceramic membranes are suitable to be used for separation of suspended solid particles in extreme conditions which could not be achieved by traditional polymer membranes, such as high temperature, highly acidic or basic feed. [3] The advantages of ceramic membranes include high thermal and chemical stability, insensitivity to swelling and ease of cleaning. For instance, aluminium oxide a commonly used and economical ceramic was proved to be far more stable than common stainless steel 316 in strong acid. [49]

However, brittleness is the major limitation for the large scale production application of ceramic membranes especially hollow fibre ceramic membranes, as most of the separation processes involve significant trans-membrane pressure where cracking and snapping of membrane could occur. The brittleness of ceramic membranes also leads to difficulty in assembly of membrane modules for practical applications. Studies on the improvement of the flexural strength of ceramic hollow fibre membranes have been carried out on the adjustment of raw particle size, which traded-off porosity of the membrane for its bending strength. [35] Nickel reinforcement was tried with the sample prepared in inert gas

atmosphere and proved to effectively strengthen fully dense alumina [93] while the toxicity of nickel makes this particle reinforcement method unfriendly to human and the environment. [94] The formation of eutectic mixture with gadolinium aluminium perovskite ($GdAlO_3$) in the alumina matrix changed brittle fracture of pure alumina to plastic deformation [95], while its raw material gadolinium oxide is of a very high cost. Fibre reinforcements were applied and showed the excellent strengthening effect on ceramic materials so far, which in comparison with particle reinforcement, have complicated preparation processes in general, such as difficulty of fibre dispersion and oxidation of many types of fibres when sintered in air. [92, 97]

In this chapter, the reinforcement of porous alumina by the formation of a second phase nickel aluminate ($NiAl_2O_4$) was investigated. The boundary strengthening effect in the matrix of the ceramic materials was a result of the stress field created by the difference in thermal expansion between alumina and $NiAl_2O_4$. The formation of $NiAl_2O_4$ has been used in waste treatment, where the toxic metal nickel is transformed into $NiAl_2O_4$ by its reaction with alumina. [133, 134] This stable and non-toxic aluminate showed even stronger reinforcement of dense alumina than nickel particles. [93] It is necessary to study the effectiveness of $NiAl_2O_4$ reinforcement in porous ceramics. The sample preparation process was simple in comparison with other ceramic reinforcement as nickel oxide particles could be evenly distributed in alumina precursor by thorough mixing and sintering could be carried out in air without unfavourable reactions. The relationship between bending strength and porosity of nickel aluminate reinforced porous alumina and the potential of using this porous ceramic as a membrane were investigated.

3.2 Experimental

3.2.1 Materials

Alumina powder of an average particle diameter of 1 μm (SLS Lapidary Product PP4) purchased from Shell-Lap Supplies Pty Ltd. (SA, Australia) was used as a raw material for the preparation of porous ceramics. Nickel (II) oxide powder was synthesized by the air-calcination method described by Xiang's group. [128] Nickel carbonate, basic hydrate (BNC) (99.9% trace metal basis) purchased from Sigma-Aldrich was a source of nickel. The BNC powder was placed in a crucible and heated in open air in a box furnace (1500 ^{o}C front load vertical door furnace, Tetlow Kilns & Furnaces Pty Ltd.) at 500 ^{o}C for 2 hours, followed by a natural cool down to room temperature of 20 ^{o}C in the furnace. The resulting NiO powder

was black in colour. The particle size of NiO measured under a Jeol 7001F scanning electron microscope (SEM) ranged from 0.30 to 0.45 μm.

3.2.2 Preparation of porous alumina/nickel oxide ceramics

Alumina and nickel oxide powder were weighed and mixed in the required ratios. The powder mixtures were dry ball-milled at 30 rpm for over 48 hours to achieve a homogeneous mixture. The number of milling ball used was 1 ball to 2 g of powder. All the milling balls were zirconia balls of a diameter of 3 mm. 1 g of the powder mixture was then dry-pressed in a rectangular die of dimension 50 mm × 5 mm for the shaping of a bar in a desktop powder presser (FY-24-A, MTI Coporation) as shown in Fig. 3.1. The pressure applied was 2.5 MPa and the pressurizing time was 5 seconds. The bars were heated up at a rate of 5 ^{o}C/min and sintered at 1500 ^{o}C and 1600 ^{o}C for 5 hours in air in a box furnace. The sample precursors contained 0, 2.5, 6.4, 12.7 and 19.1 wt% of NiO.

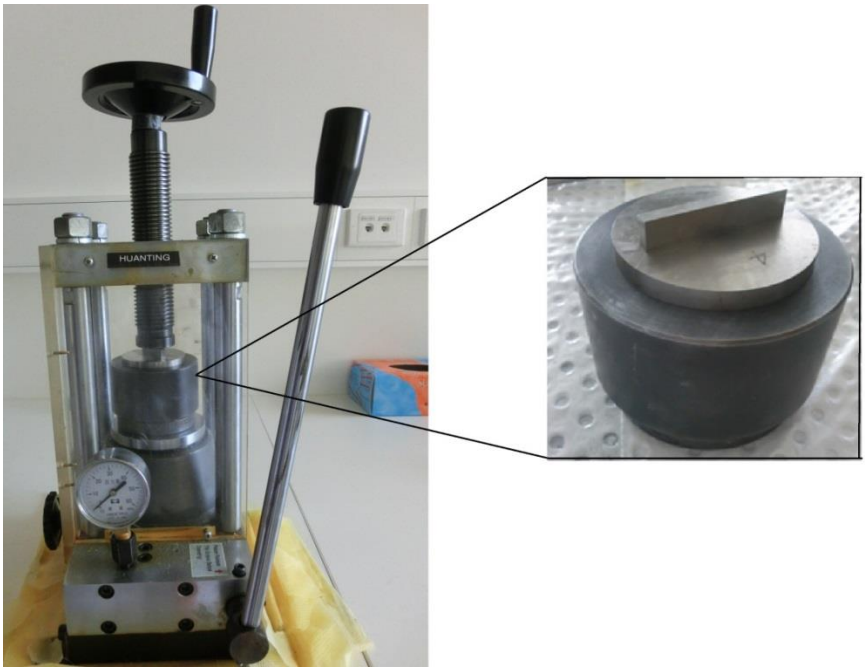

Fig. 3.1 Desktop powder presser and rectangular die for the preparation of porous ceramic.

3.2.3 Sample characterization

X-ray diffraction (XRD) was used for identifying the phases present in the samples. The ceramic bar samples were placed into a XRD sample holder without further processing. X-ray diffraction analysis was carried out in a Philips 1130 diffractomer with a scan range 10^{o}-90^{o} and a step size of 2^{o}.

Microstructures of the cross-section surface of samples were observed under a Jeol 7001F SEM at various magnifications. The cross-section cutting surfaces of the bars were obtained by manual snapping at room temperatures. All samples were coated with a platinum layer of 0.2 mm thick and SEM images were taken at 30 kV. The elemental distribution of nickel and hence $NiAl_2O_4$ in the cross section of the samples was analysed by energy-dispersive X-ray spectroscopy (EDS). EDS scans were taken at 15 kV.

The mechanical strengths of the samples were determined by the three-point bending strength. The three-point bending test was carried out with an Instron Micro Tester 5848 with a load cell of 2 kN (Instron Calibration Laboratory, U. K.). The tested sample was placed on a span of 18 mm and was extended under a crosshead speed of 0.25 mm/min until fracture occurred. The full setup of the test is shown in Fig. 3.2 Five runs for each sample were performed. The flexural strength, σ_F, of each sample was calculated from the equation [142]

$$\sigma_F = \frac{3FL}{2bt^2}$$

where F is the force measured at the fracture point of the hollow fibre. L is the span, which was kept at 18 mm. b is the width and t is the thickness of the ceramic bar. An average value of all five runs was obtained for each sample.

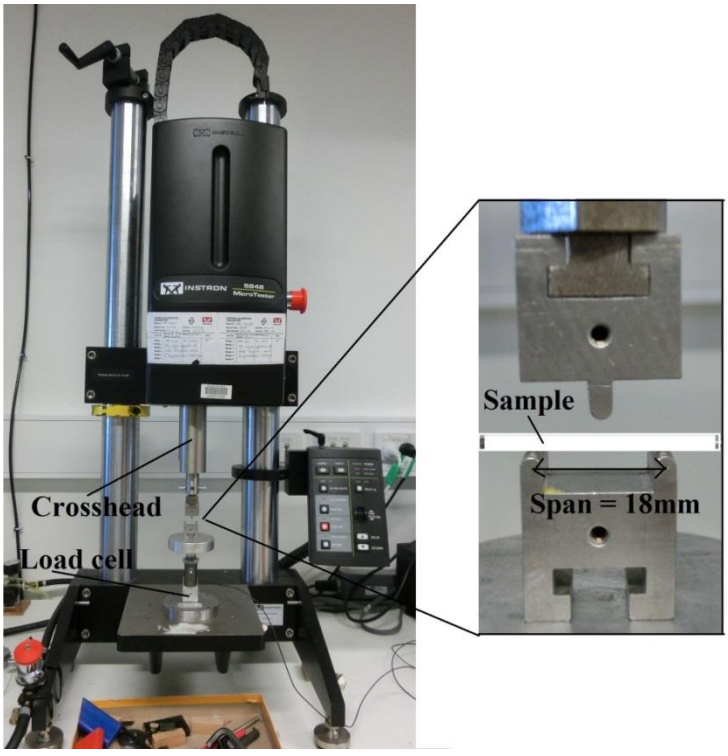

Fig. 3.2 Instron Micro Tester 5848 and three-point-bending test setup.

The porosity and pore size distribution of the samples were determined by mercury intrusion with an Auto Pore III analyser [Particle and Surface Science Pty. Ltd] The samples were first manually broken into pieces in of 5 to 10 mm, then dried and degassed to a pressure below 0.05 mbar at 350 ^{o}C in a VacPrep 061 Sample Degas System (Micromeritics) to remove all the moisture. After cooling down natural to room temperature of 20 ^{o}C, 1g of degassed samples was transferred to the chosen sample holder (07-0260 [05-11], solid 5cc, intrusion volume 0.366 cc), which was then pressurized from 38.6 mbar up to 4.2 x 10^{6} mbar for mercury intrusion. The porosity and pore size distribution were evaluated by the intrusion pressure and volume of mercury.

The gas permeance of the samples were calculated by the equation

$$Permeance = \frac{N}{\Delta PA}$$

where N is the flowrate of gas (mol/s) which is nitrogen (N_2) in this case and was measured by a MKS 628D Baratron Pressure Transducer. ΔP is the trans-membrane pressure difference (Pa) and A is the area on the sample that the gas passed through. Four trans-membrane pressures were applied on each sample. Three readings of N were taken for each ΔP applied for each sample and the average value of N was taken to calculate the gas permeance.

3.3 Results and Discussions

3.3.1 Phase identification

The X-ray diffraction patterns of samples containing different amount of NiO and sintered at different temperatures are shown in Fig. 3.3. Only peaks of alumina and $NiAl_2O_4$ were shown in the XRD patterns. The absence of NiO peaks indicated that NiO fully reacted with alumina into $NiAl_2O_4$ in all samples at both temperatures.This agreed with the NiO-Al_2O_3 binary phase equilibrium diagram presented by Phillips et al. [119], which stated at the temperatures 1500 ^{o}C and 1600 ^{o}C, when the NiO content is below 58 mol% and 57 mol% respectively, $NiAl_2O_4$ and Al_2O_4 are the only phases present at equilibrium state. The NiO content in the sample precursors ranged from 0 to 24.4 mol% fell into this two-phase range. By stoichiometry, the compositions of the final products were calculated and the results are summarized in Table 3.1.

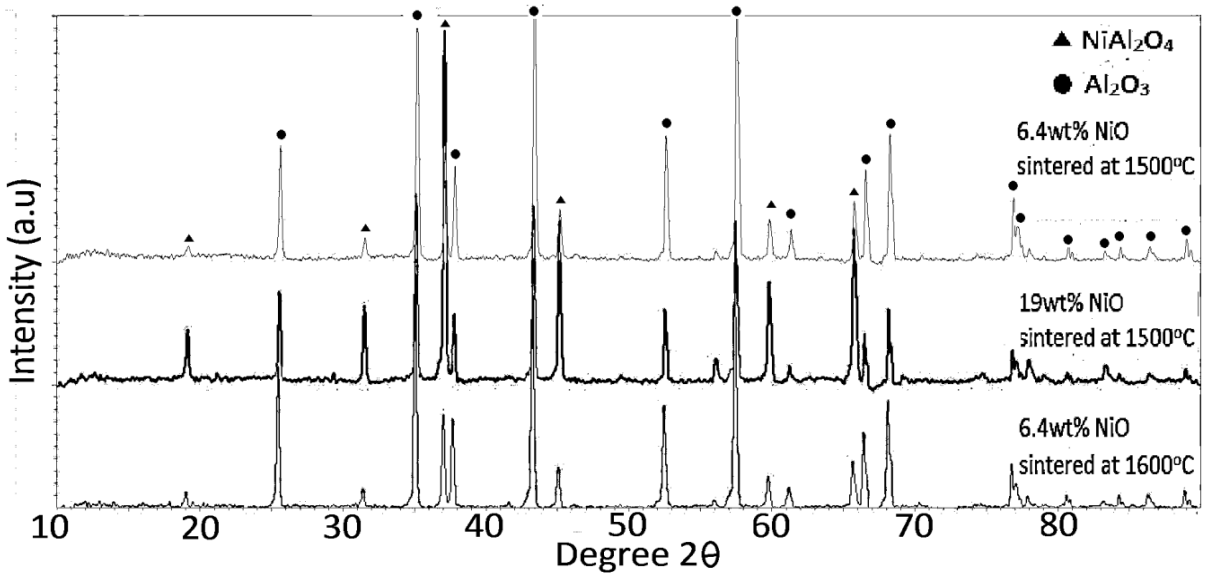

Fig. 3.3 XRD patterns of samples with 6.4 wt% NiO in precursor sintered at 1500 ^{o}C, with 19 wt% NiO in precursor sintered at 1500 ^{o}C and with 6.4 wt% NiO in precursor sintered at 1600 ^{o}C.

Table 3.1 Compositions of sintered samples by stoichiometry in weight percentage and mole percentage.

Sample	1	2	3	4	5
Al_2O_3 wt%	100	94.0	85.3	71.2	57.8
Al_2O_3 mol%	100	96.6	91.5	83.4	75.6
$NiAl_2O_4$ wt%	0	6.0	14.7	28.8	42.2
$NiAl_2O_4$ mol%	0	3.4	8.5	16.6	24.4

3.3.2 Flexural strength

Fig. 3.4 shows the flexural strength of the $NiAl_2O_4$ reinforced porous alumina sintered at different temperatures and Fig. 3.5 shows their porosities. At both sintering temperatures, the formation of $NiAl_2O_4$ increased the flexural strength of the porous alumina up to 14.7 wt%, then the flexural strength decreased with the increase in $NiAl_2O_4$ content. The change in flexural strength corresponded with that in porosity, with the porosity of 14.7 wt% $NiAl_2O_4$ reaching the minimum. There was an average of 10% drop in porosity when the sintering temperature was raised from 1500 ^{o}C to 1600 ^{o}C.

As seen in Fig. 3.5, sintering temperature is an important factor that controls the porosity of porous ceramics. Another factors that determines the porosity was particle packing which is a result of particles size [4] and pressure applied during sample preparation.

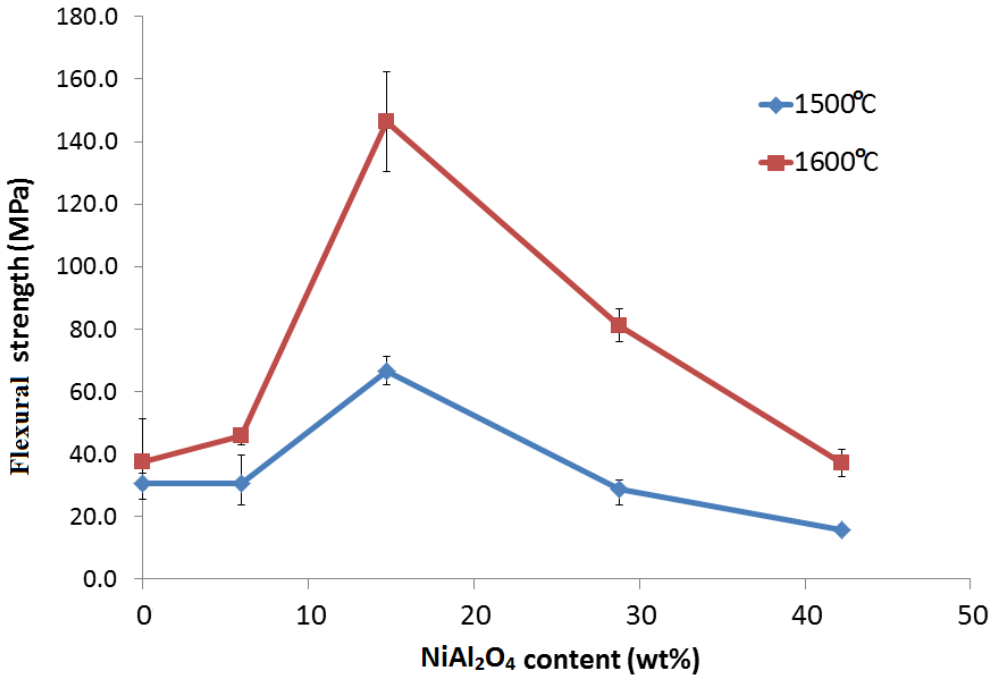

Fig. 3.4 Flexural strength of samples with various $NiAl_2O_4$ content sintered at 1500 °C and 1600 °C.

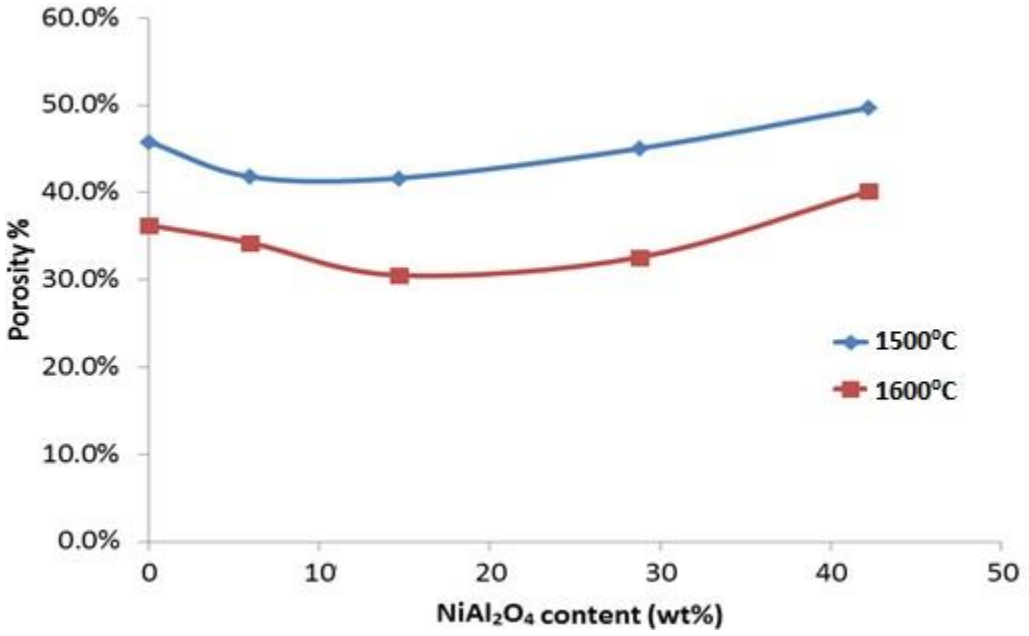

Fig. 3.5 Porosity of samples with various $NiAl_2O_4$ content sintered at 1500 °C and 1600 °C.

3.3.3 Microstructure

From the SEM images in Fig. 3.6, the change in microstructure by the addition of NiO in the precursors could be observed. With NiO in precursor and hence $NiAl_2O_4$ formation in the final product [93, 126], grains of irregular flake shapes appeared. The irregular flake shaped grains were also larger in size than grains of pure alumina. When the samples were sintered

at 1600 ^{o}C all have larger grain sizes than those sintered at 1500 ^{o}C of the sample composition, which was under expectation as a result of faster grain growth at higher temperature. Fig. 3.7 shows that $NiAl_2O_4$ was distributed evenly from a cross sectional view.

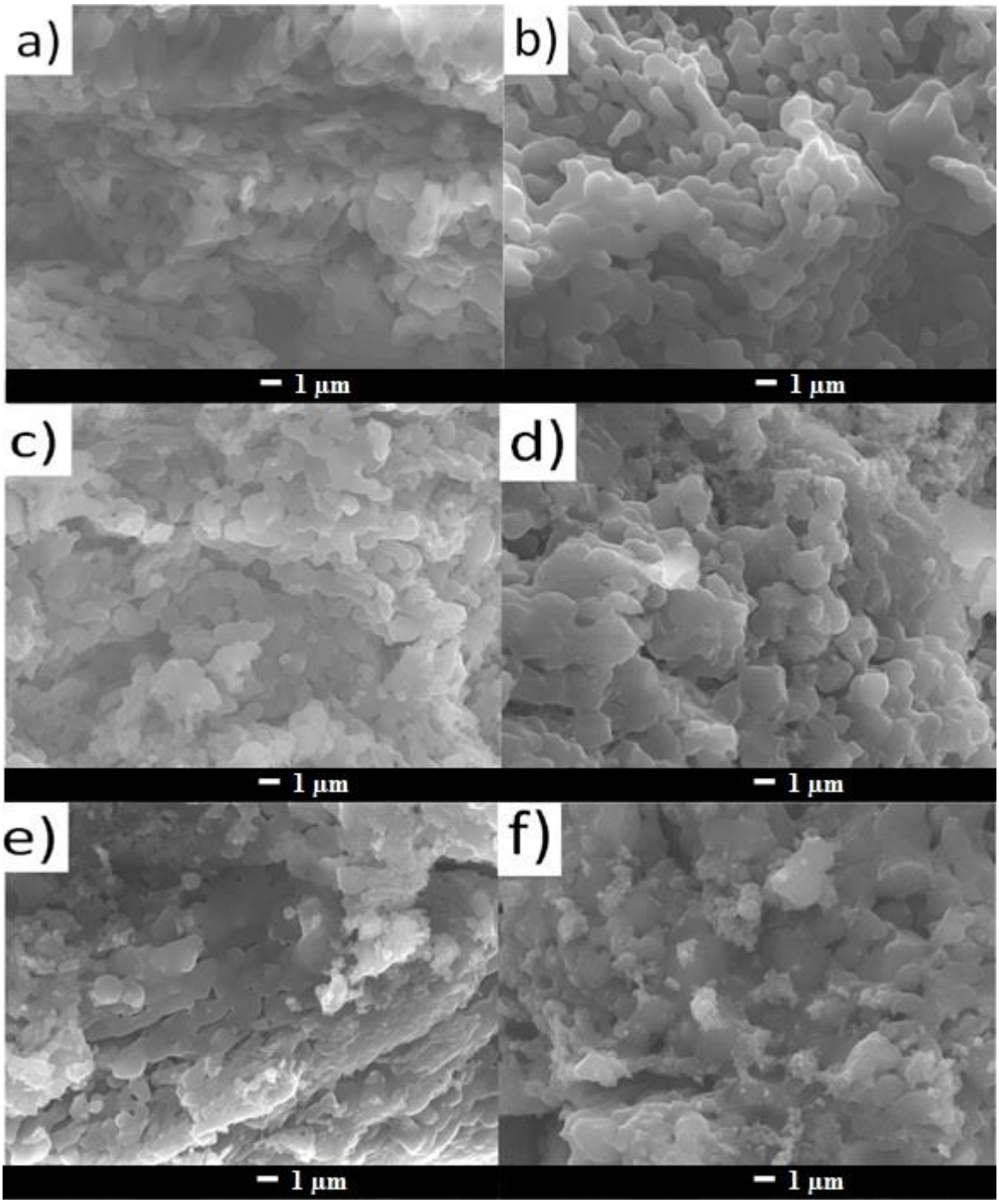

Fig. 3.6 SEM images of the cross section of samples. (a) and (b) are pure Al_2O_3 ; (c) and (d) are of 14.7 wt% $NiAl_2O_4$; (e) and (f) are 42.2 wt% $NiAl_2O_4$. (a), (c) and (e) were sintered at 1500 ^{o}C; (b), (d) and (f) were sintered at 1600 ^{o}C.

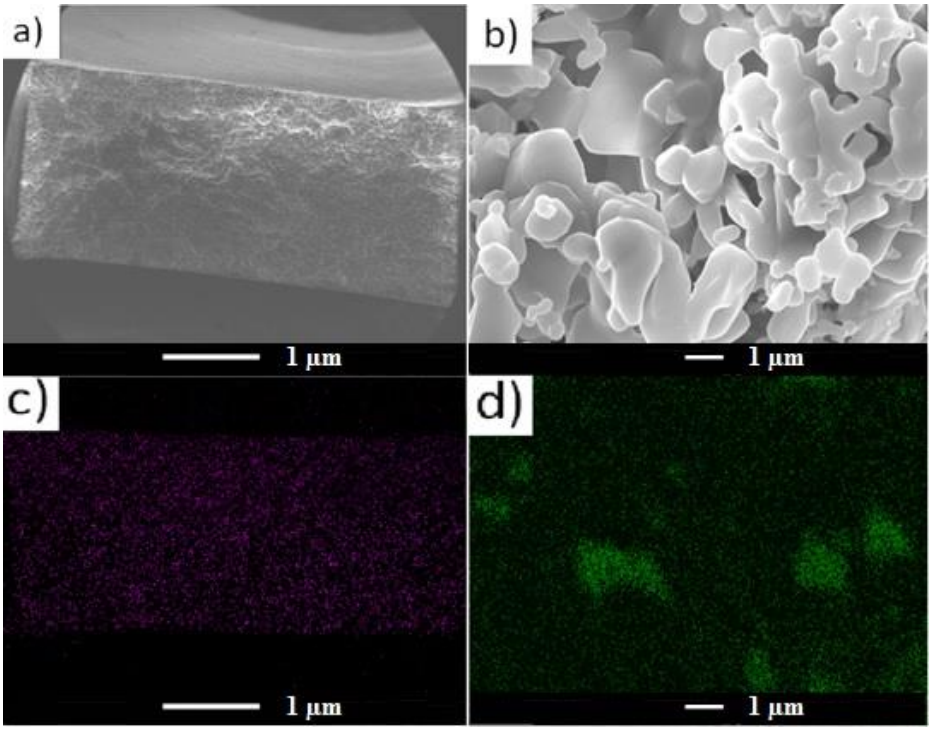

Fig. 3.7 Distribution of $NiAl_2O_4$ over the cross sectional view of sample containing 14.7 wt% $NiAl_2O_4$ sintered at 1500 ^oC ; (a) SEM image with magnification of 25X ; (b) SEM image with magnification of 10,000X ; (c) EDS mapping of Fig. 3.7a for element Ni and (d) EDS mapping of Fig. 3.7b for element Ni.

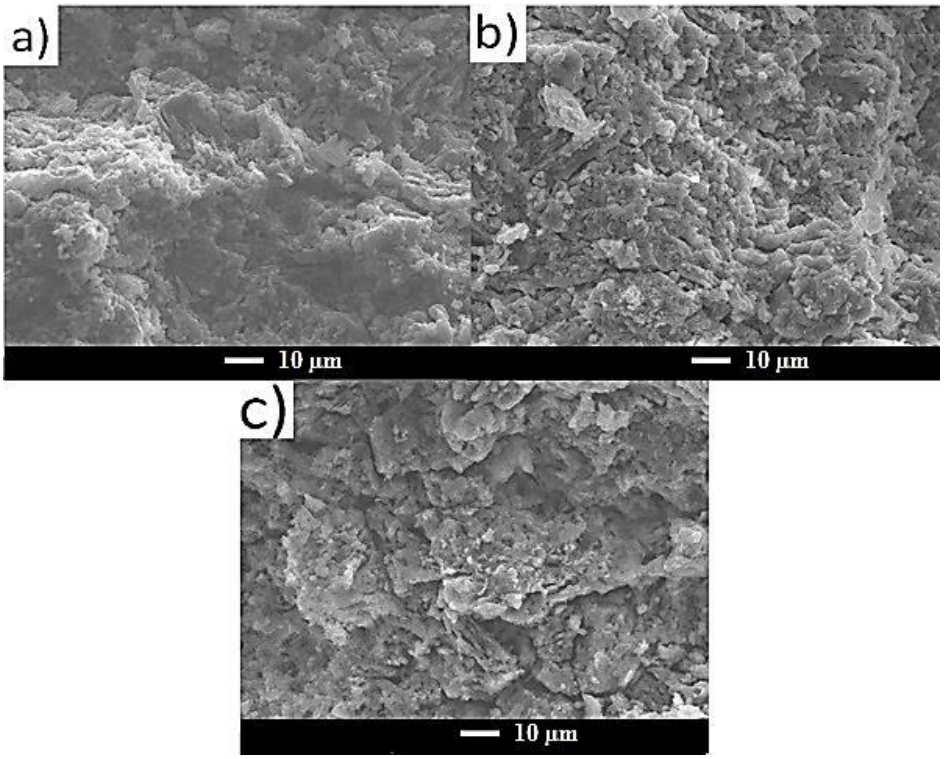

Fig. 3.8 SEM images of the cross sections of samples sintered at 1600 ^oC at low magnification showing the presence of cracks. (a) Pure Al_2O_3; (b) 14.7 wt% $NiAl_2O_4$ and (c) 42.2 wt% $NiAl_2O_4$.

When the amount of $NiAl_2O_4$ was increased over 14.7 wt%, as seen in Fig. 3.6(e) and (f), small particles and loose agglomerates appeared. These agglomerates hindered shrinkage and bonding of particles, leading to a higher porosity and lower flexural strength of the samples. Fig. 3.8(c) clearly showed the existance of pores as big as 5 μm and some slit-like cracks in the sample containing 42.2 wt% $NiAl_2O_4$. This is a result of an over-stressed ceramic matrix. As the amount of $NiAl_2O_4$ increased, tangential stress was created at various positions within the ceramic matrix. When the closure force along a grain boundary was acting in an opposite direction of that along another grain boundary, a crack would be created.

3.3.4 Pore size

The pore size distribution curves of pure alumina, 14.7 wt% $NiAl_2O_4$ which showed the highest flexural strength and 42.2 wt% $NiAl_2O_4$ which showed the lowest flexural strength as presented in Fig. 3.4 are shown in Fig. 3.9. These pore size distribution curves were obtained by mercury intrusion porosimetry. Fig. 3.9 (a) are pore size distribution curves of samples sintered at 1500 ^oC and Fig. 3.9(b) are pore size distribution curves of samples sintered at 1600 ^oC. The change in sintering temperature did not have a significant effect on the broadness of pore size distribution for samples of all three compositions. The incremental intrusion volume of mercury in samples sintered at 1600 ^oC however was obviously lower than those sintered at 1500 ^oC. This indicates that increasing the sintering temperature does not help in sharpening pore size distribution but lead to the closure of pores, which favoured flexural strength and lowered porosity as seen in Fig. 3.4 and Fig. 3.5 respectively.

At both sintering temperatures, the pore size distributions of 42.2 wt% $NiAl_2O_4$ were the broadest, with a high amount of pores in the range of 0.1 – 0.2μm which was not the case for samples of the other two compositions. The positions of major peaks and overall shape of the pore size distribution curve of 42.2 wt% $NiAl_2O_4$ also showed the least change when the sintering temperature was increased from 1500 ^oC to 1600 ^oC. These can be explained by the presence of small agglomerates when the composition of $NiAl_2O_4$ was as high as 42.2 wt%, as shown in the SEM images in Fig. 3.6(e) and (f), which hindered shrinkage and pore elimination during the sintering process. Agglomerates lead to lose packing of particles and hence reduced the effect of sintering temperature on pore size and pore size distribution.

The pore size distribution of pure alumina, on the other hand, was highly affected by the rise of sintering temperature, as observed from the shape of its pore size distribution curves. For pure alumina sintered at 1500 ^oC, major peaks of pore size distribution were at 0.3 μm and

0.9μm, while the major peaks were shifted to 0.5 μm and 1.6 μm when the sintering temperature was increased to 1600 ^{o}C. This shifting of major peaks is also shown in the pore size distribution curves of 14.7 wt% $NiAl_2O_4$, although not as significant as that in pure alumina. This indicated the addition of $NiAl_2O_4$ decreased the sensitivity of pore size to sintering temperature.

The median pore diameters are shown in Table 3.2. Median pore diameters were calculated by integrating the respective pore size distribution curve in Fig. 3.9 and determine the fifty percentile point on the x-axis. In all three compositions, the rise of sintering temperature lowered the porosity as shown in Fig. 3.5 at the same time increased the median pore diameter. Reducing of porosity during sintering process was a result of particle shrinkage, while larger pores were the consequence of grain growth. The lower porosity and larger median pore diameter shown in samples sintered at 1600 ^{o}C in comparison of those sintered at 1500 ^{o}C, regardless of composition, showed that the increase in sintering temperature enhanced both particle shrinkage and grain growth during the sintering process. The median pore diameter of pure alumina was increased by 31% when the sintering temperature was rise from 1500 ^{o}C to 1600 ^{o}C, while that of 42.2 wt% $NiAl_2O_4$ was only increased by 12%.

Table 3.2 Median pore diameter of samples with various $NiAl_2O_4$ content sintered at 1500 ^{o}C and 1600 ^{o}C.

$NiAl_2O_4$ wt%	**Median pore diameter sintered at 1500 ^{o}C (μm)**	**Median pore diameter sintered at 1600 ^{o}C (μm)**
0	0.5489	0.7213
14.7	0.4776	0.5509
42.2	0.4430	0.4981

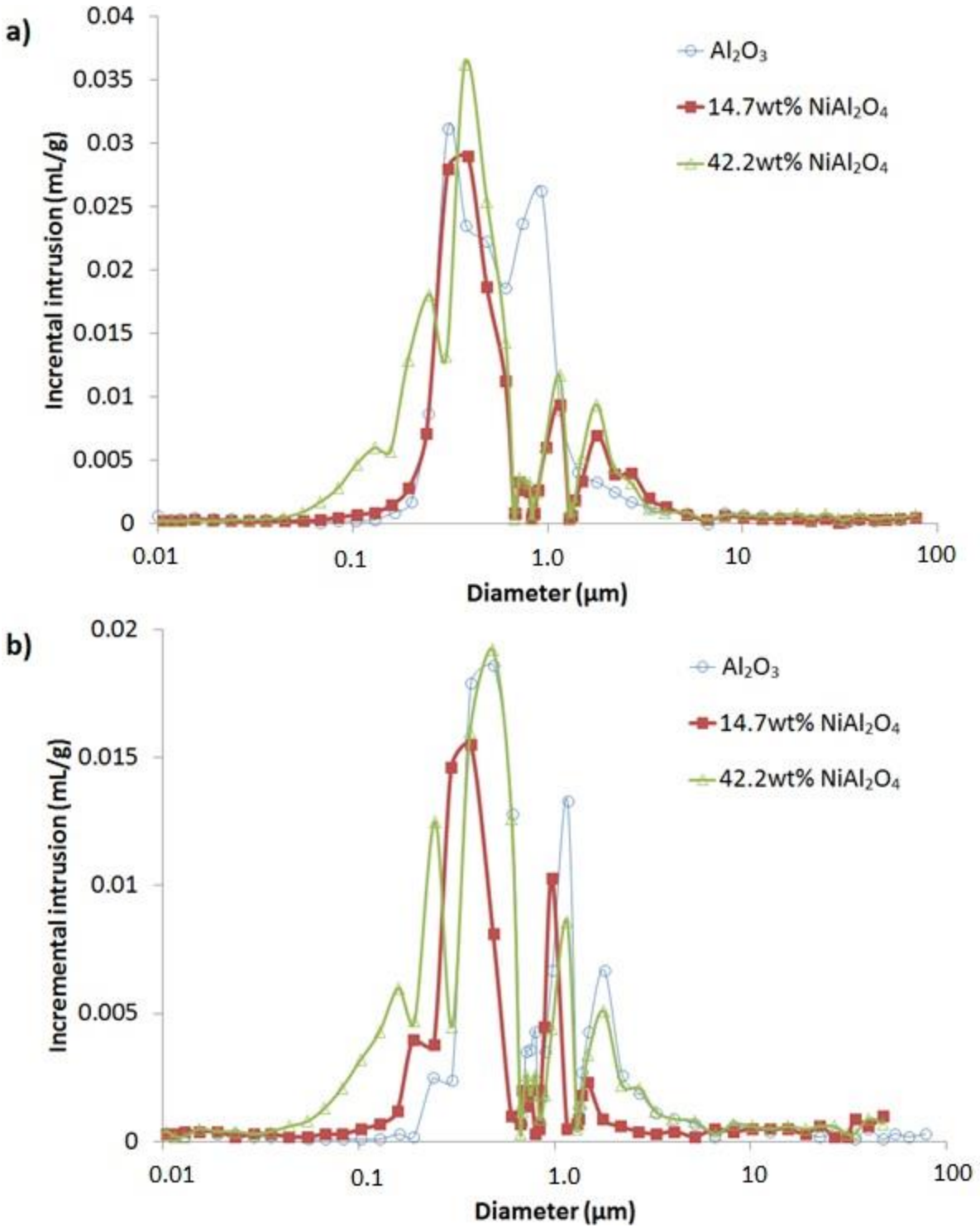

Fig. 3.9 Pore size distributions obtained by mercury intrusion a) samples sintered at 1500 ^{o}C and b) samples sintered at 1600 ^{o}C.

3.3.5 Gas Permeance

To determine the feasibility of using the $NiAl_2O_4$ reinforced porous ceramic as membranes, a nitrogen gas permeation test was carried out. The nitrogen permeance of pure Al_2O_3, 14.7 wt% $NiAl_2O_4$ and 28.8 wt% $NiAl_2O_4$ sintered at 1600 ^oC is shown in Fig. 3.10. The gas flow area, A, of the pure Al_2O_3, 14.7 wt% $NiAl_2O_4$ and 28.8 wt% $NiAl_2O_4$ sample was 23.7 mm^2, 31.5 mm^2 and 24.0 mm^2 respectively.

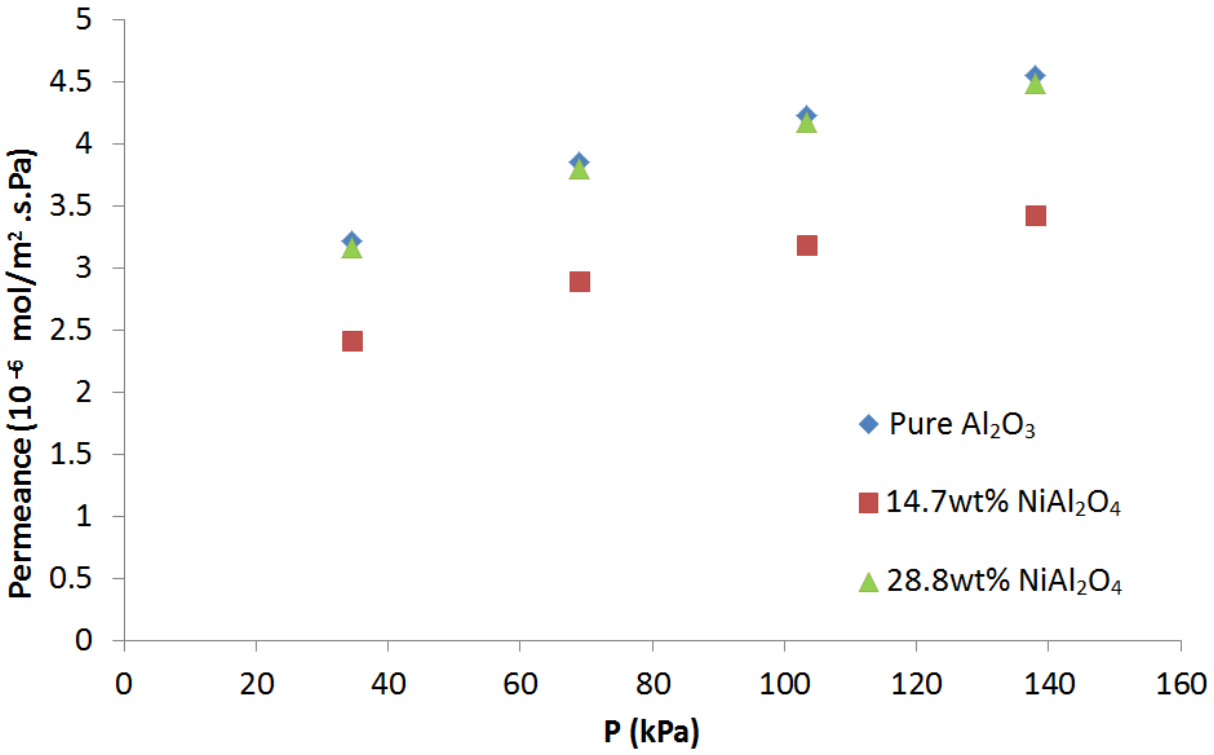

Fig. 3.10 Nitrogen permeance of Al_2O_3 and $NiAl_2O_4$ / Al_2O_3 samples sintered at 1600 ^oC.

The nitrogen permeance of the samples agreed with the porosity shown in Fig. 3.5, which the sample with 14.7 wt% $NiAl_2O_4$ had the lowest porosity and nitrogen permeance. The gas permeation of all three samples was proportional to feed pressure indicating the viscous flow of gas through the samples and hence the presence of pores larger than nano size. This shows that $NiAl_2O_4$ reinforced porous ceramics prepared was more suitable to be used as liquid separation membranes than a gas separation membranes.

3.3.6 $NiAl_2O_4$ reinforcement mechanism on porous alumina

As stated by Lieberthal and Kaplan, the formation of $NiAl_2O_4$ increased the flexural strength of dense alumina by creating a stress field in the matrix, which was a result of different thermal expansion and hence different shirinking rate between alumina and the $NiAl_2O_4$ phase in the post-sintering cool down stage. This stress field was also built up in the porous

alumina samples. $NiAl_2O_4$ contracted more than alumina when cooling down and formed a compressive tangential stress and hence a closure force along grain boundaries. This closure force slowed down the crack growth as shown in Fig. 3.11.

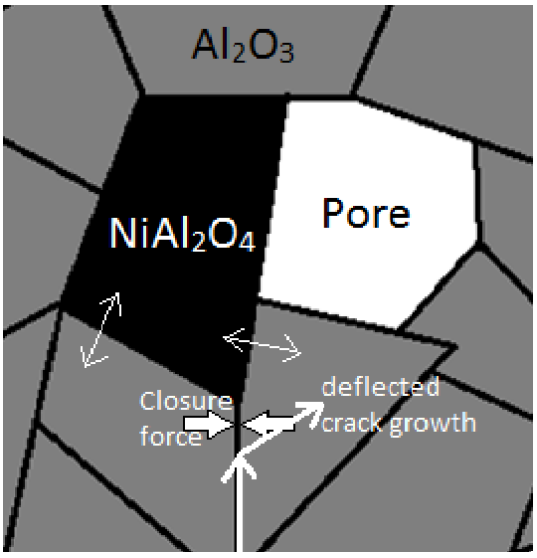

Fig. 3.11 Schematic diagram of stress field and grain boundary closure force formed by the presence of $NiAl_2O_4$

The stress field, which is created by thermal stress, is a consequence of Young's modulus, thermal expansion coefficient and temperature delta. Stress is defined as force per unit area (F/A). The closure force is a delta of force created by thermal stress mismatch in $NiAl_2O_4$ and in Al_2O_3. If grain sizes are reduced down to nanocrystal scale, the magnitude of stress mismatch would be affected by grain size because of the difference between the thermal expansion coefficients of the crystals and that of grain boundaries. The relationship between the thermal expansion coefficient of nanocrystalline material and its coarse-grain materials is defined by $\alpha_{nc}=F_{gb}\ \alpha_{gb} + (1-F_{gb})\alpha_c$ [143], where α_{nc} is the thermal coefficient expansion of nanocrystalline material, α_c is the thermal coefficient expansion of coarse-grain material, α_{gb} is the thermal coefficient expansion of grain boundary and F_{gb} is the volume faction of grain boundary. α_c is independent of grain size and is $8\times10^{-6}\ K^{-1}$ and $8.41\times10^{-6}\ K^{-1}$ for alumina and $NiAl_2O_4$ respectively. [93] With $F_{gb}=3\delta/D$, where δ is a constant relative to grain boundary thickness and D is the grain size, the relationship between the thermal expansion coefficient of nanocrystalline material and grain size becomes

$$\alpha_{nc} = \alpha_c + \frac{3\delta}{D}(\alpha_{gb} - \alpha_c)$$

This shows that at a nanocrystalline scale, a decrease in grain size of alumina and $NiAl_2O_4$ can increase their thermal expansion coefficients and hence their thermal stresses in the cooling stage after sintering. Material strengthening can be improved by increasing the difference in grain size between alumina and $NiAl_2O_4$, which leads to a more significant thermal stress mismatch between the two phases and creates a stronger boundary closure force.

Grain packing determined the contact between the $NiAl_2O_4$ grains and Al_2O_3 grains. The area of contact between $NiAl_2O_4$ grains and Al_2O_3 grains is where the stress field created by difference in thermal expansions covered. Therefore, grain packing has a significant effect on the magnitude of this crack closure force. In dense ceramics, the surface of the secondary phase is in nearly full contact with the ceramic matrix. This gives a large contact area between grains of the two phases and hence created a strong crack closure force. In porous ceramics where pores are formed by lose packing of grains, grains of the two phases are generally in less contact and the resultant crack closure force is weaker. The crack closure force still has an effect in porous ceramic reinforcement as it strengthens the obstacle for crack growth. The magnitude of closure force in relationship with porosity is demonstrated in Fig. 3.12. Both formation of $NiAl_2O_3$ and an increase in sintering temperature achieve strengthening effect on alumina. However, taking porosity which is also a key factor for membrane performance, there was a lower sacrification in porosity by $NiAl_2O_3$ reinforment in comparison. By $NiAl_2O_4$ reinforcement, there was only a 4-6% decrease in porosity when the flexural strength of alumina was doubled, while a higher sintering temperature resulted in a loss of about 10% in porosity for the same percentage increase in flexural strength.

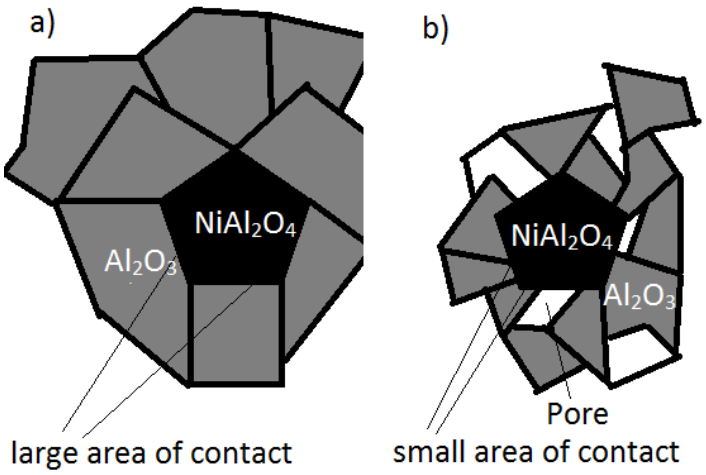

Fig. 3.12 Schematic diagram showing the contact between $NiAl_2O_4$ and alumina in (a) dense ceramic and (b) porous ceramic

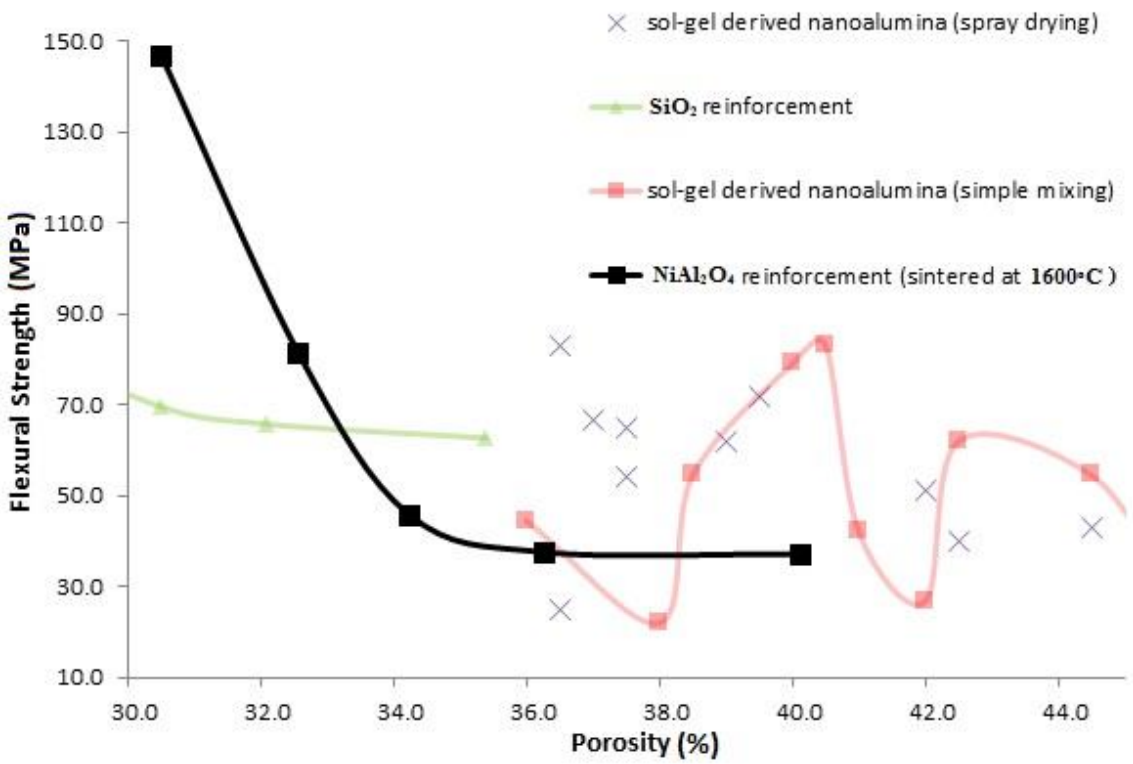

Fig. 3.13 Comparison of flexural strengths of alumina with 30% to 45% porosity reinforced by $NiAl_2O_4$, SiO_2 and sol-gel derived nanoalumina by simple mixing and spray drying.

Fig. 3.13 shows a comparison between flexural strengths of the $NiAl_2O_4$ reinforced alumina and alumina of similar porosity strengthened by sol-gel derived nanoalumina [105] and SiO_2 reinforcement. [102] In the porosity range of 30% to 45% which is appreciably high for ceramic membrane, the maximum flexural strength 146 MPa was demonstrated by $NiAl_2O_4$ reinforcement. $NiAl_2O_4$ reinforced alumina exhibited significantly higher flexural strength than alumina of the same porosity strengthened by SiO_2 reinforcement, up to a porosity of about 33%. For porosity above 33%, $NiAl_2O_4$ reinforced alumina showed lower flexural strengths than the other two reinforcement methods.

It is noted that by optimization of the preparation process, the appreciable flexural strength and porosity can be achieved by the $NiAl_2O_4$ reinforcement. This reinforcement method is promising for fabricating ceramic membranes with improved toughness in all geometries. In particular, ceramic hollow fibre membranes have attracted increasing interest for their effectiveness and efficiency in separation processes in comparison with the disc and tubular geometries because of their highest surface area to volume ratio. [4] Due to the small size and thin walls of hollow fibre membranes, reinforcement of ceramic hollow fibre membranes is a key step to extend their applications in industrial processes.

3.4 Conclusions

The formation of nickel aluminate as a second phase in aluminium oxide matrix by the reaction between nickel (II) oxide and aluminium oxide enhanced the flexural strength of porous aluminium oxide with a trade-off in porosity as low as 6%. The highest flexural strength of 146 MPa was achieved by an addition of 6.4 wt% of NiO in the precursor, after being sintered at 1600 ^{o}C in air and formed 14.7 wt% of $NiAl_2O_4$ in the alumina matrix. Porosities of all the $NiAl_2O_4$ reinforced ceramic were kept above 30%. An increase in sintering temperature from 1500 ^{o}C to 1600 ^{o}C led to a decrease of an average of 10% in porosity. The effect of sintering temperature on pore size distribution decreased with increased amount of $NiAl_2O_4$. The dependence of gas permeance on feed pressure indicated the presence of pores larger than nano size and hence made this porous ceramic suitable for separation of solid suspended particles and liquid. The appreciable flexural strength and porosity of porous $NiAl_2O_4/Al_2O_3$ showed that the boundary strengthening effect created by the difference in thermal expansion coefficient between two phases is also applicable in strengthening porous ceramics. $NiAl_2O_4$ reinforcement is therefore a potential method to improve the toughness of ceramic membranes in different geometries including hollow fibre membranes.

Chapter 4 Nickel aluminate spinel reinforced ceramic hollow fibre membrane

Overview

Ceramic hollow fibre membranes are suitable for application in many industrial processes that involve harsh conditions because of their high thermal, chemical stability and high surface area to volume ratio. The major limitation of ceramic hollow fibre membrane is the brittle nature of ceramic materials, which leads to difficulty in large scale production and failure in pressurized processes. This chapter presents the reinforcement of alumina (Al_2O_3) hollow fibre membrane by nickel aluminate spinel ($NiAl_2O_4$). The ceramic hollow fibre membrane was fabricated by the widely used phase inversion and sintering method. The $NiAl_2O_4$ phase was formed by the reaction of nickel (II) oxide (NiO) with Al_2O_3 during sintering. A maximum flexural strength of 156 MPa was achieved by the $NiAl_2O_4/Al_2O_3$ hollow fibre membrane containing 16.4 wt% of $NiAl_2O_4$, which was 2.3 times of that of the pure alumina sample. Further increasing the loading of $NiAl_2O_4$ decreased flexural strength due to uneven grain growth and neck growth in random directions and loose agglomerates that hindered shrinkage during the sintering process. The 16.4 wt% $NiAl_2O_4/Al_2O_3$ hollow fibre membrane had a porosity of 46.8% which could provide sufficiently low fluid resistance. It showed a pure water flux of 597 L/m^2.h.bar at a feed pressure 2 bar. The mean pore size of its active layer obtained by gas bubble pressure method was 330 nm which fell into the microfiltration range. $NiAl_2O_4/Al_2O_3$ hollow fibre membrane could achieve a comparable flexural strength as YSZ a stronger and higher cost ceramic and as other ceramic reinforcement methods within the porosity range of 47-55%.

4.1 Introduction

Traditional polymeric membranes are of low cost, yet they are unstable and fail under extreme conditions including temperature of over 200^oC, highly acidic or basic. [3] Ceramic membranes were therefore introduced for processes under these harsh conditions because of their high thermal and chemical stability, insensitivity to swelling and ease of cleaning. In comparison with flat sheet, capsule and tubular membranes, the hollow fibre geometry has the highest surface area to volume ratio and compactness. [4, 5]

The brittle nature of ceramic is a significant problem for industrial application of hollow fibre geometry because of their small diameters and thin membrane walls. Apart from cracking

under high operation pressure, brittleness of the hollow fibre membranes also leads to difficulty in sealing of membranes into equipment and as well-configured and orientated modules to achieve the best performance. [14] Currently a lot of studies have reported the fabrication of high porosity ceramic hollow fibre membranes, which favour high molecular transportation rate and are suitable to be used as membrane reactor and for catalyst deposition. [7, 8, 32] Study specifically on the strengthening of porous ceramic hollow fibre membranes is very limited. Addition of nano particles in micro-size powder in preparation of ceramic hollow fibre membrane favoured mechanical strength, at the same time turned the ceramic hollow fibre membrane dense and gas tight. [35, 81] The same densification effect was observed in the attempt of high temperature sintering of ceramic hollow fibre membrane. [33] Some studies focused on modifying the formation of hollow fibre precursors by the phase inversion method have produced ceramic hollow fibre membranes with outstanding properties. These included the use of sintering additive [80] and addition of non-solvent in extrusion mixture. [32] To our knowledge, nickel aluminate spinel ($NiAl_2O_4$) reinforcement, which has been applied in dense ceramic [93], has not been reported in porous ceramic membrane. The boundary strengthening effect in the matrix of alumina was a result of the stress field created by the difference in thermal expansion coefficient between alumina and $NiAl_2O_4$.

The previous chapter showed improved flexural strength of porous alumina with the inclusion of $NiAl_2O_4$ [144], which proved the feasibility of the corresponding strengthening mechanism in porous ceramic hollow fibre membranes. As a follow up, $NiAl_2O_4$/ Al_2O_3 hollow fibre membranes were prepared and investigated in this chapter. $NiAl_2O_4$ was formed by the solid state reaction between nickel oxide (NiO) and alumina. [119, 127] This reaction has been widely used in waste treatment, where the toxic metal nickel is oxidized into NiO then transformed into $NiAl_2O_4$. [133, 134] The resulting aluminate is stable, non-toxic and has a density of 4 g/cm^3 [123] which is close to that of alumina (3.983 g/cm^3). The ceramic hollow fibre membranes prepared were porous and had asymmetric structure like most of the ceramic membranes. They can be used in microfiltration of liquid, particularly in waste treatment plants where suspended large solid particles could be removed, under harsh conditions such at high temperatures and in processes that involves organic solvents where polymeric membranes are inapplicable. The enhanced flexural strength of the $NiAl_2O_4/Al_2O_3$ hollow fibre membranes can also tolerate a higher applied pressure for a more efficient separation in pressure driven separation processes.

4.2 Experimental

4.2.1 Materials

Alumina powder of a particle diameter <1 μm (alpha phase, 99.98% metals basis, APS powder, surface area 10 m^2/g) purchased from Alfa Aesar, A Johnson Matthey Company was used as a raw material for the preparation of ceramic hollow fibre membrane. Polyethylsulfone (PESf) [BASF, E6020P] was used as a binder in hollow fibre extrusion. 1-methyl-2-pyrrolidone (NMP) purchased from Sigma-Aldrich was used as a solvent of the powder, polymer and additive. Nickel (II) oxide powder was synthesized by the air-calcination method described by Xiang's group. [128] Nickel carbonate, basic hydrate (BNC) (99.9% trace metal basis) purchased from Sigma-Aldrich was a source of nickel. The BNC powder was placed in a crucible and heated in open air at 500 ^oC for 2 hours. The resulting NiO powder was black in colour, with particle size of 0.30 - 0.45 μm as observed under a JEOL 7001F scanning electron microscope (SEM).

4.2.2 Preparation of ceramic hollow fibre membranes

The well-known phase inversion and sintering method was used to prepare ceramic hollow fibre membranes. [35] The suspension mixture basis contained 15 g of alumina powder, 1.8 g of PESf and 13.2 g of NMP. Different NiO loadings were added into the alumina suspension basis for different samples. The addition of NiO powder gave a slight variation of total powder loading in the slurries, which ranged from 50.0 wt% to 51.8 wt%. The ratios of Al_2O_3 : NiO were 1:0, 1:0.0086, 1:0.022, 1:0.047, 1:0.067, 1:0.072, 1:0.075 and 1:0.106 by mass. These ratios were calculated by stoichiometry based on a 100% reaction of NiO with Al_2O_3 to form $NiAl_2O_4$, aiming at achieving final products that contained 0, 2.02 5.15, 10.62, 14.78, 15.83, 16.42 and 22.62 wt% of $NiAl_2O_4$, respectively.

The slurry was ball-milled at 30 rpm for over 48 hours on a roller miller to achieve a homogeneous mixture. The number of milling ball used was 1 ball to 2 g of slurry. The milling balls were zirconia balls of a diameter of 3 mm. The suspension was degased in room temperature for 1 hour and then was transferred to a homemade stainless steel tube-in-orifice spinneret where it was extruded into hollow fibre precursors. A schematic diagram of the extrusion process and a full setup of the fibre extrusion system are shown in Fig. 4.1 and Fig. 4.2 respectively. Nitrogen gas was used to pressurize the spinneret for the extrusion process. The outer and inner diameter of the orifice was 2.8 mm and 1.4 mm respectively. Tap water, which is a solvent of NMP, of room temperature 20 ^oC was used as both internal and external

coagulant. The internal and external coagulants were the medium for phase exchange, where NMP the solvent of the slurry was dissolved into the water. With NMP being removed, the slurry was solidified and formed the hollow fibre precursor. The same coagulants were used internally and externally to minimize the difference of phase inversion rate towards the inner and outer wall of the hollow fibre membrane, in order to avoid long finger-like pores penetrating through either side of the hollow fibre. [32] Long finger-like pores in hollow fibre membranes does not favour flexural strength. The internal coagulant flow rate was kept at 3mL/min. The air gap was kept as 1.3 cm through the extrusion process. The hollow fibre precursors were left in tab water of 20 ^{o}C for 24 hours for complete phase exchange and solidification. A detail study on the effect of extrusion process on the morphology of ceramic hollow fibre membranes was presented by Kingsbury et al. [33]

The hollow fibre precursor was heated to 580 ^{o}C in air with a heating rate of 3 ^{o}C/min and was held for 3 hours to remove the polymer binder. A low heating rate of 3 ^{o}C/min was chosen to avoid sample cracking due to a significant temperature difference between the internal and external of the samples. The samples were then sintered at 1500 ^{o}C in air for 5 hours for the purpose of grain growth and bonding. The samples were left in the furnace to be cooled down naturally to room temperature of 20 ^{o}C to prevent cracking due to a sudden temperature change.

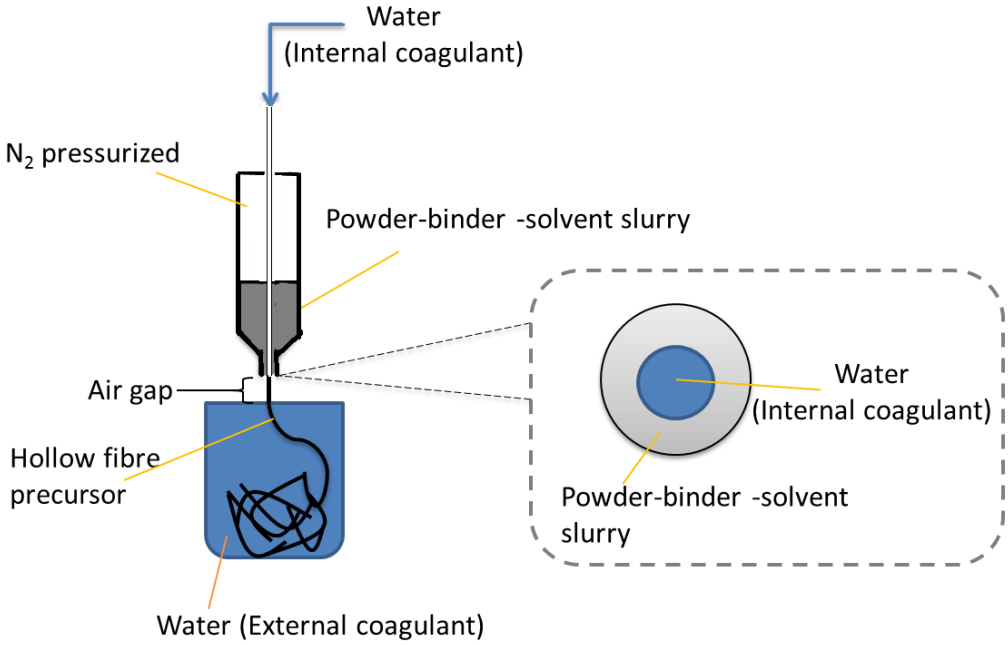

Fig. 4.1 Schematic diagram for hollow fibre precursor extrusion by phase-inversion method.

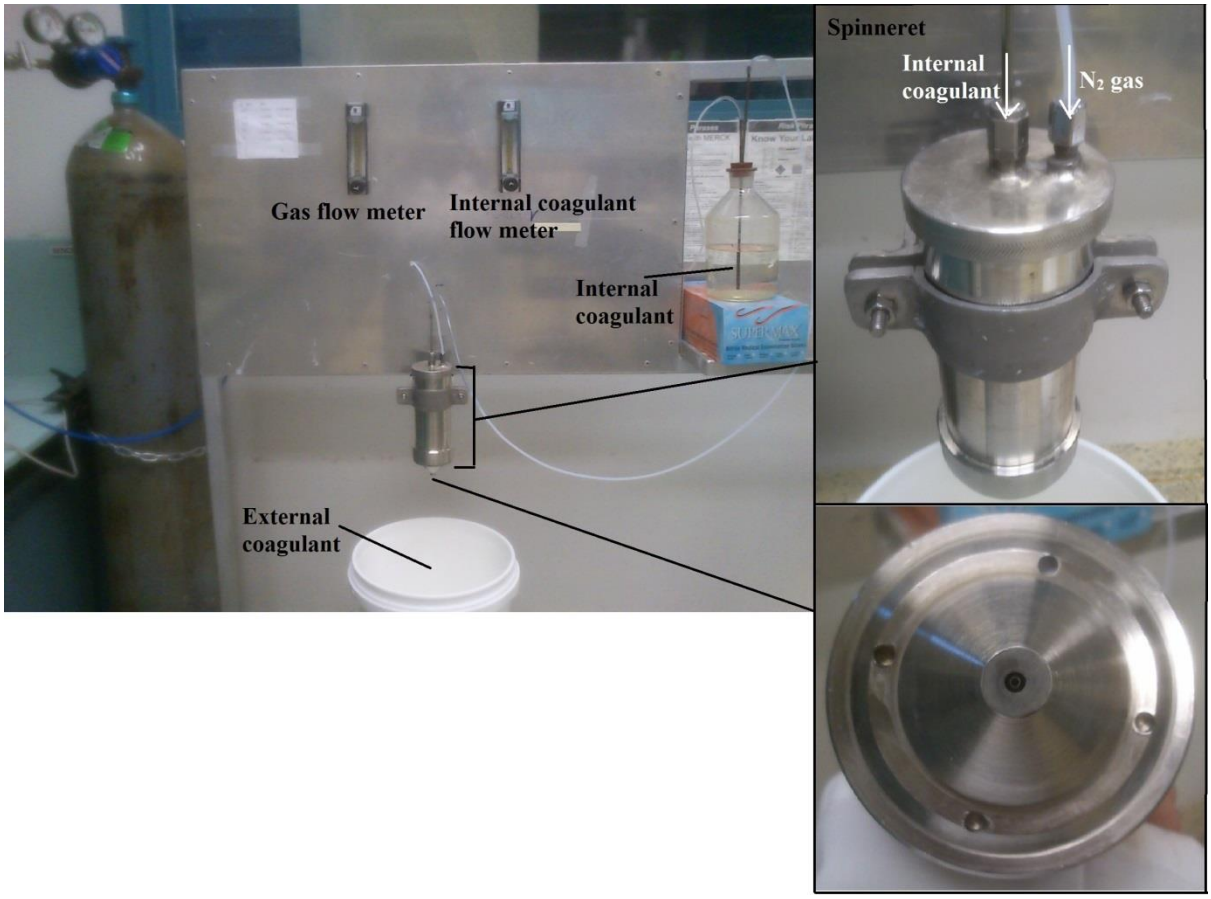

Fig. 4.2 Full setup for hollow fibre membrane precursor extrusion by phase inversion method.

4.2.3 Membrane characterizations

X-ray diffraction (XRD) was used for identifying the phase present in the samples. The XRD analysis was carried out in a Rigaku MiniFlex 600 with a scan range 10^{o}-90^{o} and a step size of 2^{o}. The samples were grinded manually for 30 minutes into powder for the XRD analysis to increase the accuracy of the result.

Structures of the cross-sectional surface and outer surface of the hollow fibre membranes were observed under a JEOL 7001F scanning electron microscope (SEM) at various magnifications. The cross-section cutting surfaces of the hollow fibres were obtained by manual snapping at room temperatures. All samples were sputter-coated with a 0.5 nm platinum layer. The SEM images were taken at 30 kV.

The flexural strengths of the samples were determined by the three-point bending test. The three-point bending test was carried out with an Instron Micro Tester 5848 with a load cell of 2 kN (Instron Calibration Laboratory, United Kingdom). The tested sample was placed on a span of 18 mm and was extended under a crosshead speed of 0.25 mm/min until fracture

occurred. The full setup of the three-point bending test was shown in Fig. 3.2 in Chapter 3. Five runs for each sample were performed. The flexural strength, σ_F, of each single hollow fibre was calculated from the equation [35]

$$\sigma_F = \frac{8FLD}{\pi(D^4 - d^4)}$$

F is the force measured at the fracture point of the hollow fibre membrane. L is the span, which was kept at 18 mm through the test. D and d is the outer and inner diameter of the hollow fibre respectively. An average value of all five runs was obtained for each sample.

The porosity and pore size distribution of the samples were determined by mercury intrusion with an Auto Pore III analyser (Micromeritics, USA). The samples were first manually broken into pieces of 5 – 10 mm and dried and degassed to a pressure below 0.05 mbar at 350 ^{o}C to ensure complete dryness. The degassed samples were naturally cooled to room temperature then transferred to the chosen sample holder (07-0260 [05-11], solid 5cc, intrusion volume 0.366 cc). The mercury intrusion was carried out from 38.6 mbar up to 4.2 x 10^6 mbar. The porosity and overall pore size distribution of the samples were obtained based on the mercury intrusion pressure and volume.

The pure water flux test was carried out in a Sterlitech HP4750 Stirred Cell (Sterlitech Corporation, USA) without a stir bar. The cell was filled up with deionized water up to three quarter full at the beginning of each run. Nitrogen gas was used as a source of pressure. The membrane supporting disc was non-porous and made of stainless steel. The disc had a diameter of 50 mm, a thickness of 2 mm and a circular hole with a diameter of 2 mm in its centre. The hollow fibre membrane was placed perpendicularly to the supporting disc in the hole. Epoxy was used to seal the top end of the membrane and the space between the membrane and the supporting disc to ensure no water leakage during the test. The setup and schematic diagram are shown in Fig. 4.3.

The gas bubble pressure (GBP) method was used to measure the mean pore size of the active layer of the hollow fibre membranes. The measurement was performed following the American Society for Testing and Materials (ASTM) Publication (F316-80). All the samples were immersed in deionized water for 2 hours under vacuum. The flow rate and trans-membrane pressure of nitrogen across the hollow fibre membranes were measured and calculated according to the standard during the measurement.

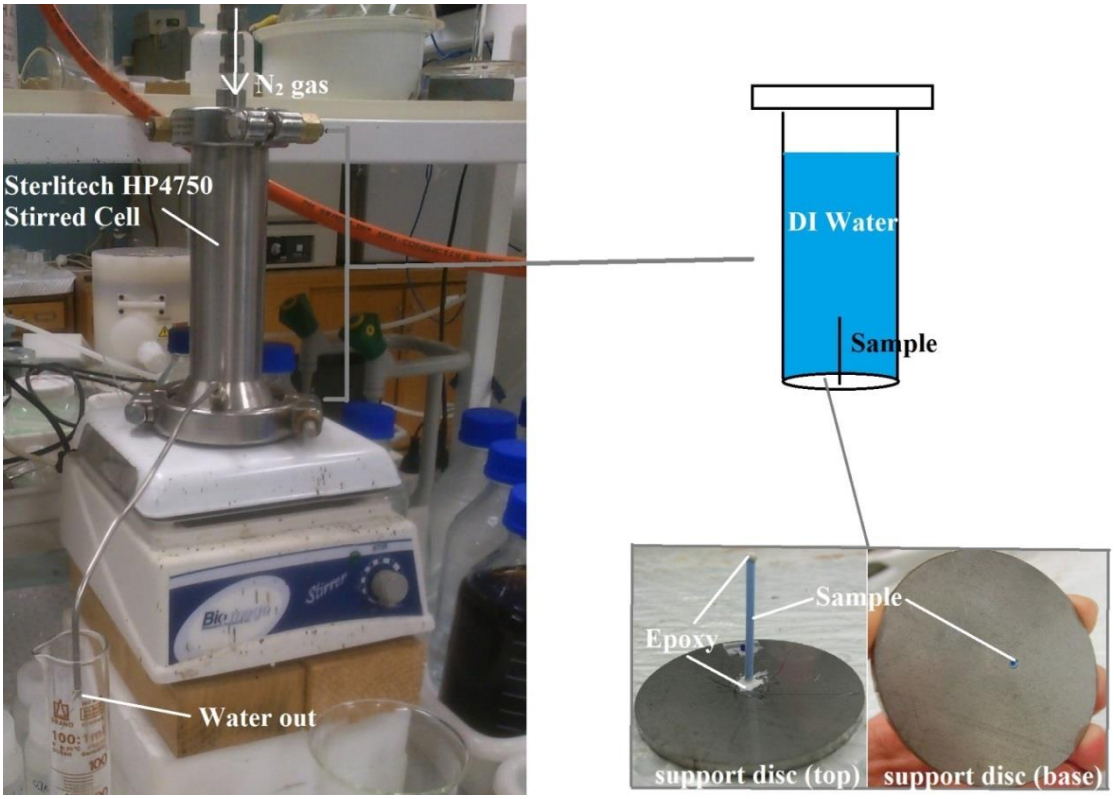

Fig. 4.3 Water Flux test setup and schematic diagram.

4.3 Results and Discussion

4.3.1 Phase identification

The XRD patterns of the pure alumina sample and that with Al_2O_3 to NiO ratio of 1:0.016 by mass are shown in Fig. 4.4. The samples tested were final products after 5 hours sintering at 1500 ^oC.

In comparison with the pure alumina sample, the other sample showed extra peaks that indicated the presence of $NiAl_2O_4$. This showed for formation of $NiAl_2O_4$ through solid-state reaction between Al_2O_3 and NiO during the sintering process. The phase equilibrium between Al_2O_3, NiO and $NiAl_2O_4$ were presented by Phillips et al. [119], who proved that when the NiO content is below 58 mol% in a NiO-Al_2O_3 mixture at 1500 ^oC, $NiAl_2O_4$ and Al_2O_3 were the only phases present at equilibrium state. Studies on the formation of $NiAl_2O_4$ by Han et al. and Kotula et al. also showed that α-Al_2O_3 react easily with NiO to form $NiAl_2O_4$ in a homogeneous mixture of α-Al_2O_3 and NiO being sintered at 1300 ^oC or over for 2 hours. [122, 125] These all supported the complete conversion of NiO to $NiAl_2O_4$ in the α-Al_2O_3-NiO mixture that contained 0-14.4 mol% NiO and were sintered at 1500 ^oC for 5 hours. By stoichiometry, the compositions of the final products were summarized in Table 4.1.

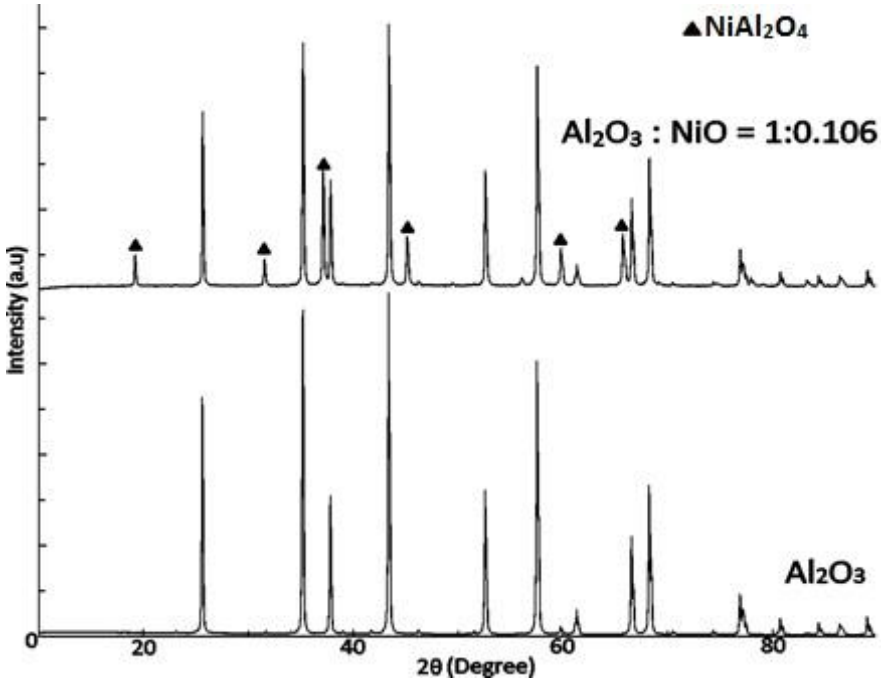

Fig. 4.4 XRD patterns of pure alumina hollow fibre membrane and a hollow fibre membrane with Al_2O_3:NiO ratio of 1:0.106 by mass.

Table 4.1 Compositions of hollow fibre membrane samples by stoichiometry in weight percentage and mole percentage.

Sample	1	2	3	4	5	6	7	8
$NiAl_2O_4$ wt%	0.00	2.02	5.15	10.62	14.78	15.83	16.42	22.62
$NiAl_2O_4$ mol%	0.00	1.18	3.04	6.42	9.10	9.79	10.18	14.43
Al_2O_3 wt%	100.00	97.98	94.85	89.38	85.22	84.17	83.58	77.38
Al_2O_3 mol%	100.00	98.82	96.96	93.58	90.90	90.21	89.82	85.57

4.3.2 Effect of $NiAl_2O_4$ content on flexural strength

Flexural strength enhancement is the main purpose of including $NiAl_2O_4$ in alumina hollow fibre membrane. The effect of $NiAl_2O_4$ content on the flexural strength of Al_2O_3 hollow fibre membrane is presented in Fig. 4.5. Ten fibres of each composition were tested for their flexural strength and an average value was calculated. It was found that a maximum flexural strength of 156 MPa was achieved by the sample containing 16.4 wt% of $NiAl_2O_4$, which was more than double of that shown by the pure alumina sample. The strengthening effect was a consequence of a stress field created in the ceramic matrix by the different thermal expansion coefficients of alumina and $NiAl_2O_4$. This stress field gave a closure force along grain boundaries, which deflected crack growth along grain boundaries. This reinforcement

mechanism was explained in more detail in our previous work on $NiAl_2O_4$ reinforced porous alumina. [144]

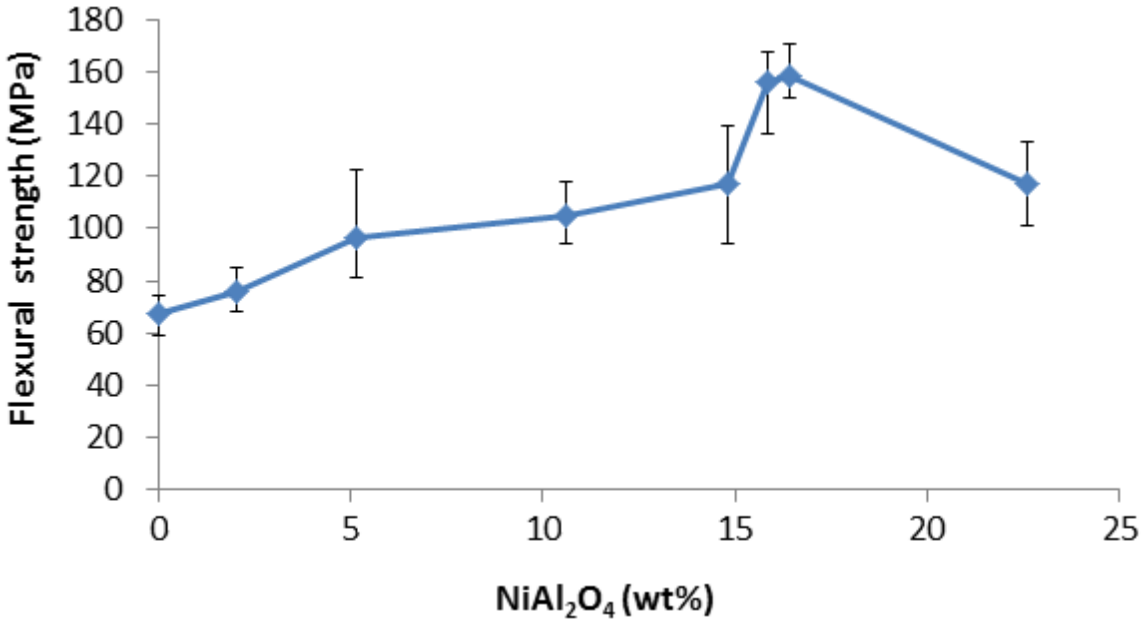

Fig. 4.5 Flexural strength of $NiAl_2O_4$ reinforced alumina hollow fibre membranes from pure alumina to 22.6 wt% $NiAl_2O_4$.

With increasing $NiAl_2O_4$ content, the flexural strength of the $NiAl_2O_4$ reinforced alumina hollow fibre membrane increased up to a $NiAl_2O_4$ loading of 16.4 wt% then dropped down when $NiAl_2O_4$ loading was further increased. The trend of this flexural strength change with $NiAl_2O_4$ loading was similar to that shown by $NiAl_2O_4$ reinforced porous alumina in our previous work. [144]

The effect of $NiAl_2O_4$ content on the flexural strength of alumina hollow fibre membranes could be explained by the packing and grain growth during the sintering stage. Comparing Fig. 4.6(a) and (b), the addition of 16.4 wt% $NiAl_2O_4$ led to a denser particle packing, which was a result of the smaller size NiO particles filling in the gaps between the alumina particles at the early particle mixing stage and hence the new phase $NiAl_2O_4$ was formed in these gaps. The grain sizes were under 1 μm. Both grain growth and neck growth by surface diffusion [4] could be observed and were developed evenly in all directions at the same rate. With 22.6 wt% of $NiAl_2O_4$, the grain growth became significantly different from that with lower $NiAl_2O_4$ loading. As shown in Fig. 4.6(c), grain growth and neck growth were at a higher rate in some directions. Some grains were joined together as random lines of over 3 μm long across the matrix, while a lot of small loose particles could be observed. These irregularly formed line structure and the peripheral small loose particles hindered shrinkage in the later

stage of sintering. The loose packing and poor bonding due to mismatched grain morphology reduced its flexural strength.

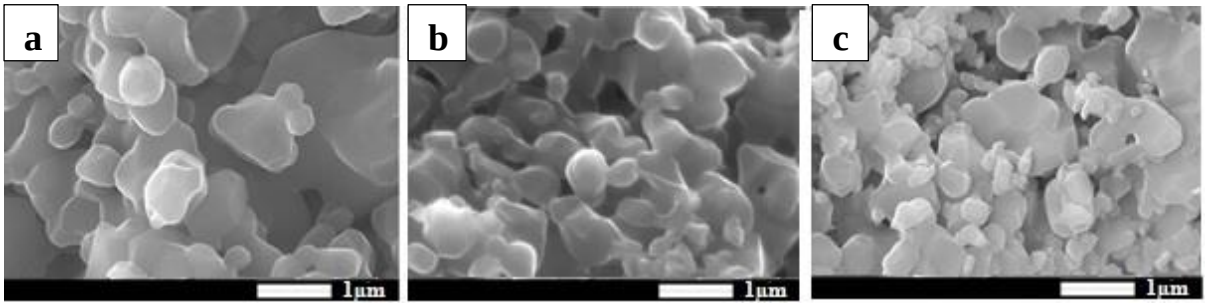

Fig. 4.6 SEM images of the cross sectional centre of (a) pure alumina; (b) 16.4wt% $NiAl_2O_4$ and (c) 22.6 wt% $NiAl_2O_4$ hollow fibre membranes.

4.3.3 Morphology and microstructure of $NiAl_2O_4$ / Al_2O_3 hollow fibre membranes

SEM images of pure alumina, 16.4 wt% and 22.6 wt% $NiAl_2O_4$ hollow fibre membranes sintered at 1500 ^oC are shown in Fig. 4.7. The average outer diameter and inner diameter of the sintered fibres were measured to be 1632 μm and 1231 μm respectively under SEM. As described in other literatures [3, 7, 33, 75, 76], ceramic hollow fibre membranes fabricated by the phase inversion method has an asymmetric structure. From a cross sectional view, a highly porous finger-like structure near the inner and outer wall of the fibre and a relatively dense sponge-like structure in the centre could be observed. The finger-like porous structure near the membrane walls was a result of rapid phase inversion, which occurred slower in the centre of the fibre and hence gave a denser sponge-like structure. The thickness of finger-like layer and sponge-like layer could be controlled in the fibre extrusion stage by adjusting factors such as air gap, internal coagulant flow rate and the coagulant used. [34] In order to study the effect of $NiAl_2O_4$ inclusion in alumina hollow fibre membrane, the extrusion conditions were kept unchanged as described in Section 4.2.2. As seen in the cross-sectional SEM images, the thickness of finger-like layer and sponge-like layer in all the hollow fibre membranes produced were approximately 1:1. The finger-like layer near the outer wall of the hollow fibre membranes was much thicker than that near the inner wall because of the instant solidification of the inner wall once the slurry was pushed out of the spinneret, while the air gap delayed the contact of the slurry with external coagulant and slowed down the solidification rate. At low magnification, the difference between the structures of hollow fibre with different composition was not obvious. Fig. 4.7(c), (d), (g), (h), (k) and (l) are SEM images of the sponge-like layer at higher magnifications. Despite being denser than the

finger-like layer from a macro view, the sponge-like layer still had a porous structure which favoured the application of this hollow fibre as a liquid separation membrane. The pores were all of irregular shapes. The 16.4 wt% $NiAl_2O_4$ sample showed denser but similar microstructure as that of the pure alumina sample. The 22.6 wt% $NiAl_2O_4$ sample on the other hand showed much more fully densified regions surrounded by many small individual particles. From a 2-dimentional view, the higher the $NiAl_2O_4$ content, the denser the sponge-like layer was. The result of flexural strength test however showed a lower flexural strength of the 22.6 wt% $NiAl_2O_4$ hollow fibre than that of 16.4 wt% $NiAl_2O_4$. As explained in Section 4.3.2, the direction and extent of grain growth, as well as the presence of small loose particles, in the 22.6 wt% $NiAl_2O_4$ would hinder shrinkage at the later sintering stage.

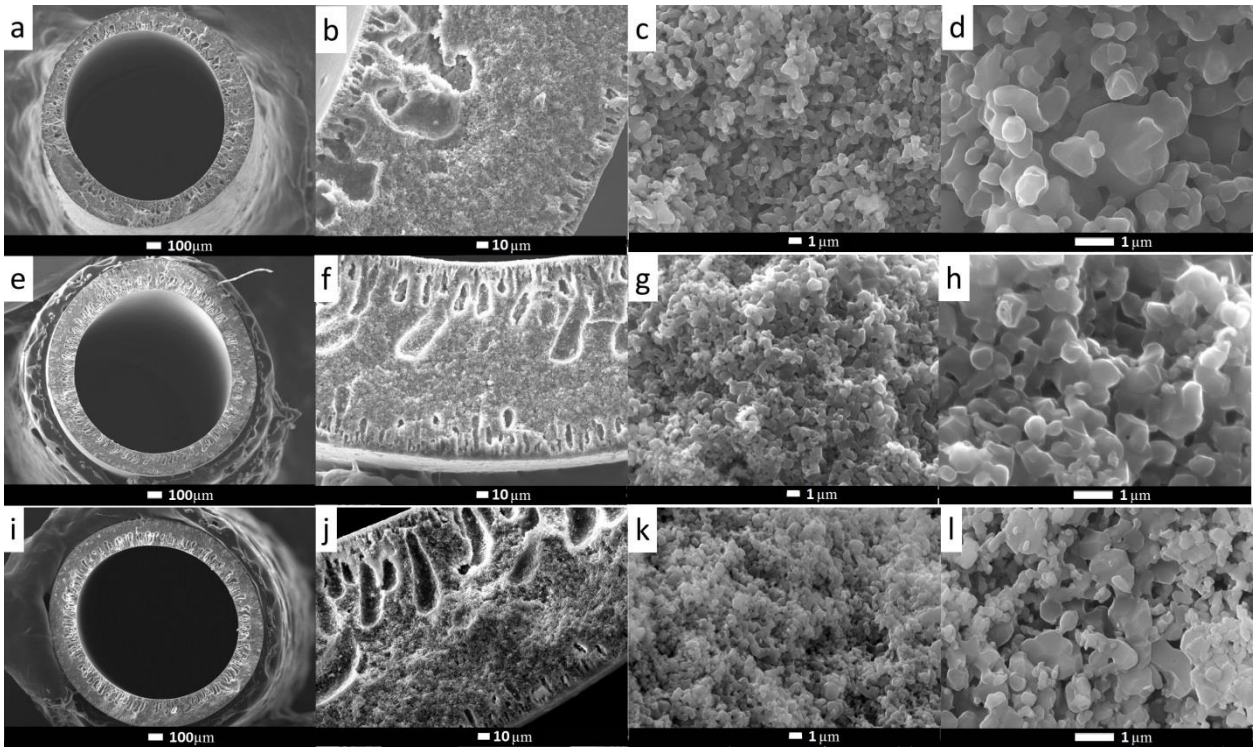

Fig. 4.7 SEM images of the cross sectional view of (a - d) pure alumina; (e-h) 16.4 wt% $NiAl_2O_4$ and (i-l) 22.6 wt% $NiAl_2O_4$ hollow fibre membrane.

4.3.4 Porosity and pore size

Porosity and pore size distributions are significant factors that affect the performance of all membranes. In separation processes, they determine the trans-membrane resistance and particle size range of retentate and hence the application of the membrane. The porosity of $NiAl_2O_4/Al_2O_3$ hollow fibre membranes with $NiAl_2O_4$ loading of 0 wt% to 22.6 wt% is shown in Fig. 4.8. An increase in $NiAl_2O_4$ content lead to a decrease in porosity, until a 16.4

wt% of $NiAl_2O_4$ loading was reached and the porosity started increasing when the $NiAl_2O_4$ loading was further raised. This trend agrees well with the effect of $NiAl_2O_4$ on flexural strength shown in Fig. 4.5. The enhancement in flexural strength came with a decrease in porosity, until the maximum flexural strength and minimum porosity were reached at 16.4 wt% of $NiAl_2O_4$ loading. Despite a loss of nearly 10% in porosity in comparison with the pure alumina sample, the 46.8% porosity of the 16.4 wt% $NiAl_2O_4$ hollow fibre membrane is still decent as a ceramic membrane. In general, a ceramic membrane of porosity of 35% or above could provide sufficiently low fluid resistance. [32, 36]

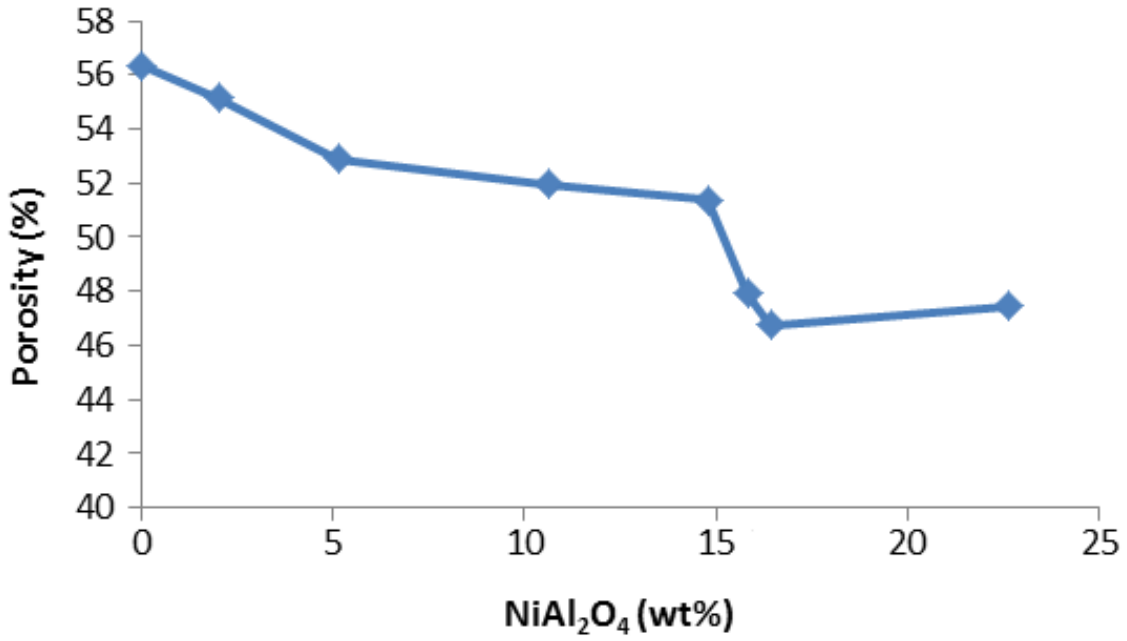

Fig. 4.8 Porosity of $NiAl_2O_4$ reinforced alumina hollow fibre membranes from pure alumina to 22.6 wt% $NiAl_2O_4$.

The pore size distribution curves of pure alumina, 16.4 wt% $NiAl_2O_4$ and 22.6 wt% $NiAl_2O_4$ hollow fibre membrane obtained from mercury intrusion porosimetry were shown in Fig. 4.9. All three pore size distribution curves show similar broadness and binomial distribution of pore size. The overall pore size of all three samples ranged from 83 nm to 606 nm. For each curve, the peak that shows a smaller pore size mainly represented the pores in the relatively dense sponge-like layer of the hollow fibre membrane, while the other peak mainly represented the pores in the finger-like highly porous layer. The peaks of the pure alumina sample appeared in 380 nm and 606 nm. With increasing $NiAl_2O_4$ content, the peaks of pore size distribution were shifted to a smaller pore size. Comparing the peak positions of the 16.4 wt% $NiAl_2O_4$ curve and those of the 22.6 wt% $NiAl_2O_4$ curve, the peak that represents the sponge-like layer shifted from 245 nm to 200 nm when the $NiAl_2O_4$ loading increased, while

the position of the peak representing the sponge-like layer remained in 380 nm. This showed as the content of $NiAl_2O_4$ increased, $NiAl_2O_4$ had a more significant effect on the pore size distribution of the sponge-like layer than on the finger-like layer.

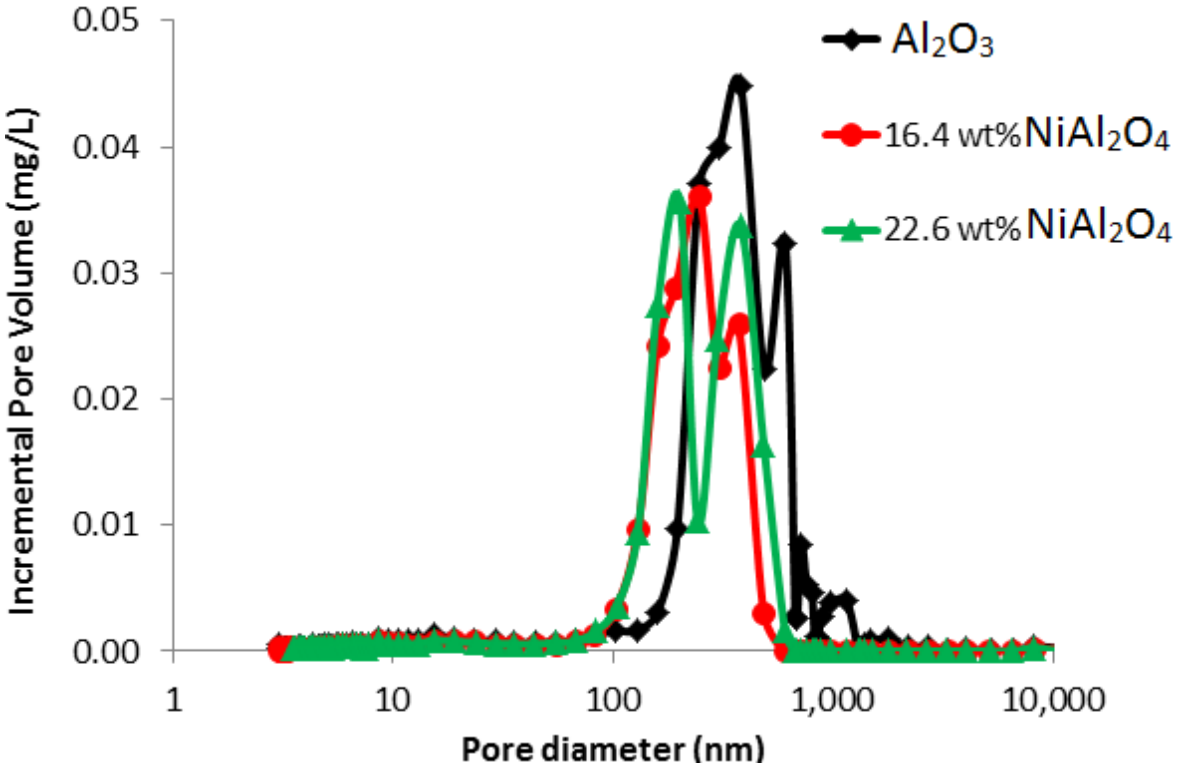

Fig. 4.9 Pore size distributions of pure alumina hollow fibre membrane, 16.4 wt% and 22.6 wt% $NiAl_2O_4$ reinforced alumina hollow fibre membrane.

4.3.5 Pure water flux and properties of active layer

Pure water flux is affected by both the porosity of the active layer and the overall porosity of a membrane and could be used to determine the trans-membrane resistance. The effect of $NiAl_2O_4$ content on the pure water flux on the $NiAl_2O_4$ reinforced alumina hollow fibre membrane at a feed pressure of 2 bar is shown in Fig. 4.10. As a combined effect of both surface porosity and overall porosity, Fig. 4.10 shows a similar trend as that of overall porosity in Fig. 4.8 with a different turning point. The minimum pure water flux was reached at 15.8 wt% $NiAl_2O_4$. The sample with 14.9 wt% of $NiAl_2O_4$ also showed a slightly lower pure water flux than that of 16.4 wt% $NiAl_2O_4$ which has the lowest overall porosity. The hollow fibre membrane with 16.4 wt% $NiAl_2O_4$ has a pure water flux of 597 L/m^2.h.bar at 2 bar. As the pure water flux of the $NiAl_2O_4$ reinforced hollow fibre membrane substantially decreased, a balance between flexural strength and flux has to be taken when choosing the

most suitable composition. The more than doubled flexural strength of the $NiAl_2O_4$ reinforcement would allow the membrane to be used under higher pressure where the overall flux would be increased. Other factors that could be changed to adjust strength and flux of a hollow fibre membrane include diameter and wall thickness.

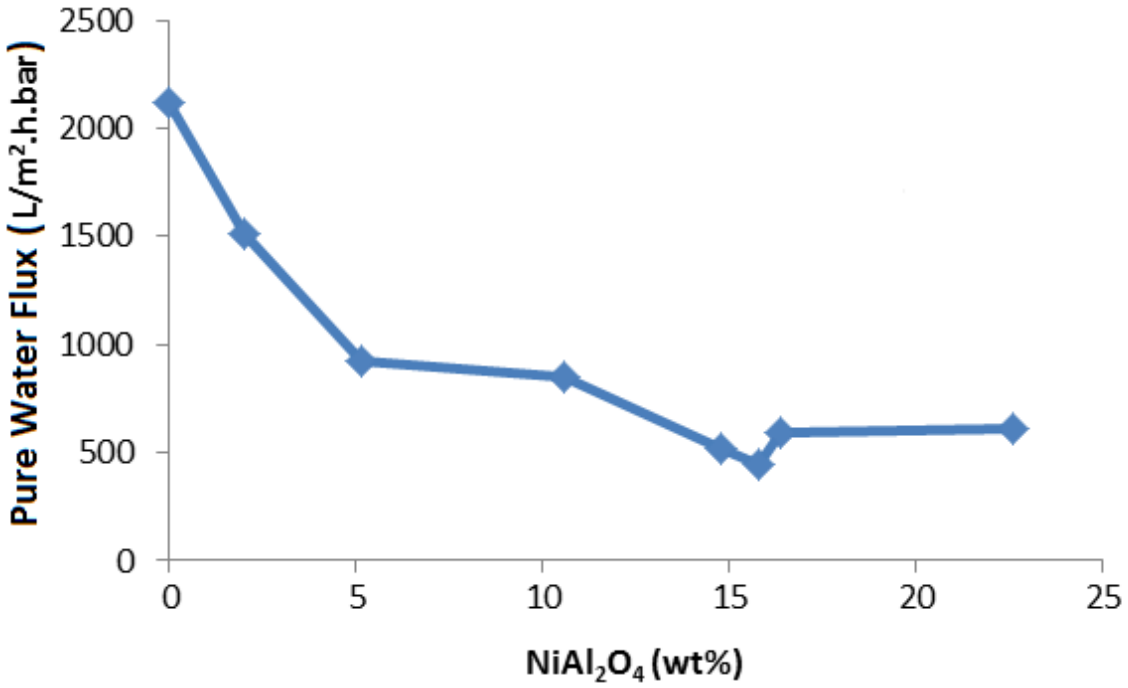

Fig. 4.10 Pure water flux of $NiAl_2O_4$ reinforced alumina hollow fibre membranes at a feed pressure of 2 bar.

The pore size and porosity of active layer significantly affect the mass transport through the membrane. Wang and Chung reported three molecular transport mechanisms in asymmetric hollow fibre membranes that have a dense selective layer: Knudsen flow, solution diffusion and poiseuille flow. [37] Knudsen flow occurs when the free mean path of the transporting molecules is large compared to the passage in the membrane, which is not expected to take place in water permeation through a microfiltration membrane. The effect of solution diffusion which occurs through non-porous dense region of the active layer was negligible because of the relatively large molecular size of water and the porous membrane surface. Poiseuille flow was therefore the dominating transport mechanism in the pure water flux test.

Li et al. presented a model to describe the relationship between water permeability and microstructure parameters in a ceramic membrane [39]. Taken into account the deformation of ceramic particles and change in particle aggregation during sintering, Li et al. modified the well-known Carman-Kozeny equation and applied it in Darcy's Law, giving the relationship between pure water flux and the membrane parameter as

$$j = \frac{\Delta P {d_m}^{k_2} \varepsilon^3}{k_1 \mu (1-\varepsilon)^2 L}$$

j was the pure water flux, ΔP was the pressure difference across the membrane, d_m was the mean pore size, ε was the overall porosity, μ was the viscosity of pure water and L was the membrane thickness. k_1 and k_2 were constants developed by experimental data as correction factors for the deformation of ceramic particles and change in particle aggregation and were 2.499×10^7 $m^{-0.892}$ and 1.108 respectively. The general Hagen-Poiseuille equation

$$j = \frac{\Delta P {d_m}^2 \varepsilon}{32 \mu L \tau}$$

was also modified by Li et al. from experimental data, giving the tortuosity $\tau = \frac{4.000}{\varepsilon}$.

To apply this model in asymmetric ceramic hollow fibre membranes, the assumptions made include the active layer had a uniform thickness and its resistance was more significant than the other layers of the membrane. For a simple estimation of pore size of the active layer of the three samples presented in Fig. 4.7 using these two modified equation, the overall porosity of the active layer was assumed to be the same as the outer surface porosity of the hollow fibre membrane. The outer surface porosities were determined by the image tool ImageJ which turns SEM images into black and white regions that represent particless and pores respectively and calculates the ratio of black and white pixels. The SEM images of outer surface of pure alumina, 16.4 wt% $NiAl_2O_4$ and 22.6 wt% $NiAl_2O_4$ hollow fibre membrane and their corresponding ImageJ image are shown in Fig. 4.11.

As a validation of the active layer pore size estimated by the above equations, the active layer pore sizes of the same samples were measured by gas bubble pressure method (GBP). The results of GBP measurement is shown in Fig. 4.12. Table 4.2 summarized the mean pore sizes of active layer obtained by the two modified equations and GBP method.

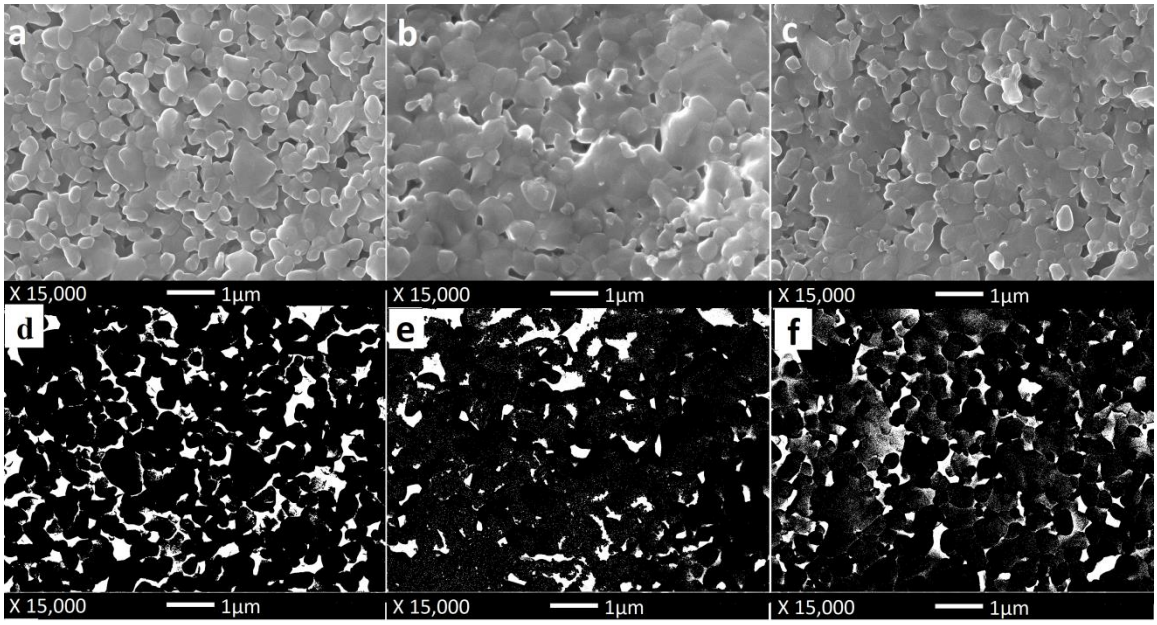

Fig. 4.11 SEM images of outer surface of (a) pure alumina, (b) 16.4 wt%$NiAl_2O_4$, (c) 22.6 wt% $NiAl_2O_4$ hollow fibre membrane. (d), (e) and (f) are the ImageJ images for calculating the surface porosity of (a), (b) and (c) respectively.

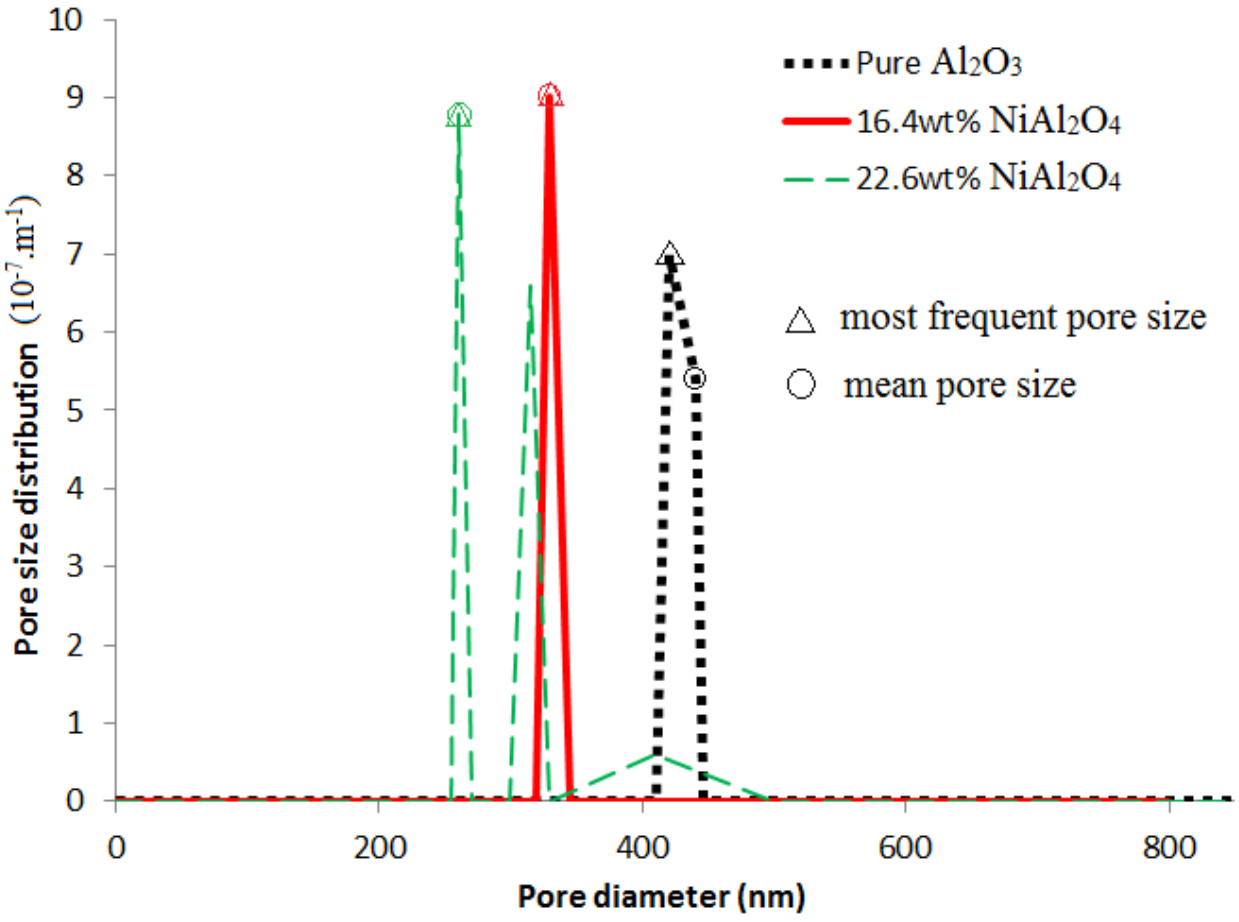

Fig. 4.12 Pore size distribution of active layer of (a) pure alumina (b) 16.4 wt% $NiAl_2O_4$ (c) 22.6 wt% $NiAl_2O_4$ hollow fibre membrane by GBP method.

Table 4.2 Summary of mean pore size of active layer determined by the modified Carman-Kozeny equation, modified Hagen-Poiseuille equation and GBP method.

$NiAl_2O_4$ wt%	Outer surface porosity (%)	Mean pore size of active layer, d_m (nm)		
		C-K equation	H-P equation	GBP method
0.0	15.5	482	334	440
16.4	12.0	334	230	330
22.6	13.1	258	211	260

As shown in Fig. 4.12, the mean pore size of active layer decreased with increasing $NiAl_2O_4$ loading same as the overall pore size shown in Fig. 4.9. 16.4 wt% $NiAl_2O_4$ gave the sharpest active layer pore size distribution. Out of the three samples tested by GBP method, only the pore size distribution of 22.6 wt% $NiAl_2O_4$ showed multiple peaks and had the broadest range. As explained in Section 4.3.3, the presence of large grains and loose particles in the 22.6 wt% $NiAl_2O_4$ led to board range of pore size. Comparing the results in Table 4.2, the active layer mean pore sizes estimated by the modified Carman-Kozeny equation were close to those obtained by the GBP method, with the largest difference of 9.5% in the pure alumina hollow fibre membrane. This validated the three assumptions of applying the modified Carman-Kozeny for surface pore size estimation. The modified Carman-Kozeny equation was therefore more accurate than the modified Hagen-Poiseuille equation in estimating the mean pore size of active layer of the hollow fibre membranes described in this paper. This is a combine effect of membrane parameters such as porosity, pore size range and active layer thickness and the trans-membrane pressure during the pure water flux test.

4.3.6 Comparison of $NiAl_2O_4$ reinforcement with other reinforcement methods

The $NiAl_2O_4$ reinforced alumina hollow fibre membranes fabricated had porosities 46.8-55.2%. The flexural strengths of these $NiAl_2O_4/Al_2O_3$ hollow fibre membranes and those of other ceramic hollow fibre membranes with similar porosities are shown in Fig. 4.13. In comparison with the yttria-stabilized zirconia (YSZ), Ni/YSZ and NiO/YSZ hollow fibres prepared by Yang's, Zhang's and Meng's group [32, 34, 114], the flexural strengths of $NiAl_2O_4$ reinforced alumina hollow fibre membranes was placed in the middle range. It showed that within the porosity range of 46.8-55.2%, $NiAl_2O_4$ reinforcement could raise the flexural strength of alumina hollow fibre membranes to that given by YSZ a stronger ceramic material of a higher cost. The $NiAl_2O_4$ reinforced alumina membranes with porosity over

45.0% also had a flexural strength significantly higher than the alumina and silicon nitride (Si_3N_4) hollow fibres prepared by Smid et al.[3]

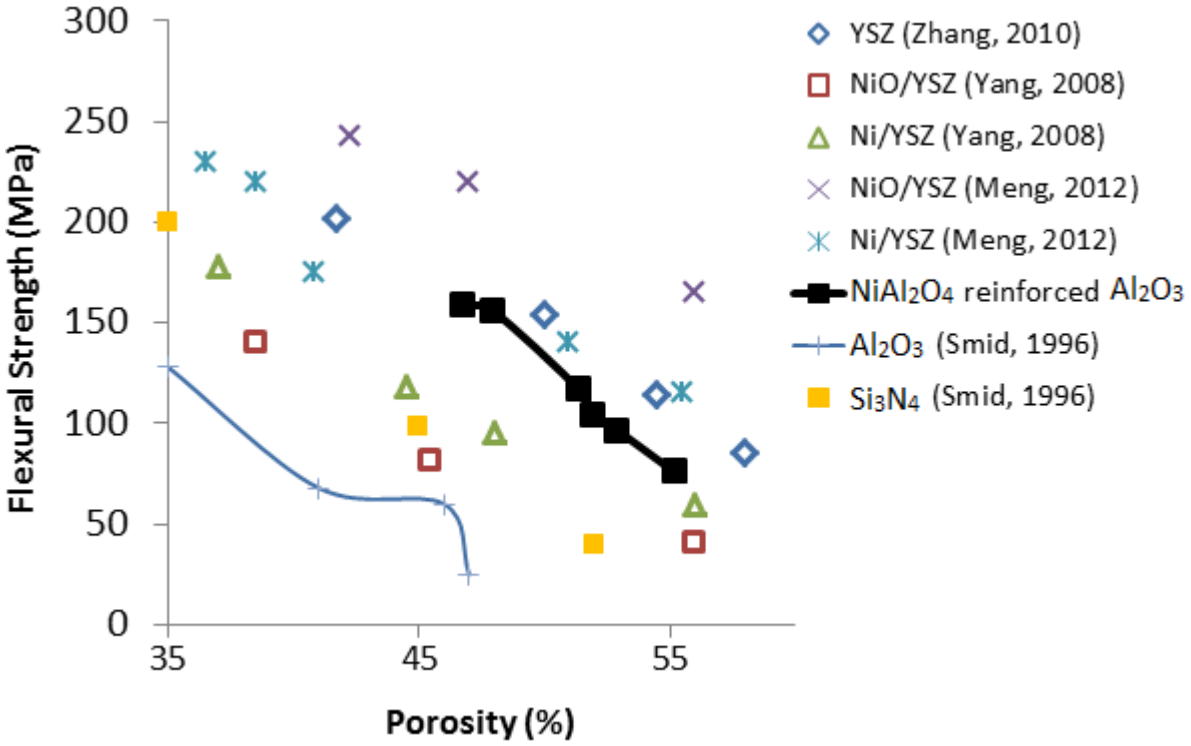

Fig. 4.13 Flexural strengths of various ceramic hollow fibre membranes with porosity of 35.0% to 60.0%.

4.4 Conclusions

The presence of $NiAl_2O_4$ phase enhanced the flexural strength of alumina hollow fibre membrane. A maximum flexural strength of 156 MPa was achieved by the $NiAl_2O_4/Al_2O_3$ hollow fibre membrane containing 16.4 wt% of $NiAl_2O_4$, while the porosity was still maintained at 46.8%. This porosity is significantly higher than the generally recommended 35% for ceramic membranes to provide sufficiently low fluid resistance. The 16.4 wt% $NiAl_2O_4$ reinforced membrane had a flexural strength 2.3 times of that of the pure Al_2O_3 membrane with a 10% trade-off in porosity. Further increasing the loading of $NiAl_2O_4$ led to uneven grain growth and neck growth in random directions and loose agglomerates, hence hindered shrinkage during the sintering process and decreased flexural strength. The pure water flux of the 16.4 wt% $NiAl_2O_4/Al_2O_3$ hollow fibre membrane was 597 L/m^2.h.bar at 2 bar. The mean pore size active layer measured by the gas bubble pressure method was 330 nm which fell into the microfiltration range. A modified version of the well-known Carman-Kozeny

equation and Hagen-Poiseuille equation were applied to estimate the mean pore size on active layer from the pure water flux. Comparing with the measurement from the GBP method, the modified Carman-Kozeny equation obtained a closer estimation on the mean active layer pore size. The largest difference between the estimated mean pore size by the modified Carman-Kozeny equation and that obtained from GBP measurement was 9.5% among all the samples tested. $NiAl_2O_4/Al_2O_3$ hollow fibre membrane could achieve a comparable flexural strength as YSZ a stronger and higher cost ceramic material and as other ceramic reinforcement methods within the porosity range of 46.8-55.2%. In a liquid separation process, the resistance caused by the centre layers in an asymmetric hollow fibre membrane is negligible in comparison with the active layer. Therefore, a potential approach to further improve the flexural strength of $NiAl_2O_4/Al_2O_3$ hollow fibre membrane without affecting the mass transport efficiency is adjusting the fibre extrusion parameters to minimize the thickness of the finger-like porous layer which does not favour mechanical strength.

Chapter 5 Nickel aluminate chains reinforced ceramic hollow fibre membrane

Overview

Apart from discrete elements, continuous fibres and chains were also suitable reinforcement medium in material strengthening. The previous chapter reports the reinforcement of alumina (Al_2O_3) hollow fibre membrane through the inclusion of nickel (II) oxide (NiO) powder which reacted with Al_2O_3 to form discrete nickel aluminate ($NiAl_2O_4$) particles within the Al_2O_3 matrix. In this chapter, nickel nanowire (Ni NW) which has a continuous structure was added into the extrusion of Al_2O_3 hollow fibre membrane precursor. Ni NW was oxidized into NiO chains after being sintered in air and react with Al_2O_3 to form $NiAl_2O_4$ chains within the Al_2O_3 matrix. The thermal expansion mismatch between $NiAl_2O_4$ and Al_2O_3 and crack bridging effect of the $NiAl_2O_4$ chains both led to crack growth deflection, hence a strengthening effect was achieved. Flexural strength was increased by the presence of $NiAl_2O_4$ up to a loading of 2.00 wt% and decreased with further increase in $NiAl_2O_4$. As porosity and pure water flux were decreased with flexural strength, for a balance between flexural strength and liquid flux, 5.00 wt% of $NiAl_2O_4$ was determined to be the most suitable loading for this reinforcement method. 5.00 wt% $NiAl_2O_4$ / Al_2O_3 hollow fibre membrane had a flexural strength of 135 MPa, porosity of 48 % and pure water flux of 160 L/m^2.h.bar and active layer pore size of 0.079 – 0.24 μm. These $NiAl_2O_4$ / Al_2O_3 membranes were suitable for microfiltration separation processes.

5.1 Introduction

Hollow fibre membranes are widely used in many industrial applications because of their high surface area to volume ratio and high compactness. [4, 5] Separation processes that hollow fibre membrane systems are involved include water desalination, waste treatment, chemical filtration and gas separation. With controllable porosity and pore size, hollow fibre membranes were also used as catalytic reactors, chemical reactors and bioreactors. [7, 10, 110]

Ceramic hollow fibre membranes have high thermal and chemical stability and are also insensitive to swelling and easy for cleaning. They are therefore suitable for harsh conditions that traditional polymer hollow fibre membranes foul in, such as high temperature, highly

acidic or basic feed or permeate and processes that involve organic solvents [3]. The brittleness of ceramic hollow fibre membranes, however, hindered their large scale production and application. The small size and thin membrane walls of ceramic hollow fibre membrane lead to membrane failure under high operation pressure and difficulty in being sealed the into equipment as well-configured and orientated modules for the best performance. [14]

The previous chapters showed the enhancement of flexural strength in porous alumina and alumina hollow fibre membrane by the formation of a second phase nickel aluminate spinel ($NiAl_2O_4$). [144, 145] $NiAl_2O_4$ was a ceramic formed by the solid-solid reaction between nickel oxide powder (NiO) and alumina powder. This reaction has been widely demonstrated in many literatures [122, 123, 125, 127] and was used in the removal of toxic nickel in waste treatment. [133, 134, 146] This boundary strengthening effect in the matrix of alumina was a result of the stress field created by the difference in thermal expansion between alumina and $NiAl_2O_4$. [93] This stress field created a closure force which deflects crack growth along grain boundaries.

In this chapter, the use of nickel nanowire as a starting material for the formation of $NiAl_2O_4$ in porous alumina hollow fibre membrane for the purpose of flexural strength enhancement is presented. In air atmosphere, nickel (Ni) as a transition metal is oxidized into nickel (II) oxide (NiO) when the temperature is over 500 ^oC. [147, 148] At lower temperatures oxidation of nickel could only occur under ultra-high vacuum. [149] Nickel could therefore also be a starting material for the formation of $NiAl_2O_4$ via the oxidation of nickel to nickel (II) oxide and the reaction with alumina. Apart from existing and being used as individual particles, many studies have reported the synthesis of nickel nanowire, nanotubes, fibres, chains, nanospheres and nanoflowers. Among all these morphologies of nickel, its nanowire have been widely studied and used in solid oxide fuel cells (SOFC) and batteries.

Many literatures have reported the properties of nickel nanowire such as mechanical properties, melting behaviour, oxidizing processes and magnetic properties. Mechanical strength, melting behaviour and oxidizing processes are important for the feasibility of applying nickel nanowire in ceramic hollow fibre membrane reinforcement, while magnetic properties are relatively more vital for the production of SOFC.

The mechanical properties of nanowires therefore determine the performance of its reinforced ceramic because crack-bridging is the major toughening mechanism when nanowires are used

for reinforcement purpose, in which nanowires acts as a crack-bridging element on crack faces of a material. When a crack grows, the nanowire exerts a closing force and partially retains the load carrying capacity behind the crack tip, hence increasing the driving force required for the crack to continue growing. [85] Cheng's group has reported the relationship between the mechanical properties of single crystalline nickel nanowires and their sizes. [150] Their results from a uniaxial tensile test showed that single crystalline nickel nanowires within the diameter range of 100-300 nm all had high breaking strength of over 1 GPa which were more than five times higher than that of bulk nickel. Breaking strength of single crystalline nickel nanowire could be further enhanced by 50% by decreasing the diameter of nickel nanowire from 300 nm to 100 nm. Before a critical loading was applied, nickel nanowires showed insignificant change in morphology and surface structure. Limited plasticity was shown in fractured nickel nanowires.

Melting behaviour of nickel nanowire is important for its involvement with ceramics because of the typical high temperature sintering process in all ceramic productions. Hui et al. has reported a detail study on how multi-shell structured nickel nanowires melt upon heating from 400 K to 1500 K. Their result showed the melting of nickel nanowire started from the central interior atom which moved along the axial direction of the nanowire. The moving atoms from the centre of the nanowire were inline and formed a monostrand atomic chain when temperature reached 900 K. Further heating deformed this atomic chain into a cluster and lost the nickel nanowire lost its original crystalline structure. [151] Li et al. developed a model to describe the relationship between size and melting temperature of many pure metallic and bimetallic nanowires including pure nickel nanowires. The computational model in Li's group considered the effects of all surface atoms, lattice and surface packing factors and the cross sectional shape of the nanowires. The model was then compared with experimental data. The simulation and experimental results showed a melting temperature of 1300 – 1400 K for nickel nanowires of a diameter of 5 nm. Further increase in diameter did not show a significant increase in melting temperature according to the computation model. [152]

The high temperature required for sintering in ceramics also leads to thermal oxidation of metals in the presence of oxygen. The oxidation process of nickel nanowire therefore also determines the final products in a ceramic material and its performance. Unlike the formation of other metal oxide, nickel nanowire was found to form void and bamboo-like structure during thermal oxidation to nickel (II) oxide. This unique oxidation behaviour has

been studied in details, especially for the production of NiO nanowire a semiconducting oxide. Ren et al. has compared the oxidation mechanism of nickel nanowire at different temperatures and ramp rates. The nickel nanowires underwent oxidation had a diameter of about 80 nm and a length of approximately 30 μm. No oxidation was observed at temperature below 350 ^{o}C. Voids were formed along the nanowire when the oxidation temperature was raised up to 450 ^{o}C as a consequence of partial oxidation, while a tube like structure of the nanowire was formed. Complete oxidation was achieved when temperature was increased to 650 ^{o}C when a bamboo-like structure with uneven wall thickness was formed. It was suggested that to achieve NiO tubes with a uniform wall thickness, low oxidation temperature between 400 – 450 ^{o}C should be used, followed by the removal of unoxidized nickel residual through wet etching in ferric chloride ($FeCl_3$) solution. [153]

A lot of methods have been reported for the fabrication of nickel nanowire and fibres of different diameter and length. Gong et al. prepared nanocrystallites nickel fibres with diameter of 250 nm through the reduction of Ni^{2+} ions in nickel chloride hexahydrate ($NiCl_2 . 6H_2O$) by hydrazine monohydrate ($N_2H_4 . H_2O$) a reducing agent in an external magnetic field. Their results showed that pH of the reduction condition, which was controlled by sodium hydroxide (NaOH) concentration, had an effect on the morphology. The suggested optimal concentration of NaOH was 0.02 – 0.04 M and a higher concentration of NaOH resulted in rough and clustered fibres. Nickel chloride concentrations of 0.003 – 0.05 M were tried and found to have an effect on the length of nickel fibre. The average lengths of nickel fibre fabricated ranged from 20 – 100 μm. Further increasing the concentration of nickel chloride hindered the reduction process and produced some unknown nickel compounds. Another factor that affected the morphology and length of the nickel fibres was the magnetic field intensity. Magnetic fields of 0.13 - 0.35 T were tried. Smooth fibres were obtained in the presence of magnetic fields below 0.22 T. Further increasing in magnetic field intensity led to elongated and tangled nickel fibres of over 100 μm long. [154] As reported by Jia et al, nickel nanowires were formed by the controlled aggregation of nickel nanospheres drawn together by attractive magnetic forces. Growth of nickel nanoparticles in the absence of an external magnetic field is random, in which individual particles would be formed. The dipolar interactions between individual nickel nanoparticles are too weak for the assembly of nanowires. [155] Tang et al. reported the synthesis of nickel nanowire with the assistance of microwave. Polycrystalline nickel nanowires with an average diameter of 25±2 nm and up to several hundred microns long. Same as the fabrication of nickel nanowire in a

magnetic field, $NiCl_2 \cdot 6H_2O$ was the source of nickel and $N_2H_4 \cdot H_2O$ was used as a reducing agent. The mixture was microwaved for the production of nickel nanoparticles. In contrast to conventional heating which thermal energy is transferred from outside to inside of the particles, microwave irradiation is absorbed as electromagnetic energy by the particles then converted to thermal energy and hence heating up the particles from inside, which results in more rapid heating. Instead of magnetic field, the role of particle assembling was taken by Polyvinylpyrrolidone (PVP). Different amount of PVP was added and proved the role of PVP in joining nickel nanoparticles to nanowires and smoothening nanowires surfaces. Only nickel nanospheres were synthesized with the absence of PVP. 0.2 M of PVP was sufficient to join nickel particles to form a chain-like structure with rough surface. Nickel nanowires with smooth surfaces and lengths up to several hundred microns were formed with a PVP concentration of 0.75 M. [156] Tang's group then introduced the microwave-assisted polyol method for the synthesis of polycrystalline nickel nanowires with adjustable diameters of 70 – 380 nm. Concentration of $NiCl_2 \cdot 6H_2O$ as low as 5 mM was found to result in meander nickel nanowires of diameter of about 70 nm and tens of micrometers long with rough surfaces. Higher concentration of $NiCl_2 \cdot 6H_2O$ increased the diameter of final product. Irregular nanoparticles were mainly produced if the concentration of $NiCl_2 \cdot 6H_2O$ was as low as 0.1 mM. [157]

In this work, the use of nickel nanowires as a raw material for the formation of $NiAl_2O_4$ with chain structure in alumina hollow fibre membrane for reinforcement purpose was attempted. The mechanical properties of nickel nanowires used was important as mixing of raw materials and extrusion of hollow fibre membrane precursors involved shearing which could damage nickel nanowires. The formation of $NiAl_2O_4$ involved the oxidation of nickel nanowire to NiO wires, hence oxidation behaviour of nickel nanowires was considered. Melting temperature of nickel nanowires and NiO wires were critical in the formation of $NiAl_2O_4$ chains in alumina hollow fibre membrane. Chain structure of $NiAl_2O_4$, which could only be formed if nickel nanowires were oxidized to NiO wires which react with alumina before melting of the wires occurred, is expected to be a crack bridging medium for the reinforcement of alumna hollow fibre membranes. The crack bridging mechanism has been proved to be very effective in reinforcement of many materials including ceramics. [85, 158] The $NiAl_2O_4/Al_2O_3$ hollow fibre membranes prepared in this experiment therefore achieved comparable flexural strength with lower loading of $NiAl_2O_4$ in comparison with those using NiO particles as a starting material. With further improved flexural strength, these

$NiAl_2O_4/Al_2O_3$ hollow fibre membranes maintained their porous and asymmetric features and can be used in microfiltration of liquid.

5.2 Experimental

5.2.1 Materials

Alumina powder of a particle diameter <1 μm (alpha phase, 99.98 metals basis, APS powder, surface area 10 m^2/g) purchased from Alfa Aesar, A Johnson Matthey Company was used as a raw material for the preparation of ceramic hollow fibre membrane. Polyethylsulfone (PESf) [BASF, E6020P] was used as a polymer binder in hollow fibre membrane extrusion. 1-methyl-2-pyrrolidone (NMP) purchased from Sigma-Aldrich was used as a solvent of the polymer binder. Nickel nanowires were prepared by electroless deposition in an external magnetic field [159]. 0.912 g of nickel (II) nitrate hexahydrate ($Ni(NO_3)_2 . 6H_2O$) [Sigma Aldrich, crystal], a source of nickel and 0.800 g of sodium hydroxide (NaOH) [Merck, pellets GR for analysis] used for pH neutralizing were dissolved in 50 mL of ethylene glycol [Merck, reagent grade] separately. The two solutions were then mixed together and 1.625 g of hydrazine monohydrate ($N_2H_4.H_2O$) [Sigma Aldrich, N_2H_4 64-65%, reagent grade 98%] which act as a reducing agent was added. The solution was placed in a 75 ^oC water bath under a 0.2 T static magnetic field for 20 minutes. Nickel nanowires were formed as black floccules in the solution, which was collected and washed by deionized water and ethanol three times. The Ni nanowires were placed in a 60 ^oC oven for 24 hours to be dried thoroughly. The Ni nanowires had an average diameter of 300 nm and average length of 5 μm.

5.2.2 Preparation of ceramic hollow fibre membranes

The well-known phase inversion and sintering method was used to prepare ceramic hollow fibre membranes. Detailed description of the phase inversion and sintering method is reported in many literatures. [35, 76, 114] 1.5 g of PESf which act as a binder for the hollow fibre membrane precursor was dissolved in 13.5 g of NMP the solvent. Different nickel nanowire loadings were added into the PESf-NMP solution and were placed in sonication for 30 minutes for dispersion purpose. 15 g of Al_2O_3 powder was added into the mixture and ball-milled at 30 rpm for 24 hours to form homogeneous slurry. The low rotation speed of 30 rpm was applied to keep the length of the nickel nanowires. The different loading of Ni NW gave a slight variation of total powder loading in the slurries, which ranged from 50.0 wt% to 51.3 wt%. The ratios of Al_2O_3 to Ni NW were 1:0, 1:0.0040, 1:0.0067, 1:0.0170, 1:0.0347

and 1:0.0532 by mass. These ratios were calculated by stoichiometry based on a 100% reaction of Ni NW with Al_2O_3 to form $NiAl_2O_4$, aiming at achieving final products that contained 0 wt%, 1.20 wt%, 2.00 wt%, 5.00 wt%, 10.0 wt% and 15.0 wt% of $NiAl_2O_4$ respectively.

The ball-milled slurry was degased at room temperature for 20 minutes and was transferred to a stainless steel tube-in-orifice spinneret where it was extruded into hollow fibre precursors. Nitrogen gas was used to pressurize the spinneret for the extrusion process. The outer and inner diameter of the orifice was 2.8 mm and 1.4 mm respectively. Tap water of room temperature 20 ^oC was used as external coagulant. The internal coagulant was of 50 vol% ethanol and 50 vol% tap water and its flowrate was kept at 3 mL/min through the extrusion process. The effect of using ethanol-water mixture in replace of water as internal coagulant is discussed in Section 5.3.3. The air gap was fixed at 1.3 cm. The hollow fibre precursors were left in tap water of 20 ^oC for 24 hours for complete phase exchange and solidification. A schematic diagram and the full setup of the extrusion process were shown in Fig. 4.1 and Fig. 4.2 in Chapter 4 respectively.

The hollow fibre precursor was heated to 580 ^oC in air with a heating rate of 5 ^oC/min and was held for 3 hours in a high temperature tube furnace to remove the polymer binder. They were then sintered at 1500 ^oC for 5 hours for the purpose of grain growth and bonding. The samples were left in the furnace to be cooled down naturally to room temperature to prevent cracking caused by a sudden temperature change.

5.2.3 Membrane characterizations

X-ray diffraction (XRD) was used for identifying the phase present in the samples and hence confirmed the reaction between Ni nanowire and alumina for the formation of $NiAl_2O_4$. The XRD analysis was carried out in a Rigaku MiniFlex 600 with a scan range 10^o-90^o and a step size of 2^o.

The cross-sectional surface and outer surface of the hollow fibre membranes were observed under a JEOL 7001F scanning electron microscope (SEM). The cross-sectional surfaces of the hollow fibres were obtained by manual snapping at room temperatures. All samples were sputter-coated with a 0.5 nm platinum layer. The SEM images were taken at 30 kV.

The flexural strengths of the samples were determined by a three-point bending test which was carried out in an Instron Micro Tester 5848. A 2 kN load cell (Instron Calibration

Laboratory, United Kingdom), 18 mm span and crosshead speed of 0.25 mm/min were used throughout the test. The full setup of the three-point bending test was shown in Fig. 3.2 in Chapter 3. The crosshead was stopped automatically once fracture occurred in the hollow fibre. Five runs for each sample were performed. The flexural strength, σ_F, of each single hollow fibre was calculated from the following equation [35]

$$\sigma_F = \frac{8FLD}{\pi(D^4 - d^4)}$$

F is the force measured when the hollow fibre fractured. L is magnitude of the span, which was fixed at 18 mm. D and d is the outer and inner diameter of the hollow fibre respectively. The inner and outer diameters were measured under the JEOL 7001F SEM.

The porosity of each hollow fibre membrane was measured by Archimedes' principle based method. Boiling water was used as a wetting liquid. The dry mass of all samples were first measured. All samples were then immersed in boiling water for over 30 minutes for filling all the pores in the membrane with water. The wet mass of the samples was then measured. The porosity of each hollow fibre membrane were calculated by the difference between its wet mass and dry mass, which the volume of water immersed into the membrane equals to the volume of space present in the membrane.

The pure water flux test was carried out in a Sterlitech HP4750 Stirred Cell (Sterlitech Corporation, USA). Nitrogen gas was used to pressurize the cell and the feed preasure was fixed at 2 bar. The customized membrane supporting disc was non-porous and made of stainless steel. The disc had a diameter of 50 mm, a thickness of 2 mm and a circular hole with a diameter of 2 mm in its centre. The hollow fibre membrane was placed in the hole perpendicularly to the supporting disc. Epoxy was used to seal the top end of the membrane and the space between the membrane and the supporting disc. The setup and a schematic diagram of the water flux test were shown in Fig. 4.3 in Chapter 4. The pure water flux of each sample was measured over a time period of 10 minutes.

Mercury porosimetry was carried out in a Poremaster GT-60 (Quantachrome, USA) to obtain the pore size distribution of the hollow fibre membranes. Mercury was forced into the porous samples under pressure. By measuring the pressure required to force mercury through the pores, the pore volumes were estimated.

5.3 Results and Discussion

5.3.1 Phase identification

The phases present in the hollow fibre membranes were identified by XRD. Fig. 5.1 shows the XRD pattern of the sample which had Al_2O_3 to Ni nanowire ratio of 1:0.0532 by mass in its precursor and has undergone a sintering process at 1500 ^oC in air for 5 hours. Peaks representing alumina and $NiAl_2O_4$ were present and hence confirmed the reaction between alumina and Ni NW for the formation of $NiAl_2O_4$ and a complete removal of PESf polymer binder under a temperature of 1500 ^oC in air for 5 hours. With this sample containing the highest Ni nanowire loading in its precursor among all the samples, it is concluded that under the same sintering condition, reaction between alumina and Ni NW had also successfully took place in other hollow fibre precursors with lower Ni NW loading and formed $NiAl_2O_4$. The final products were therefore $NiAl_2O_3$ / Al_2O_3 ceramic hollow fibre membrane, without any polymeric or metallic component. This maintained all the advantages of ceramic materials including insensitivity to swelling, ease of cleaning and high thermal and chemical stability [49]

The stoichiometric compositions of all final products were calculated in both weight and mole percentage and displayed in Table 5.1. Base on a mass balance of one mole of Ni NW producing one mole of $NiAl_2O_4$, the six ceramic hollow fibre membrane samples prepared contained a $NiAl_2O_4$ loading of 0, 1.20, 2.00, 5.00, 10.0 and 15.0 wt%.

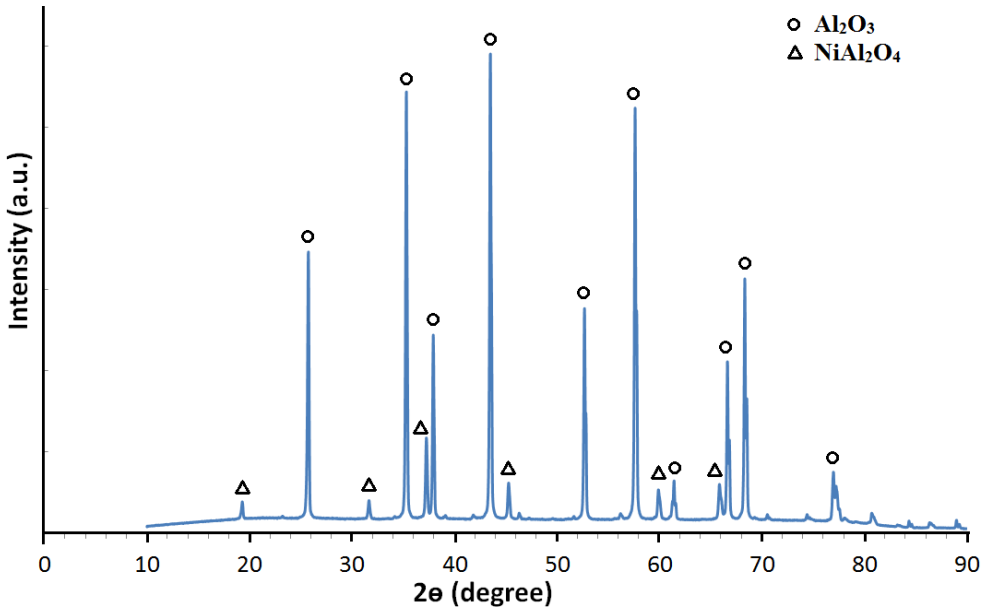

Fig. 5.1 XRD pattern of hollow fibre precursor with Al_2O_3 to Ni NW ratio of 1:0.0532 by mass, after a sintering at 1500 ^oC for 5 hours in air.

Table 5.1 Compositions of ceramic hollow fibre membrane samples by stoichiometry in weight percentage and mole percentage.

Sample	1	2	3	4	5	6
$NiAl_2O_4$ wt%	0	1.20	2.00	5.00	10.0	15.0
$NiAl_2O_4$ mol%	0	0.700	1.17	2.95	6.03	9.24
Al_2O_3 wt%	100	98.8	98.0	95.0	90.0	85.0
Al_2O_3 mol%	100	99.3	98.8	97.05	93.97	90.76

5.3.2 Effect of $NiAl_2O_4$ content on flexural strength

The effect of $NiAl_2O_4$ on the flexural strength of alumina hollow fibre membrane, which is the main focus of this study, is shown in Fig. 5.2. In comparison with pure alumina hollow fibre membrane, the inclusion of $NiAl_2O_4$ through the reaction between Ni NW and alumina in the alumina matrix showed an increase in flexural strength up to 2.00 wt% of $NiAl_2O_4$, followed by an obvious drop in flexural strength with further increase in $NiAl_2O_4$ loading. The maximum flexural strength achieved by 2.00 wt% $NiAl_2O_4$ was 172 MPa, which was 2.5 times of the 69.6 MPa shown by the pure alumina sample. This relationship between flexural strength and $NiAl_2O_4$ loading was similar to that reported in our previous work which NiO powder was used as a raw material for the formation of $NiAl_2O_4$ [145], while the maximum flexural strength was achieved at a much lower $NiAl_2O_4$ loading in this work.

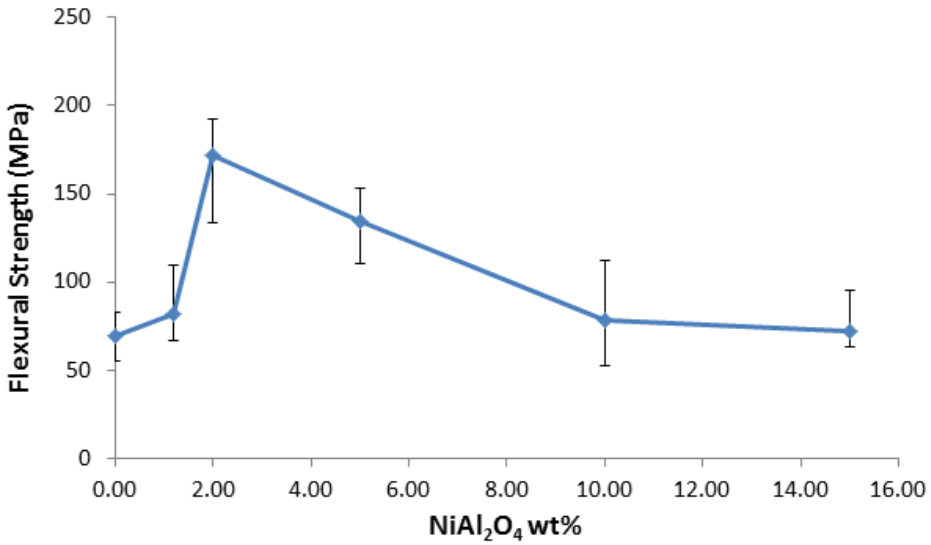

Fig. 5.2 The change in flexural strength of $NiAl_2O_4$ / Al_2O_3 hollow fibre membrane with increasing $NiAl_2O_4$ content.

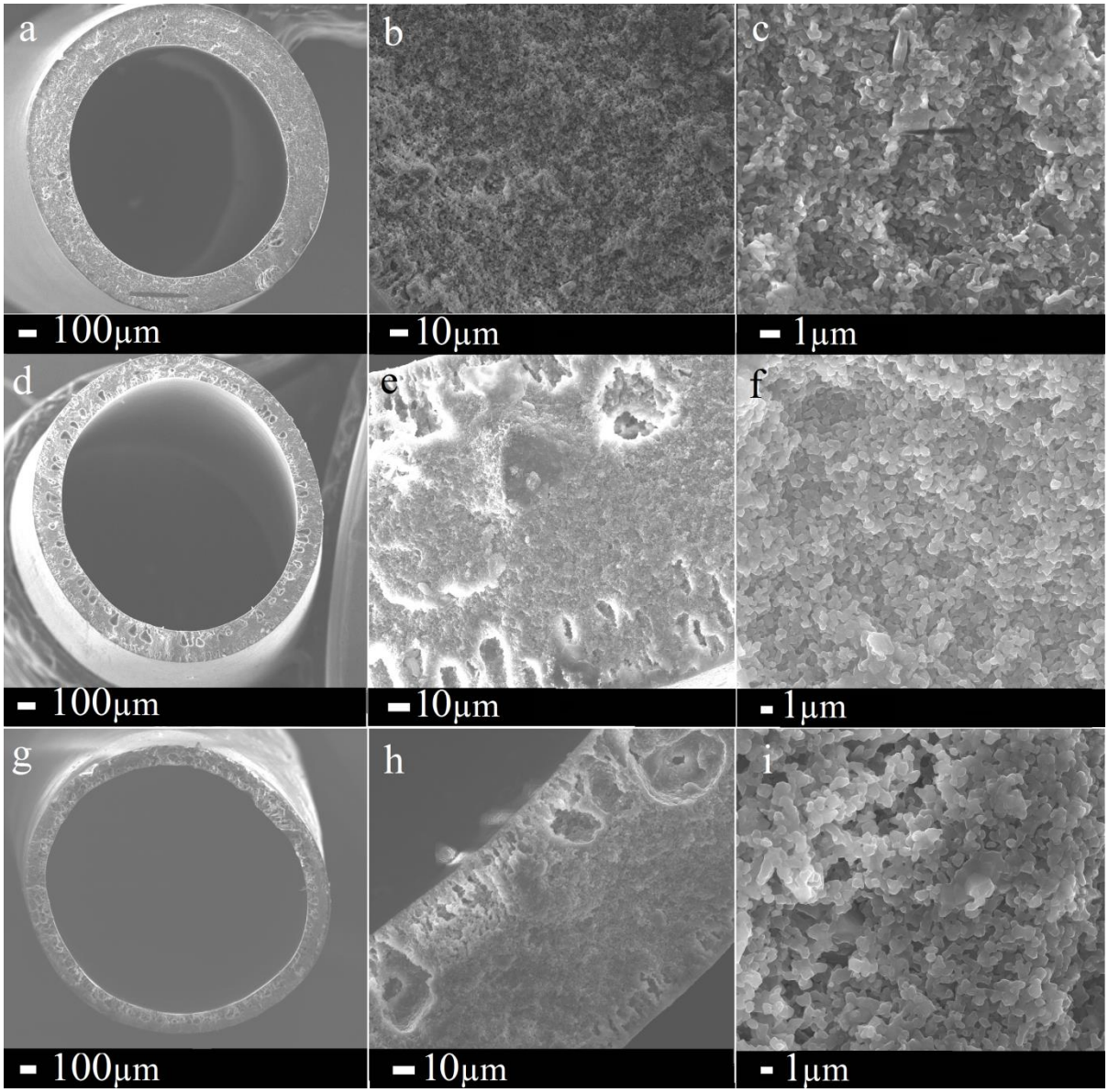

Fig. 5.3 Cross sectional SEM images of $NiAl_2O_4$ / Al_2O_3 hollow fibre membranes sintered at 1500 ^oC for 5 hours at various magnifications. (a) – (c) is pure alumina, (d) – (f) contained 2.00 wt% $NiAl_2O_4$ and (g) – (i) contained 10.0 wt% $NiAl_2O_4$.

The change in flexural strength of the $NiAl_2O_4$ / Al_2O_3 hollow fibre membranes with the loading of $NiAl_2O_4$ is explained by shrinkage and bond formation during the sintering stage. From Fig. 5.3, at low magnifications, the cross sectional morphology of all three samples of different $NiAl_2O_4$ loading were similar, with a sponge-like dense central layer and relatively porous finger-like structure in the outer and inner wall of the hollow fibre. The dense layer in the centre of the hollow fibre membranes contributed significantly to its mechanical properties including flexural strength. Fig. 5.3(c), (f) and (i) showed the dense layer of $NiAl_2O_4$ / Al_2O_3 hollow fibre membranes. In comparison, as observed in Fig. 5.3(i), the 10.0 wt% $NiAl_2O_4$ sample which achieved the lowest flexural strength among these three

compositions, showed larger pores and cracks than the other two samples. The packing of particles in the 10.0 wt% $NiAl_2O_4$ sample was less dense than samples of the other two compositions. With the same extrusion and sintering condition, the change in flexural strength of the $NiAl_2O_4$ / Al_2O_3 was a result of shrinkage and particle packing through the variation of composition. The reinforcement mechanism is explained in details in Section 5.3.4.

5.3.3 Morphology and microstructure of $NiAl_2O_4$ / Al_2O_3 hollow fibre membranes

To ensure the nickel nanowires were damaged neither over the applied ball-milling time and speed nor during the hollow fibre precursor extrusion process, SEM images of the cross-section and inner wall of the hollow fibre membrane precursor were obtained and shown in Fig. 5.4. No nanowire was observed in the outer surface of the precursors. This is a consequence of air gap delaying the phase exchange towards the outer direction. In the slurry preparation process, polymer was dissolved in NMP while nickel nanowires were dispersed in NMP. When inner coagulant entered the slurry, NMP was drawn towards the inner wall of the precursor together with the nanowires dispersed in it. The nanowires were caught by the solidified inner surface of the precursor and hence did not leave the system with NMP. After the sintering process at 1500 ^oC in air, as seen in Fig. 5.3, there was no sign of nanowire in all cross-sectional, inner and outer surfaces of the $NiAl_2O_4$ / Al_2O_3 hollow fibre membranes.

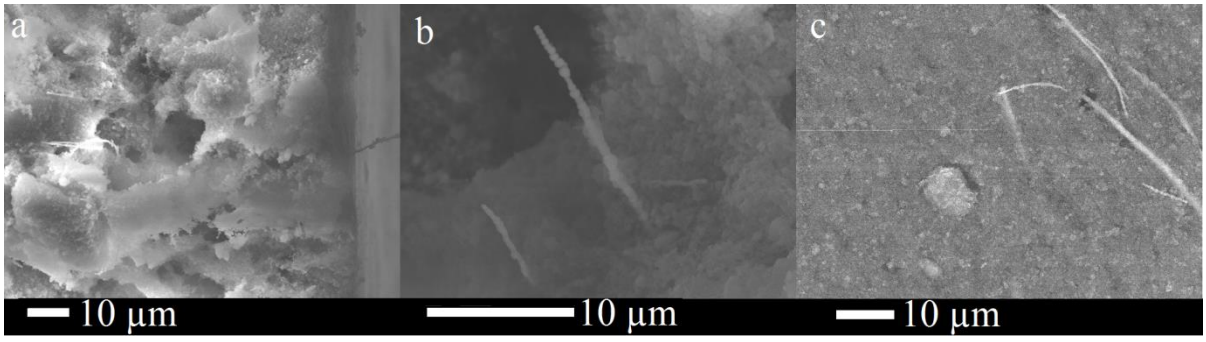

Fig. 5.4 SEM images of hollow fibre precursors with Al_2O_3 to Ni nanowire of 1:0.0347 by mass (a) and (b) are the cross sectional surface at different magnifications and (c) is the inner surface.

In a typical phase inversion process for producing hollow fibre membrane precursors, water as a non-solvent of polymer is used as both internal and external coagulant. [35, 76, 114] Some literatures have reported the mixing of polymer solvent NMP and ethanol a weak coagulant into water for internal and external coagulation for the preparation of highly porous

hollow fibre membranes, in which highly porous finger like structure dominated their cross-section [31, 32]. The polymer solubility and flow rate of the coagulants, together with the size of air gap, determine the rate of phase exchange towards the inner and outer directions and hence the cross sectional morphology of the hollow fibre membrane precursors. Low coagulant flow rate and narrow air gap lower precipitation rate and hence favour the formation of thick sponge-like layer. [33] The mechanical strength of hollow fibre membranes, which is the key study of this paper, is mainly contributed by the sponge-like layer. To focus on the effect of $NiAl_2O_4$ formed by nickel nanowire on the flexural strength of the $NiAl_2O_4$ / Al_2O_3 hollow fibre membranes, the sponge-like region in the cross-section was maximized in this experiment in order to minimize the effect of cross-sectional structure variation on flexural strength. Due to the simplicity of the homemade hollow fibre extrusion system used in this experiment, a minimum internal coagulant flow rate was necessary to push the hollow fibre precursor out of the spinneret. A certain air gap size was also needed to prevent blockage of the spinneret. The composition of internal coagulant was therefore adjusted for the formation of sponge-like structure. Fig. 5.5 shows the cross-sectional structures of alumina hollow fibres extruded using water, 50 vol% ethanol / water and 75 vol% ethanol / water as internal coagulant. The internal coagulant flow rate was kept at 3 mL/min and the air gap stayed at 1.3 cm. The hollow fibre precursors were sintered under the same condition of 1500 ^{o}C in air. Using water as internal coagulant formed thick finger-like porous structure close to the inner wall. Addition of ethanol a weaker coagulant than water lowered the overall coagulation power of the internal coagulant and hence lowered the precipitation rate towards the inner wall of the hollow fibre precursor. With 50 vol% of ethanol in the internal coagulant, the cross-section structure was close to fully sponge-like. Increasing ethanol in internal coagulant up to 75 vol% over weakened its coagulation power, hence failed to keep the cylindrical shape of the hollow fibre before it passed through the air gap and reached the external coagulant. 50 vol% ethanol / water was therefore selected as the internal coagulant for the extrusion of all the nickel nanowire / alumina hollow fibre membrane precursors.

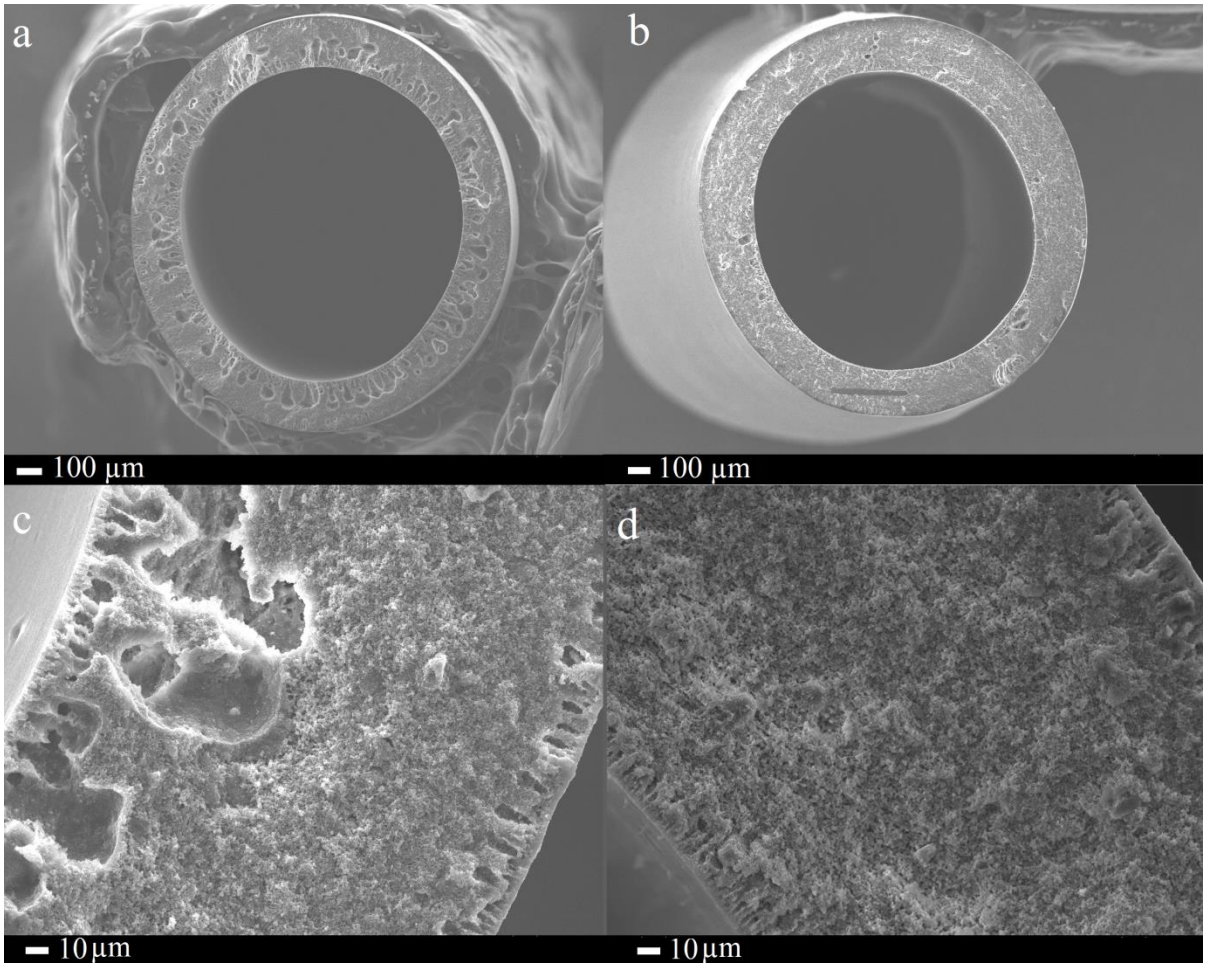

Fig. 5.5 SEM images of sintered pure alumina hollow fibre membrane extruded with different internal coagulant. (a) and (c) were obtained with water as internal coagulant, (b) and (d) were had 50 vol% ethanol / water as internal coagulant.

The microstructures and particle packing of all samples with $NiAl_2O_4$ loading from 0 to 15.0 wt% are shown in Fig. 5.6. The SEM images were taken from the cross section, inner and outer surfaces of the sintered ceramic hollow fibre membranes. Porous structure is shown for the view of all surfaces in all samples. The pure alumina hollow fibre membrane showed the smallest grain size of less than 300 nm with a narrow size range. From the cross sectional view, particles in the pure alumina sample were loosely packed with large pores and gaps in between. With $NiAl_2O_4$ included in the alumina matrix, larger grains of 1 µm could be observed. Grain growth and neck growth were more obvious and more bonds between grains were formed with increasing $NiAl_2O_4$ loading. This could be explained by the reaction between alumina and NiO which was formed by oxidized Ni nanowires. This solid-solid reaction occurred when alumina and NiO were physically in contact at a temperature over 1100 ^oC. $NiAl_2O_4$ was formed as a new phase at the alumina-NiO boundaries [122, 127]. Larger grains were formed when alumina particles combined with NiO and turned into

$NiAl_2O_4$. Formation of the $NiAl_2O_4$ therefore also helped joining adjacent alumina particles. When the $NiAl_2O_4$ content was increased over 2.00 wt%, some oversize grains as large as 2 μm appeared. As the solid-solid alumina-NiO reaction is non-directional, grains were bonded in random directions. The broadness of grain size and random bonding of grains hindered further shrinkage and pore closure in the ceramic membrane, hence lowered the membrane flexural strength and increased porosity of the membrane which is presented in Section 5.3.5. The inner surface of the hollow fibre membrane showed the least changes with composition.

Inner surface of all samples had the highest surface porosity in comparison with the cross sectional and outer surfaces. Enlarged grain size, grain growth and bonding in random directions were not obvious until the amount of $NiAl_2O_4$ was increased up to 10.0 wt%, as seen from Fig. 5.6(n) and (q). Some small loose particles were also observed in the inner surface of the 10.0 wt% and 15.0 wt% $NiAl_2O_4$ samples. Apart from having higher surface density, the outer surface of $NiAl_2O_4$ / Al_2O_3 showed similar changes with composition as their cross sectional surfaces. The outer surface of the 2.00 wt% $NiAl_2O_4$ sample was close to fully dense as seen in Fig. 5.6 (i). With 5.00 wt% or above of $NiAl_2O_4$, large grains and grains joined in random directions were present. Some small loose particles were also observed in the outer surface of the 10.0 wt% and 15.0 wt% $NiAl_2O_4$ / Al_2O_3 hollow fibre membranes.

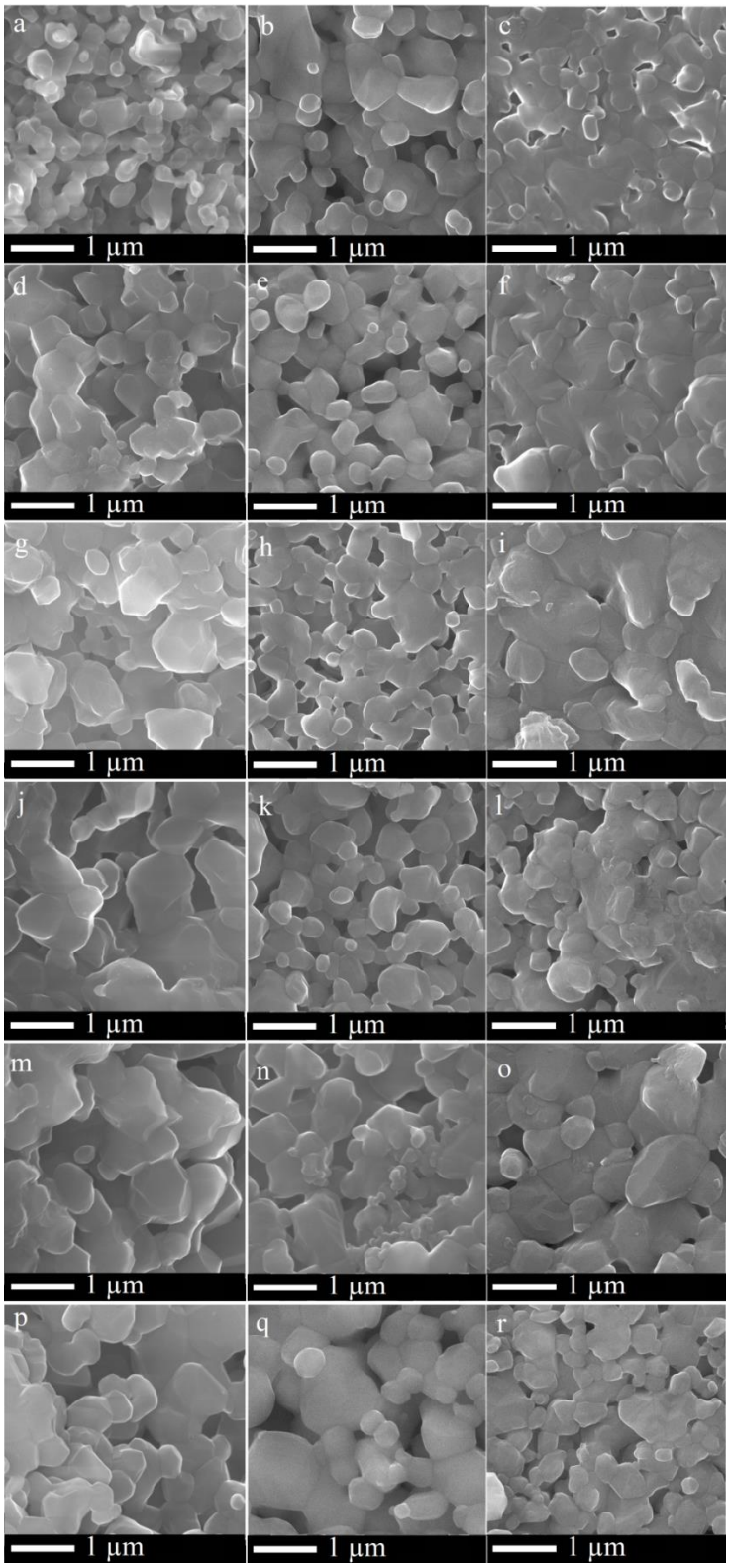

Fig. 5.6 SEM images of microstructure of 0 – 15.0 wt% $NiAl_2O_4$ / Al_2O_3 hollow fibre membranes. (a) – (c) was pure alumina, (d) – (f) contained 1.20 wt% $NiAl_2O_4$, (g) – (i) contained 2.00 wt% $NiAl_2O_4$, (j) – (l) contained 5.00 wt% $NiAl_2O_4$, (m) – (o) contained 10.0 wt% $NiAl_2O_4$, (p) – (r) contained 15.0 wt% $NiAl_2O_4$. The left column showed cross-sections, middle column showed inner surfaces and the right column showed outer surfaces.

5.3.4 Reinforcement mechanism

Formation of only 2.00 wt% of $NiAl_2O_4$ in alumina hollow fibre membrane improved its flexural strength by 1.5 times. The reinforcement effect was a combination of crack deflection due to thermal expansion mismatch between alumina and $NiAl_2O_4$ and the crack bridging mechanism.

The effect of thermal expansion mismatch between alumina and $NiAl_2O_4$ on flexural strength has been explained in details in our previous work. [144] The stress field formed by different contracting rates of alumina and $NiAl_2O_4$ at the post-sintering cooling stage created a closure force that deflects crack growth along grain boundaries. In this work, thermal expansion mismatch also took a role in flexural strength enhancement of ceramic hollow fibre membranes, while the difference was the positioning of $NiAl_2O_4$ the phase with a higher thermal expansion coefficient. Instead of existing as individual particles distributed evenly across the ceramic hollow fibre membrane, the $NiAl_2O_4$ in this work was structured as chains. As seen in Fig. 5.7(a), the Ni nanowires used as raw materials for the extrusion of hollow fibre precursor was formed by joined Ni particles. Many studies have been carried out on the oxidation of Ni nanowires to NiO wires through heat treatment in open air and proved that under atmospheric pressure, oxidation occurs when the temperature is over 500 ^oC. [147, 153, 160] According to literatures that reported the melting temperature and behaviour of Ni nanowires, Ni nanowires with a diameter as small as 2.5 nm have a melting point of over 900 ^oC and melting point increases with diameter. The hollow fibre precursors in this experiment were all heat treated at 580 ^oC in air for the removal of polymer binder, which is below the melting temperature of Ni nanowires and suitable for its oxidation to occur. These support that the Ni nanowires were kept at nanowire structure when being oxidized. Fig. 5.7(b) and (c) show the SEM images of Ni nanowires undergone heat treatment in air at 1100 ^oC and 1500 ^oC, which were the minimum temperature for the solid-solid reaction between alumina and NiO and the sintering temperature of the ceramic hollow fibre membranes in this experiment respectively. The diameter of the wires has increased to about 1 μm after heat treatment in air. Its colour turned from black to green, which indicated the oxidation of Ni nanowires to micron size NiO wires. At both temperatures the NiO remained as wires without separating into individual particles. Many studies on $NiAl_2O_4$ have proved its formation at the interface of solid alumina and NiO. [93, 122, 134] Chains structures were found in the $NiAl_2O_4$ / Al_2O_3 hollow fibre membranes as shown in Fig. 5.7 (d) and (e) which proved the formation of $NiAl_2O_4$ chains through the reaction between alumina and NiO wires.

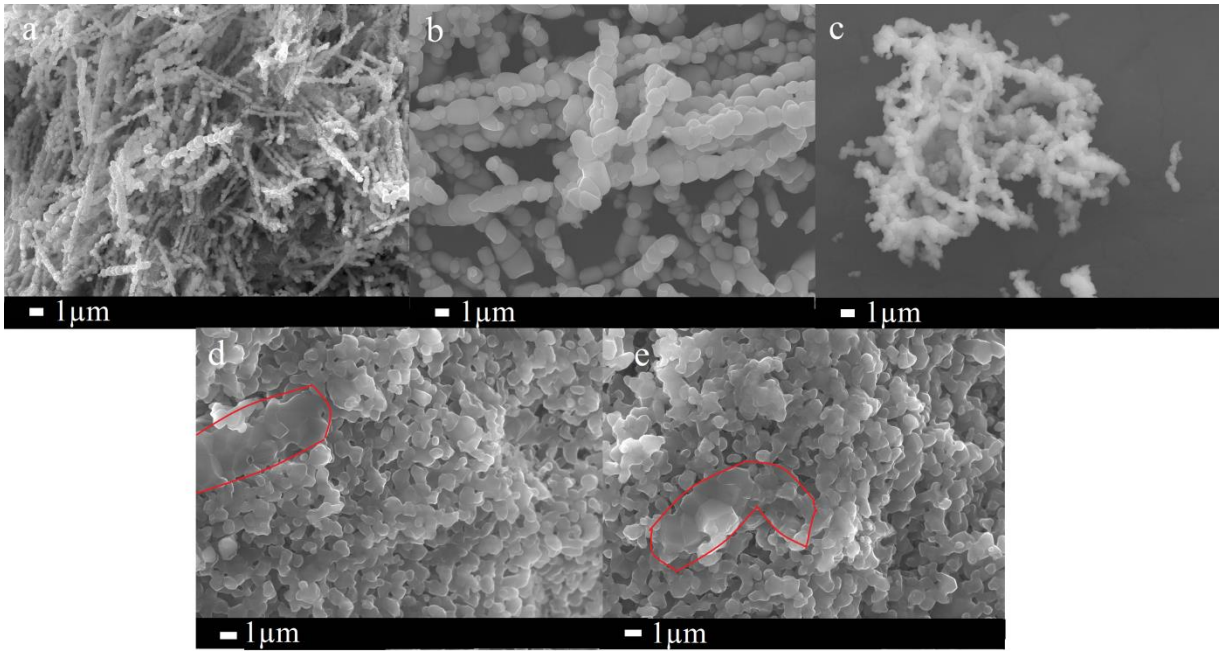

Fig. 5.7 Nickel nanowires undergone different heating profiles in air (a) raw nickel nanowires included in hollow fibre membrane precursors, (b) after heat treatment of 580 ^{o}C for three hours then 1100 ^{o}C for 5 hours, (c) after heat treatment of 580 ^{o}C for three hours then 1500 ^{o}C for 5 hours, (d) $NiAl_2O_4$ chain formation in 5.00 wt% $NiAl_2O_4$ sample and (e) $NiAl_2O_4$ chain formation in 10.0 wt% $NiAl_2O_4$ sample.

A schematic diagram of reinforcement mechanism of $NiAl_2O_4$ chains in porous alumina membrane is shown in Fig. 5.8. Crack bridging and crack deflection were the two major toughening mechanisms [83] that contributed to the reinforcement of the ceramic hollow fibre membranes. The thermal expansion mismatch between $NiAl_2O_4$ and alumina created a stress field that deflected crack growth along the alumina grain boundaries to the interface of $NiAl_2O_4$ chain and alumina. This change in crack growth direction increased its resistance and hence toughened the alumina. The crack growth direction would also no longer be perpendicular to the stress direction, which also hindered further growth of the crack. Crack bridging of ceramic for reinforcement purpose has been reported in detail in many literatures. [85, 158] The role of fibres and chains as a bridging medium is to share partial or full stress in the ceramic matrix as a crack develops and disperses the stress intensity through fibre pull-out. Beyond failure of the ceramic matrix, the bridging material remains intact and bridges the cracked surfaces, hence complete failure of the material only occurs when the stress is sufficient to cause bridges failure. $NiAl_2O_4$ as an inflexible ceramic was not expected to show much pull-out, yet the $NiAl_2O_4$ chains formed by closely joined particles were believed to be tougher than the porous ceramic matrix and hence could bridge cracked matrix surfaces.

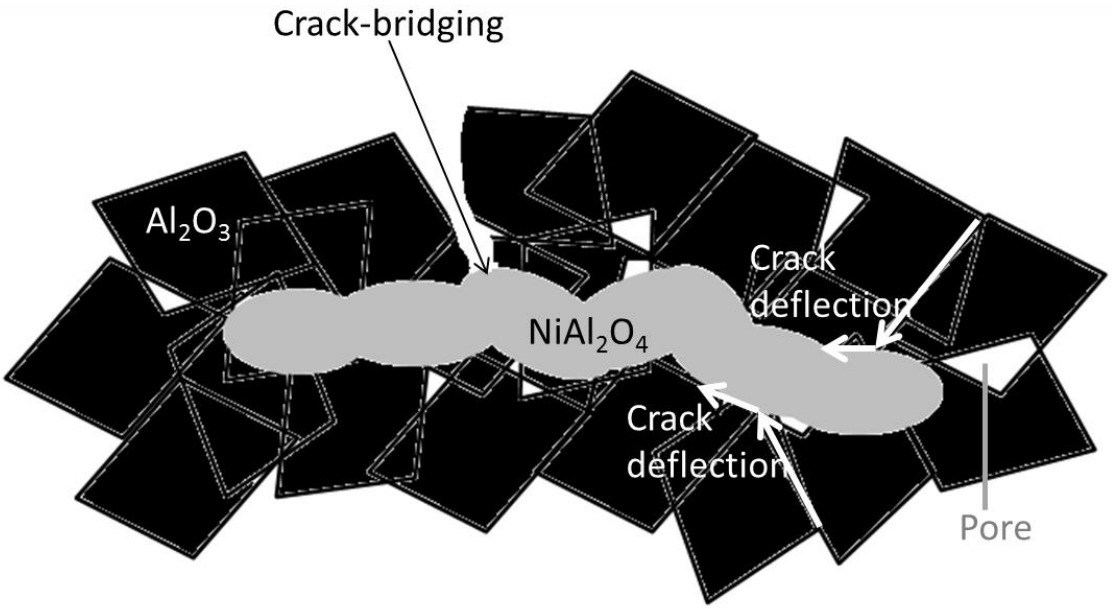

Fig. 5.8 Schematic diagram of reinforcement mechanism of $NiAl_2O_4$ chains in porous alumina membrane.

5.3.5 Porosity

Porosity of hollow fibre membranes is an important factor that determines their trans-membrane fluid resistance and hence liquid fluxes and energy consumption in a separation process. The porosities of all $NiAl_2O_4$ / Al_2O_3 hollow fibre membranes were obtained by Archimedes' principle and are shown in Fig. 5.9. The pure alumina sample showed a porosity of 44%. As the loading of $NiAl_2O_4$ increased, the porosity of the $NiAl_2O_4$ / Al_2O_3 hollow fibre membranes dropped down to 35% as the amount of $NiAl_2O_4$ reached 2.00 wt%. Porosity was regained as the $NiAl_2O_4$ loading went over 2.00 wt%. The effect of $NiAl_2O_4$ loading on porosity was less significant as $NiAl_2O_4$ loading increased further. The sample that contained 15.0 wt% of $NiAl_2O_4$ which was the highest out of all samples prepared had the highest porosity of 56%. The large difference in porosity between the ceramic hollow fibre membranes of different compositions can also be observed in Fig. 5.6, which showed the increase in grain density from pure alumina to 2.00 wt% $NiAl_2O_4$ and large pores and cracks were regained with further increased $NiAl_2O_4$ loading.

There is no clear definition on the minimum porosity required in a liquid separation membrane for sufficiently low trans-membrane resistance as it is not the only factor that contributes to the separation performance of a membrane. Burggaraaf stated that the porosities of membrane components ranged widely from 20% to 60%, with 30% to 40% being commonly reported. [36] Zhang et al. stated that a minimum open porosity of 35% is necessary to lower fluid resistance in a porous ceramic membrane. [32] The porosity of $NiAl_2O_4$ / Al_2O_3 hollow fibre membranes prepared ranged from 35% to 56%, which fell into the ranges reported by Burggaraaf and Zhang et. al.

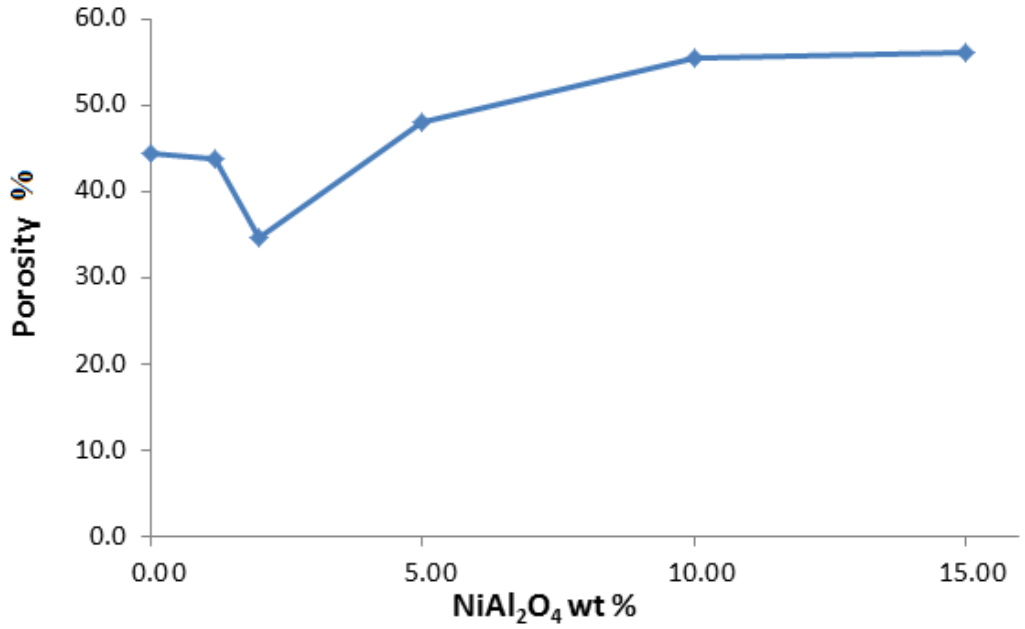

Fig. 5.9 Porosity of $NiAl_2O_4$ / Al_2O_3 hollow fibre membranes with $NiAl_2O_4$ loading ranged from 0 to 15.0 wt%.

5.3.6 Pure water flux

For practical industrial scale applications, apart from mechanical properties, the liquid permeability of ceramic hollow fibre membranes is an indicator for the efficiency of a separation process. The pure water flux of the $NiAl_2O_4$ / Al_2O_3 hollow fibre membranes were measured under a feed pressure of 2 bar and reported in Fig. 5.10. Pure water flux of a membrane is affected by both overall porosity and porosity of the selective layer. The SEM images in Fig. 5.6 showed that for all samples of pure alumina and $NiAl_2O_4$ / Al_2O_3 hollow fibre membranes, the inner surface contained significantly larger pores than its outer surface, with some pores in the inner wall as large as 1 µm. The outer surface layer was therefore the active layer of these ceramic hollow fibre membranes, where separation is carried out by sieving mechanism. The pure water flux of 0 – 15.0 wt% $NiAl_2O_4$ / Al_2O_3 hollow fibre

membranes ranged from 35 – 601 L/m^2.h.bar which was significantly lower than those presented in our previous work on $NiAl_2O_4$ reinforced ceramic hollow fibre membrane. [145] The thick relatively dense sponge-like layer was a main source of fluid resistance. The right column of Fig. 5.6 showed the SEM images of the outer surface of all samples. The selective layers of all samples were porous, with even grain structure and distribution of pores.

As expected, the enhancement of flexural strength with the presence of $NiAl_2O_4$ decreased both the overall porosity and pure water flux. The 2.00 wt% $NiAl_2O_4$ / Al_2O_3 hollow fibre membranes achieved the highest flexural strength and an overall porosity of 35% showed a low pure water flux of only 10% of that of the pure alumina sample. The low pure water flux was explained by the highly dense selective layer as observed in Fig. 5.6(i), which limited number of pores was shown. In comparison with the other samples, the 2.00 wt% $NiAl_2O_4$ sample had the densest outer surface and had the smallest and lowest number of pores. Apart from the number of pores, the density of cracks and slit-like pores also decreased with increasing $NiAl_2O_4$ content until 2.00 wt%, then increased with further increasing loading of $NiAl_2O_4$. Same as the overall porosity, pure water flux was increased with the amount of $NiAl_2O_4$ when the $NiAl_2O_4$ loading was over 2.00 wt%. This is a combined effect of increasing overall porosity and surface porosity. The 15.0 wt% $NiAl_2O_4$ sample showed a highest water flux and surface porosity with large pores and cracks of about 800 nm as seen in Fig. 5.6(r).

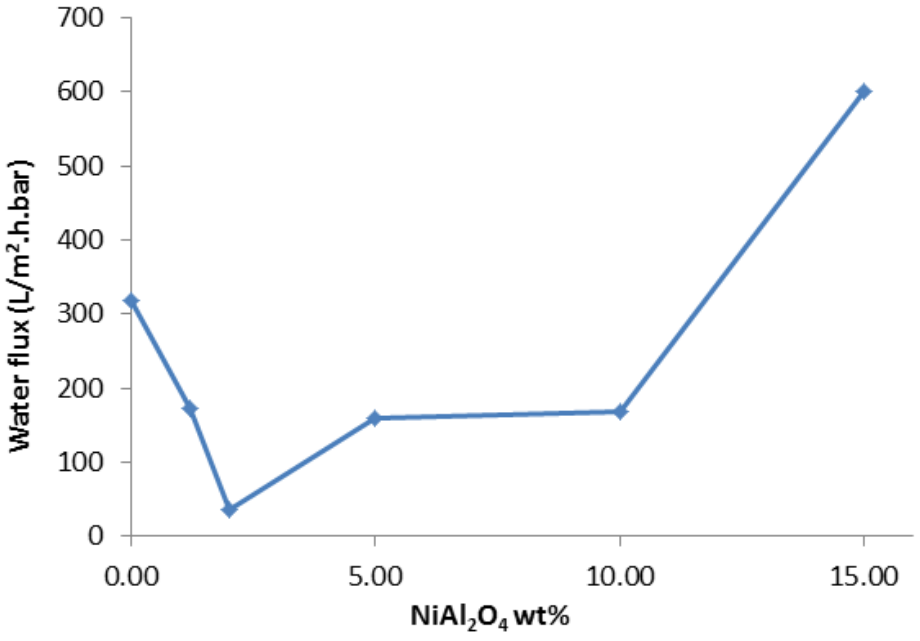

Fig. 5.10 Porosity of $NiAl_2O_4$ / Al_2O_3 hollow fibre membranes with $NiAl_2O_4$ loading range from 0 to 15.0 wt% measured at a feed pressure of 2 bar.

5.3.7 Pore size distribution

The overall pore size distribution of four samples – pure alumina, 2.00 wt% $NiAl_2O_4$, 5.00 wt% $NiAl_2O_4$ and 15.0 wt% $NiAl_2O_4$ obtained from mercury porosimetry are shown in Fig. 5.11. Two pore size distributions appeared in each overall pore size distribution curve. The binomial distributions of pore size diameter over 60 µm represented the finger-like layers and the sharp peaks below 2 µm represented the active layer and the sponge-like layer of each sample, as visually observed from SEM images in Fig. 5.3 and Fig. 5.6. The pore size of finger-like layers was mainly a consequence of the precursor extrusion process and the binomial distributions were a result of inner and outer finger-like layers of each sample.

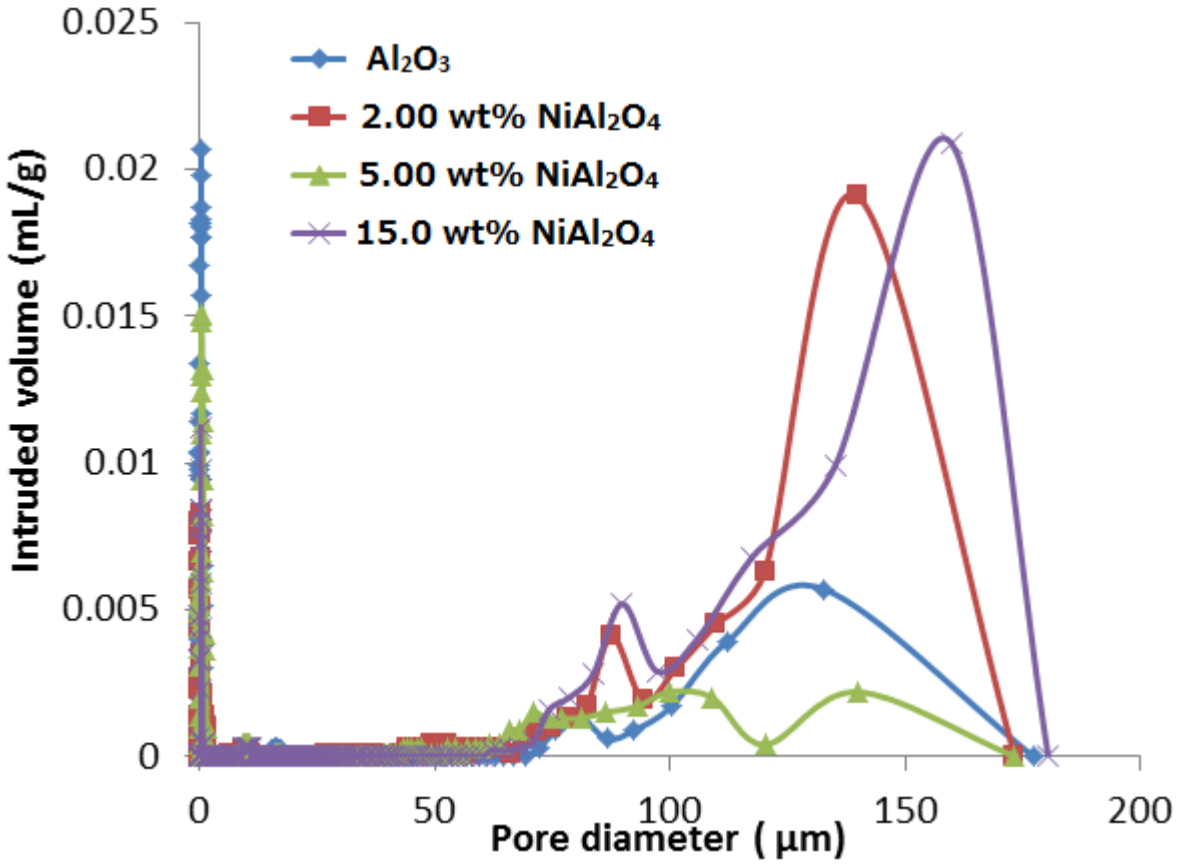

Fig. 5.11 Overall pore size distribution of pure Al_2O_3, 2.00 wt% $NiAl_2O_4$, 5.00 wt% $NiAl_2O_4$ and 15.0 wt% $NiAl_2O_4$ hollow fibre membranes.

The pore size distribution of the selective layer, which is also the active layer of a membrane, determines the size range of particles that a membrane could filter off and hence its suitability in a separation process. Minimum broadness of pore size range in the membrane active layer contributes to the effectiveness of a separation process. Fig. 5.12 showed the same pore size distribution curves as Fig. 5.11 at a different scale, with the X-axis in the range of 0 – 2 µm, for a clear display of the pore size distribution of the active layer and sponge-like centre of

each sample. Although not as obvious as that representing the finger-like layers, binomial distribution was also shown in each pore size distribution curve in Fig. 5.12. As observed in Fig. 5.6, pores on the outer surface of all samples were smaller than 0.5 µm. It is therefore reasonable to conclude that the left peak of the binomial curve gave the pore size distribution of the active layer. The pore size on the active layer of the ceramic hollow fibre membranes prepared ranged from 0.074 – 0.30 µm.

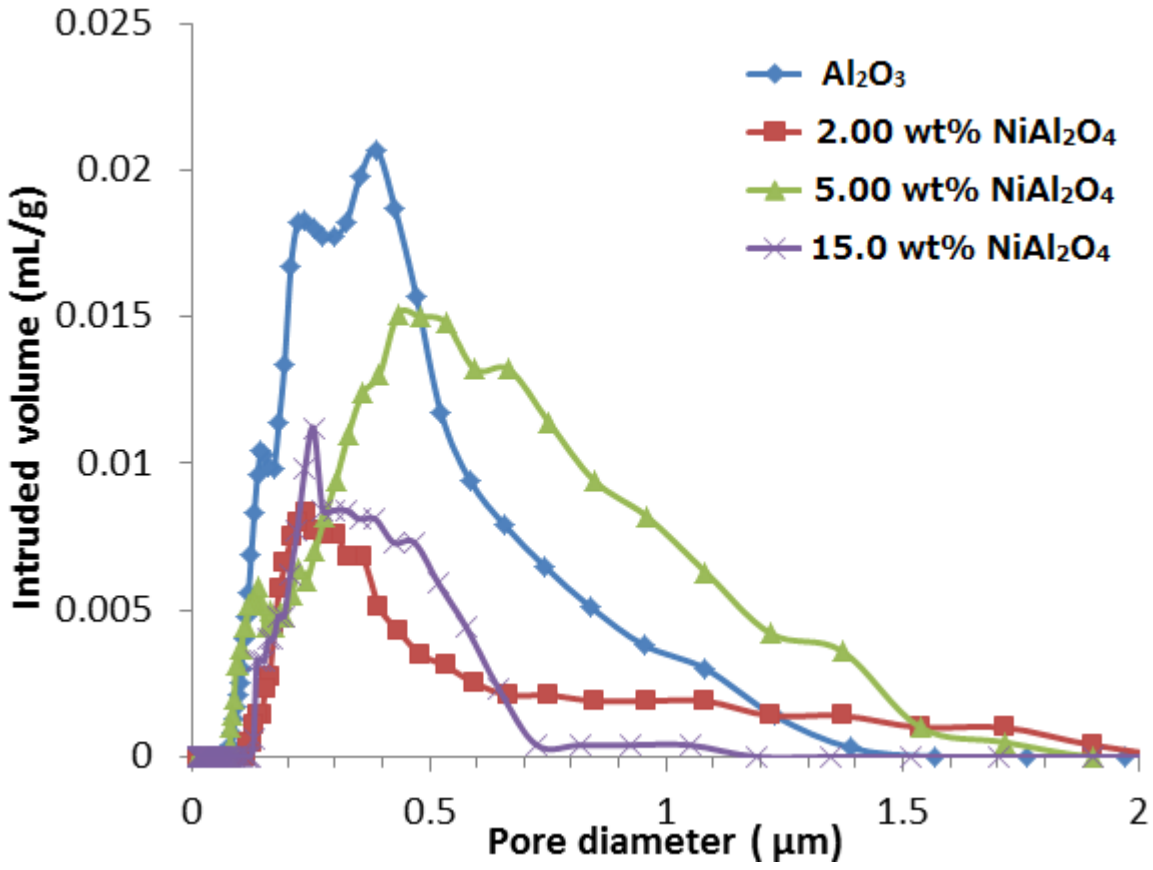

Fig. 5.12 Pore size distribution of the active layer and sponge-like centre of pure Al_2O_3, 2.00 wt% $NiAl_2O_4$, 5.00 wt% $NiAl_2O_4$ and 15.0 wt% $NiAl_2O_4$ hollow fibre membranes.

5.4 Conclusions

$NiAl_2O_4$ was formed in porous alumina hollow fibre membrane for flexural strength enhancement using nickel nanowire as a raw material. The hollow fibre precursors with nickel nanowire included was prepared by phase inversion method, followed by sintering in 1500 ^oC in air for the purpose of particle bonding and grain growth. During the heat treatment in air atmosphere, nickel nanowires were oxidized into NiO wires which would react with alumina and formed $NiAl_2O_4$ chains. The final products contained 0 to 15.0 wt%

$NiAl_2O_4$. Flexural strength was increased by the presence of $NiAl_2O_4$ up to a $NiAl_2O_4$ loading of 2.00 wt%. The strengthening effect was a consequence of crack growth deflection caused by thermal expansion mismatch between $NiAl_2O_4$ and alumina and crack bridging effect of the $NiAl_2O_4$ chains formed. Further increase in $NiAl_2O_4$ loading led to a decrease in flexural strength. The 2.00 wt% $NiAl_2O_4$ / Al_2O_3 sample showed the highest flexural strength of 172 MPa and 35% porosity but a low pure water flux of 35 L/m^2.h.bar. For a balance between flexural strength and liquid flux, the 5.00 wt% $NiAl_2O_4$ sample which had a porosity of 48% and a pure water flux of 160 L/m^2.h.bar while keeping its flexural strength at 135 MPa was more suitable for practical applications. The active layer pore size of 5.00 wt% $NiAl_2O_4$ / Al_2O_3 hollow fibre membrane ranged from 0.079 – 0.24 μm. The $NiAl_2O_4$ / Al_2O_3 membranes prepared were suitable for microfiltration separation processes.

Chapter 6 Nickel aluminate hollow fibre membrane

Overview

Nickel aluminate ($NiAl_2O_4$) was formed in the alumina (Al_2O_3) matrix in the previous chapters for reinforcement purpose of the ceramic membranes. Despite being a non-toxic ceramic with high thermal and chemical stability, the use of pure $NiAl_2O_4$ as membrane has never been reported. This chapter reported the preparation of pure $NiAl_2O_4$ hollow fibre membrane through the phase-inversion and sintering method. $NiAl_2O_4$ was formed by the complete solid-solid reaction between homogeneously mixed alumina and nickel (II) oxide (NiO) powder in 1 : 1 molar ratio. A sintering time of 10 hours and sintering temperature of 1600 ^oC was found to be sufficient for the formation and sintering of $NiAl_2O_4$. The maximum flexural strength of the $NiAl_2O_4$ hollow fibre membrane achieved in this chapter was 101 MPa with a high porosity of 55% and pure water flux of 862 $L/m^2.h.bar$ at a feed pressure of 2 bar after being sintered at 1630 ^oC. This flexural strength is higher than ceramic hollow fibre membranes of similar porosity prepared in previous chapters and comparable to yttria-stabilized zirconia (YSZ) samples reported in other literatures. A further increase in flexural strength is expected if porosity could be further lowered by increasing the sintering temperature. The active layer pore size of all the $NiAl_2O_4$ hollow fibre membranes prepared fell into the microfiltration range. The active layer pore size of the sample with highest flexural strength ranged from 0.05 – 0.14 μm. The static corrosion test showed high stability of the $NiAl_2O_4$ hollow fibre membrane under acidic and basic conditions, which proved the suitability of chemical cleaning for flux recovery in industrial applications of $NiAl_2O_4$ membranes.

6.1 Introduction

Nickel aluminate spinel ($NiAl_2O_4$) is a non-toxic ceramic materials with high melting temperature [119] and strong resistance to acids and bases. [120] It is formed by the reaction between alumina and a source of nickel ion under high temperature calcination. Combinations of raw materials that have successfully formed $NiAl_2O_4$ include α-alumina (α-Al_2O_3) with nickel (II) oxide (NiO) [122, 123, 125], aluminium nitrate ($Al(NO_3)_3$) with nickel (Ni) [121] and aluminium hydroxide ($Al(OH)_3$) with nickel nitrate ($Ni(NO_3)_2$). [126] The oxidation of nickel aluminide (NiAl) single crystal with (1 1 1) orientation have also formed $NiAl_2O_4$. [124]

$NiAl_2O_4$ has been a by-product in the waste treatment industry for the removal of nickel a toxic metal. Because of the high chemical stability of $NiAl_2O_4$, reacting nickel with alumina and formed $NiAl_2O_4$ was a safe solution to capture and store nickel for disposal. [133, 134] Apart from acting as a by-product, $NiAl_2O_4$ has also been formed in dense alumina for reinforcement which was a result of boundary strengthening effect caused by the thermal expansion mismatch between $NiAl_2O_4$ and alumina. [93] The previous chapters of this thesis $NiAl_2O_4$ has introduced as a reinforcement medium in porous alumina and alumina hollow fibre membranes for the enhancement of flexural strength, based on the same boundary strengthening effect. This improvement in mechanical property further extent the pressure limit that alumina hollow fibre membranes could withstand for and increased their service life.

$NiAl_2O_4$ / Al_2O_3 hollow fibre membranes reported in this thesis were multi-phase systems formed by the solid state reaction between NiO and α-alumina. It has been reported that a sufficiently long mixing time of a 1:1 molar ratio NiO and alumina powder could create a homogeneous mixture that resulted in a complete solid-solid reaction and formed pure $NiAl_2O_4$. [127] Despite its high thermal and chemical stability and existence as a single phase, as far as our knowledge, pure $NiAl_2O_4$ has never been used as a membrane.

This chapter reports the preparation of pure $NiAl_2O_4$ hollow fibre membrane through the phase-inversion and sintering method. The major differences between the preparation of $NiAl_2O_4$ and that of alumina hollow fibre membrane were the higher requirement on homogeneity of the mixture slurry for precursor extrusion and the extra time taken for the NiO-Al_2O_3 solid-solid reaction to complete before sintering of $NiAl_2O_4$ happened. The relationship between sintering conditions and flexural strength of $NiAl_2O_4$ hollow fibre membrane was studied and a suitable sintering condition for this ceramic hollow fibre membrane was determined. Porosity, pore size distributions and pure water flux of the $NiAl_2O_4$ hollow fibre membranes were tested to show determine their application and efficiency in a separation process. The chemical stability of these $NiAl_2O_4$ hollow fibre membranes in acidic and basic solvents was also tested to further understand its practicality.

6.2 Experimental

6.2.1 Materials

Alumina powder of a particle diameter <1 μm (alpha phase, 99.98 metals basis, APS powder, surface area 10 m^2/g) purchased from Alfa Aesar, A Johnson Matthey Company was used as a raw material for the preparation of ceramic hollow fibre membrane. Polyethylsulfone (PESf) [BASF, E6020P] was used as a binder in hollow fibre extrusion. 1-methyl-2-pyrrolidone (NMP) purchased from Sigma-Aldrich was used as a solvent of the powder and polymer. Nickel carbonate, basic hydrate (BNC) (99.9% trace metal basis) purchased from Sigma-Aldrich was a source of nickel for the synthesis of nickel (II) oxide, as described in Section 4.2.1 in Chapter 4.

6.2.2 Preparation of nickel aluminate hollow fibre membranes

Phase inversion and sintering method was used to prepare the nickel aluminate hollow fibre membranes. PESf which act as a binder for the hollow fibre membrane precursor was dissolved in NMP the solvent, at the ratio of 1:9 by mass. By stoichiometry, every mole of $NiAl_2O_4$ is formed by reaction between one mole of Al_2O_3 and one mole of NiO. A powder mixture of alumina and NiO at a ratio of 1:0.73 by mass, which was 1:1 by mole, was therefore prepared. The overall mixture formed by 50 wt% PESf/NMP and 50 wt% powder was ball-milled at 30 rpm for 120 hours to form homogeneous slurry.

The ball-milled slurry was degased at room temperature for 20 minutes and was transferred to a stainless steel tube-in-orifice spinneret where it was extruded into hollow fibre precursors. Nitrogen gas was used to pressurize the spinneret for the extrusion process. The outer and inner diameter of the orifice was 2.8 mm and 1.4 mm respectively. Tap water of room temperature 20 ^oC was used as external coagulant. The internal coagulant was of 50 vol% ethanol and 50 vol% tap water and its flowrate was kept at 3 mL/min through the extrusion process. The air gap was fixed at 1.3cm. The hollow fibre precursors were left in tap water of 20 ^oC for 24 hours for complete phase exchange and solidification. A schematic diagram and the full setup of the extrusion process were shown in Fig. 4.1 and Fig. 4.2 in Chapter 4 respectively.

The hollow fibre precursor was heated to 580 ^oC in air at a rate of 5 ^oC/min and was held for 3 hours in a furnace to remove the polymer binder. They were then sintered at different temperatures from 1400 ^oC to 1640 ^oC for 5 hours or 10 hours for the purpose of grain growth

and bonding. The samples were left in the furnace to be cooled down naturally to room temperature to prevent cracking caused by a sudden temperature change.

6.2.3 Membrane characterizations

X-ray diffraction (XRD) was used for identifying the phase present in the samples and confirming the formation of $NiAl_2O_4$ and the absence of excess Al_2O_3 and NiO. The XRD analysis was carried out in a Rigaku MiniFlex 600 with a scan range 10^o-90^o and a step size of 2^o.

The cross-sectional surface, inner and outer surface of the hollow fibre membranes were observed under a JEOL 7001F scanning electron microscope (SEM). The cross-sectional surfaces of the hollow fibres were obtained by manual snapping at room temperatures. All samples were sputter-coated with a 0.5 nm platinum layer. The SEM images were taken at 30 kV.

The flexural strengths of the samples were determined by the three-point bending test which was carried out in an Instron Micro Tester 5848. A 2 kN load cell (Instron Calibration Laboratory, United Kingdom), 18mm span and crosshead speed of 0.25 mm/min were used throughout the test. The full setup of the three-point bending test was shown in Fig. 3.2 in Chapter 3. The crosshead was stopped once fracture occurred in the hollow fibre. Five runs for each sample were performed. The flexural strength, σ_F, of each single hollow fibre was calculated from the following equation [35]

$$\sigma_F = \frac{8FLD}{\pi(D^4 - d^4)}$$

F is the force measured when the fibre fractured. L is magnitude of the span, which was 18 mm. D and d is the outer and inner diameter of the hollow fibre respectively. The inner and outer diameters were measured under SEM. A mean flexural strength was calculated for each sample.

Archimedes' principle based method was used to obtain the porosity of each sample. The dry mass of all samples were first measured. All samples were then immersed in boiling water for over 30 minutes for filling all the pores in the membrane with water. The wet mass of the samples was then measured. The porosity of each hollow fibre membrane were calculated by the difference between its wet mass and dry mass, which the volume of water immersed into the membrane equals to the volume of space present in the membrane.

The pure water flux test was carried out in a Sterlitech HP4750 Stirred Cell (Sterlitech Corporation, USA). Nitrogen gas was used to pressurize the cell. The test was carried out under a fixed feed pressure of 2 bar. The customized membrane supporting disc was non-porous and made of stainless steel. The disc had a diameter of 50 mm, a thickness of 2 mm and a circular hole with a diameter of 2 mm in its centre. The hollow fibre membrane was placed in the hole perpendicularly to the supporting disc. Epoxy was used to seal the top end of the membrane and the space between the membrane and the supporting disc. The setup and a schematic diagram of the water flux test were shown in Fig. 4.3 in Chapter 4.

Mercury porosimetry was carried out in a Poremaster GT-60 (Quantachrome, USA) to obtain the pore size distribution of the hollow fibre membranes. Mercury was forced into the porous samples under pressure. By measuring the pressure required to force mercury through the pores, the pore volumes were estimated.

The chemical stability of $NiAl_2O_4$ hollow fibre membrane was determined by a static corrosion test. [49] Their stabilities in acidic and basic solvents were considered. Samples were weighed then immersed into corrosive solvents in room temperature of 20 ^oC. Continuous mixing was carried out by ball-milling at 50 rpm to minimize concentration gradient near the membrane surface. The test was carried out over a time period of 72 hours. Samples taken out of the solvents were rinsed with distilled water and dried in an oven at 150 ^oC to remove all the water vapour. The masses of acid / base treated samples were measured and the weight loss percentages were obtained.

6.3 Results and Discussions

6.3.1 $NiAl_2O_4$ phase identification

The formation of $NiAl_2O_4$ hollow fibre membrane without excess alumina and NiO was proved by phase identification in XRD. Fig. 6.1 shows the XRD diagram of the 1:1 mole NiO/Al_2O_3 hollow fibre precursor after being sintered in air at 1400 ^oC for 10 hours. 1400 ^oC was the lowest tested sintering temperature, which was the temperature Kotula et al. successfully reacted NiO and α-Al_2O_3 and formed $NiAl_2O_4$ at their boundary. [122] Han et al. reported the formation of $NiAl_2O_4$ as a single phase with a minimum sintering temperature of 1300 ^oC and a milling time as long as 168 hours. [125] Although the slurry for hollow fibre precursor extrusion was only ball-milled for 120 hours, Fig. 6.1 shows peaks of $NiAl_2O_4$ and absence of peaks representing NiO and Al_2O_3. 120 hours was therefore a sufficient ball-

milling time to achieve uniformity of the slurry for the formation of pure $NiAl_2O_4$. With all the hollow fibre precursors extruded from phase-inversion of the same slurry and were sintered at 1400 ^oC or above, it was concluded that $NiAl_2O_4$ was the only phase presented in all the samples prepared.

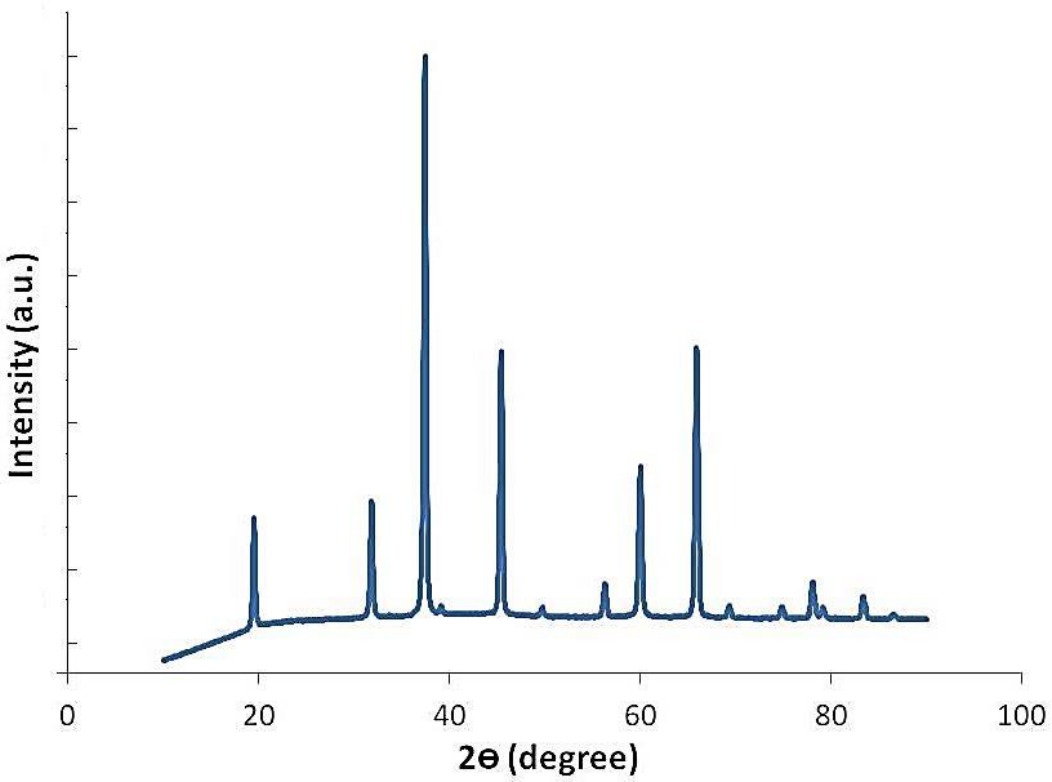

Fig. 6.1 XRD diagram of NiO/Al_2O_3 hollow fibre precursor sintered at 1400 ^oC for 10 hours in air.

6.3.2 Effect of sintering conditions on flexural strength

In Chapter 3 - 5, the sintering time for all the ceramic samples were kept at 5 hours which was shown to be sufficient for grain growth and bonding. The maximum amount of $NiAl_2O_4$ formed in these samples were 22.6 wt%. For the formation of 100% $NiAl_2O_4$, more time was required for the complete reaction between NiO and Al_2O_3, followed by grain growth and bonding of $NiAl_2O_4$ which provided the hollow fibre membrane with mechanical strength. As shown in Fig. 6.2, the flexural strength of $NiAl_2O_4$ was more than quadrupled when the sintering time was increased from 5 hours to 10 hours after being sintered at the same temperature of 1600 ^oC. The low flexural strength with a 5 hour sintering time showed insufficient grain growth and bonding, as $NiAl_2O_4$ was still being formed from the reaction between Al_2O_3 and NiO within this time period. Extending the sintering time up to 10 hours

allowed extra time for grain growth and bonding between the $NiAl_2O_4$ and hence significantly raised the flexural strength of the hollow fibre membranes. Further increase in sintering time did not show a significant change in flexural strength, hence 10 hours was considered as the suitable heat treatment time for $NiAl_2O_4$ formation and grain growth.

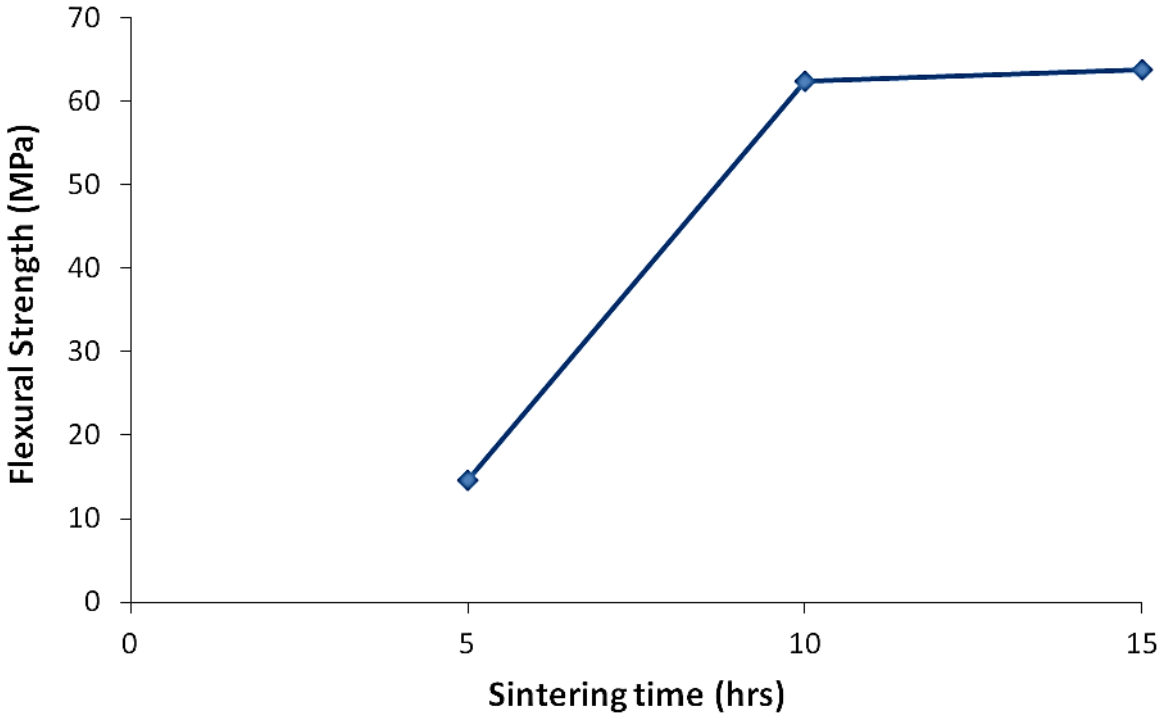

Fig. 6.2 Change in flexural strength of $NiAl_2O_4$ hollow fibre membrane with sintering time at a sintering temperature of 1600 ^oC.

Based on a sintering time of 10 hours, the effect of sintering temperature on the flexural strength of $NiAl_2O_4$ hollow fibre membrane are shown in Fig. 6.3. Similar to Al_2O_3 and $NiAl_2O_4/Al_2O_3$ hollow fibre membranes studied in Chapter 3 -5, flexural strength increased with sintering temperature. There was a sharp rise in flexural strength when the sintering temperature was increased over 1600 ^oC. Within the tested temperature range of 1400 – 1630 ^oC, the higher the sintering temperature the more significant effect it had on flexural strength. The flexural strengths of $NiAl_2O_4$ hollow fibre membranes were lower than $NiAl_2O_4/Al_2O_3$ hollow fibre membranes fabricated by the same methods and materials and sintered at the same temperature as presented in Chapter 4. One of the explanations of this difference was the material nature of Al_2O_3 and $NiAl_2O_4$. $NiAl_2O_4$ has a melting temperature of 2110 ^oC which is higher than the 2044 ^oC of Al_2O_3 [119]. Sintering of a ceramic commonly occurs when temperature reaches half to two-third of its melting point [4], hence $NiAl_2O_4$ has a higher melting temperature than Al_2O_3. The particle size of $NiAl_2O_4$ was another reason for

the lower flexural strength of $NiAl_2O_4$ hollow fibre membranes in comparison with $NiAl_2O_4/Al_2O_3$ hollow fibre membranes. The $NiAl_2O_4$ formed by sold-solid reaction between Al_2O_3 and NiO are larger than Al_2O_3 particles. The mean particle size in the $NiAl_2O_4$ matrix is therefore larger than that in the $NiAl_2O_4$ / Al_2O_3 matrix. Finer particle size can be sintered more rapidly at a lower temperature than coarser particles [60]. The larger particle size of $NiAl_2O_4$ also led to looser packing of particles. Microstructures of $NiAl_2O_4$ hollow fibre membranes are further discussed in Section 6.3.3.

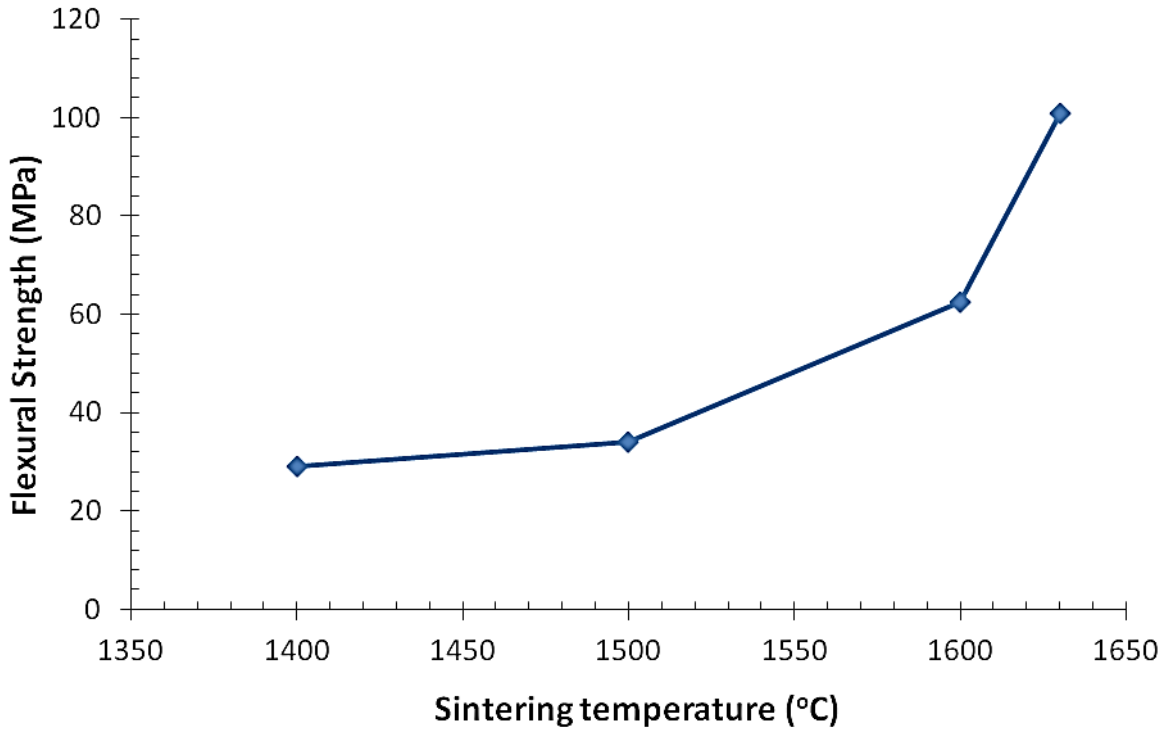

Fig. 6.3 Change in flexural strength of $NiAl_2O_4$ hollow fibre membrane with sintering temperature with a sintering time of 10 hours.

6.3.3 Morphology and microstructure of $NiAl_2O_4$ hollow fibre membranes

The microstructures of $NiAl_2O_4$ hollow fibre membranes sintered at 1600 ^oC for different time are shown in Fig. 6.4. The SEM images were taken from the cross-sectional view of the centre of the sponge-like layer in Fig. 6.5(b). As seen in Fig. 6.4(a), most of the $NiAl_2O_4$ were still individuals and were not bonded to adjacent particles. The average grain size was also smaller than those appeared in Fig. 6.4(b) and (c). This showed that 5 hours was insufficient for both the formation of $NiAl_2O_4$ and sintering, which explained its low flexural strength. Bonding and growth of grains were more obvious in Fig. 6.4(b) and (c) which the hollow fibre membranes were sintered for 10 hours and 15 hours respectively. With 15 hours

of sintering, random grains of over 1 μm were formed. This broadened the grain size range within the hollow fibre membrane, which did not favour particle packing and hence flexural strength. 10 hours was therefore concluded as a suitable time for the formation and sintering of $NiAl_2O_4$ with even and consistent microstructure.

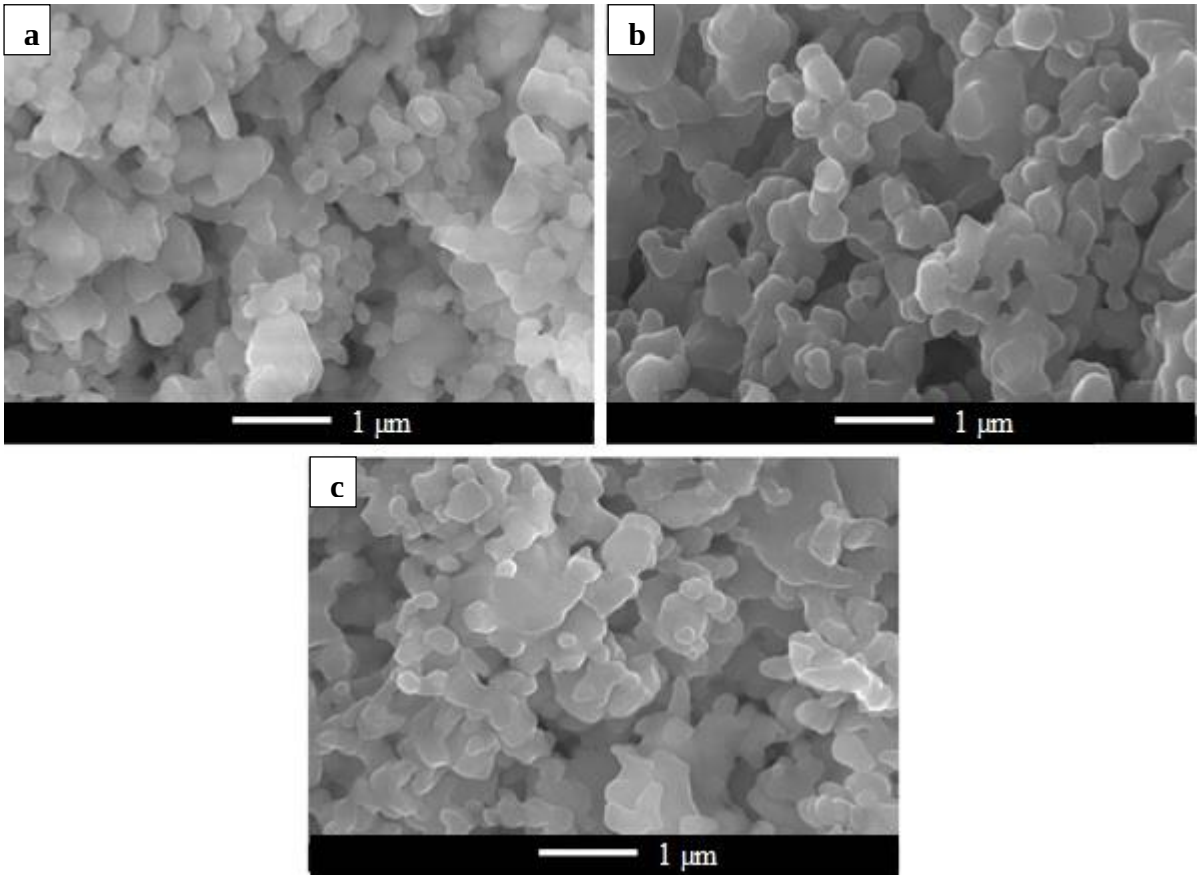

Fig. 6.4 Cross-sectional SEM images of $NiAl_2O_4$ hollow fibre membranes sintered at 1600 ^{o}C for (a) 5 hours, (b) 10 hours and (c) 15 hours.

The full cross-sectional surface and wall of the $NiAl_2O_4$ hollow fibre membrane are shown in Fig. 6.5. The fibre extrusion process was kept constant and hence all $NiAl_2O_4$ hollow fibre membranes had similar cross-sectional structure. Same as most ceramic hollow fibre membranes fabricated by the phase inversion method, the $NiAl_2O_4$ membrane had an asymmetric structure formed by a dense selective layer, finger-like porous layers near the inside and outside membrane walls and a relatively denser sponge-like layer in the centre. The different thickness of finger-like layer near the inside and outside membrane wall was a consequence of different phase exchange rate with the use of 50 vol% ethanol / water as internal coagulant and tap water as external coagulant. The relationship between membrane structure and the use of coagulants was explained in Chapter 4 and Chapter 5. .

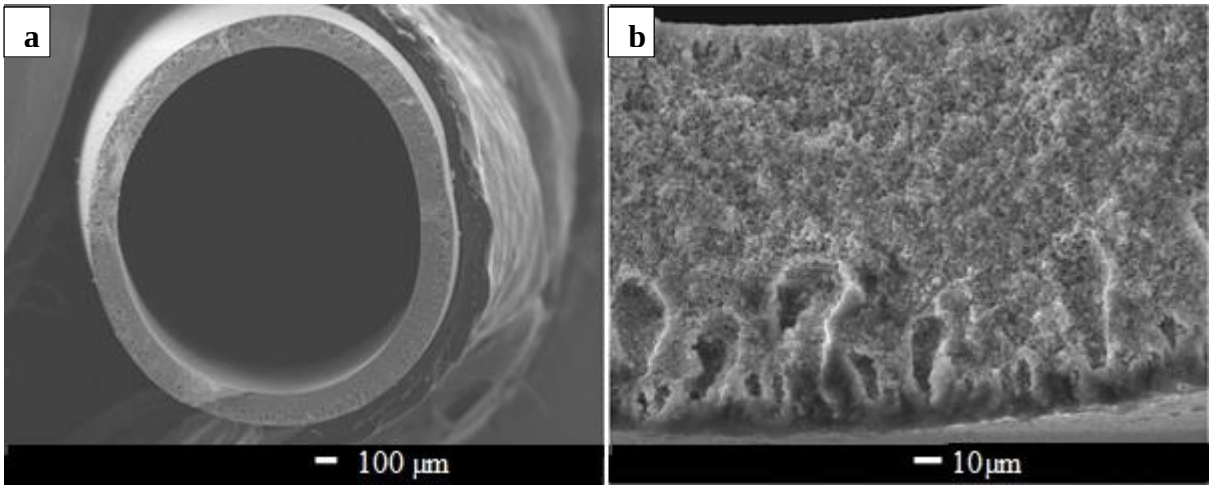

Fig. 6.5 SEM image of the cross-sectional view of $NiAl_2O_4$ hollow fibre membrane sintered at 1600 ^oC for 10 hours (a) full hollow fibre and (b) full membrane wall.

Despite having similar cross-sectional structure, different microstructures were formed in $NiAl_2O_4$ hollow fibre membranes sintered at different temperatures, as shown in Fig. 6.6 which shows SEM images of the sponge-like centre of the membranes. Mechanical strength of the hollow fibre membranes is highly dependent on their sponge-like central layer [4, 35]. Very limited sintering occurred under 1400 ^oC and 1500 ^oC shown in Fig. 6.6 (a) and (b) respectively regardless of a long sintering period of 10 hours. Most particles were 500 µm or under, which indicated limited grain growth. These explain the low flexural strength of $NiAl_2O_4$ hollow fibre membranes sintered at 1500 ^oC and under. As the temperature was increased to 1600 ^oC, sintering was more obvious and grains were joined together with adjacent ones, with a lot less loose individual particles in comparison with those sintered at lower temperatures. A significant increase in flexural strength was therefore obtained. Sintering was completed further as the temperature was risen to 1630 ^oC. Although still being highly porous, majority of the particles were bonded to adjacent particles in Fig. 6.6 (d). Grain growth and neck growth were both observed [4], which further increased the flexural strength up to 101 MPa.

The microstructures of inner and outer surfaces of $NiAl_2O_4$ hollow fibre membrane sintered at different temperatures were shown in Fig. 6.7. At all sintering temperatures, the outer surface had a higher density than the inner surface, which made the outer surface the active layer in practical applications of these hollow fibre membranes in separation processes. Same as the cross-sectional microstructures in Fig. 6.6, at 1400 ^oC and 1500 ^oC, very limited sintering occurred and majority of the particles remained as individuals, with very little bonding and grain growth. The surface porosity differences between inner and outer surfaces

were not obvious at these temperatures. As the temperature was increased to 1600 ^{o}C or above, all grains were bonded to adjacent grains and grain growth occurred. The outside surface became significantly less porous than the inner surface. This made the resistance of the inner wall negligible in comparison with the active layer. As seen in Fig. 6.7 (h), at a sintering temperature of 1630 ^{o}C, although not being fully dense, closure of pores on the outer surface was more significant than at 1600 ^{o}C. The change in microstructure of the inner surface, on the other hand, was less significant. At 1630 ^{o}C the inner surface looked as porous as that treated in 1600 ^{o}C.

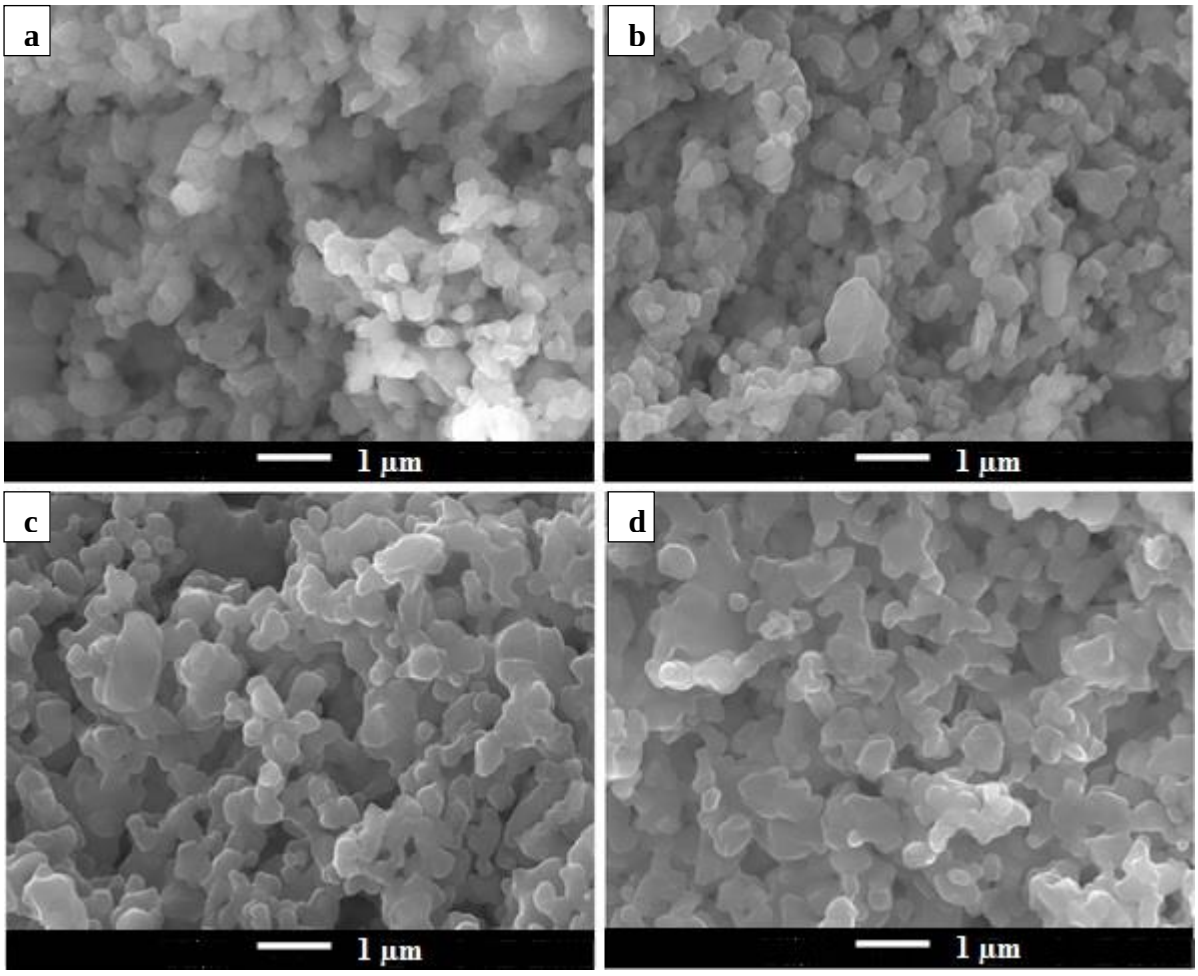

Fig. 6.6 Cross-sectional SEM images of sponge-like centre of $NiAl_2O_4$ hollow fibre membranes sintered for 10 hours at (a) 1400 ^{o}C, (b) 1500 ^{o}C hours, (c) 1600 ^{o}C and (d) 1630 ^{o}C.

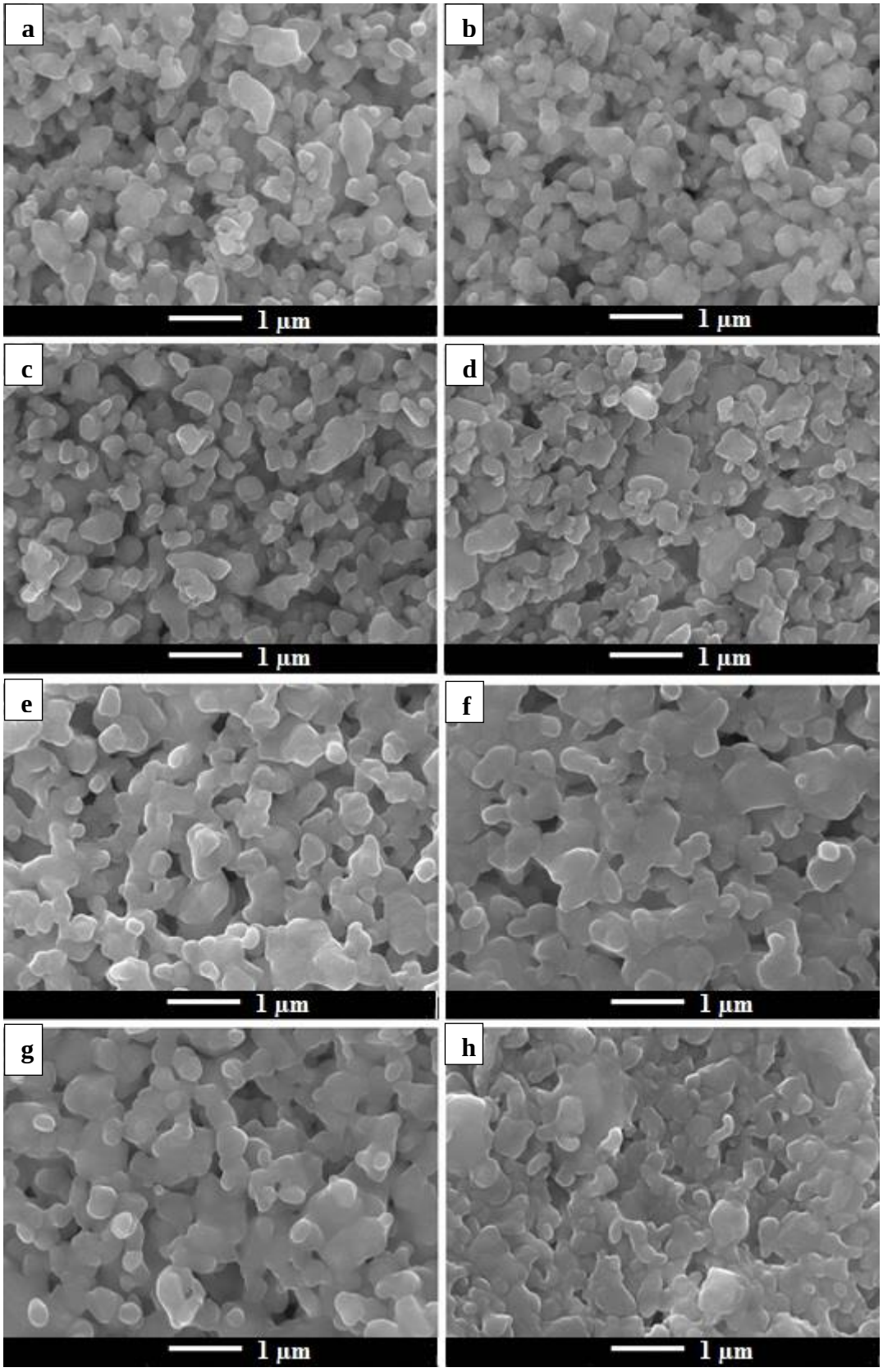

Fig. 6.7 SEM images of the inside and outside surface of $NiAl_2O_4$ hollow fibre membranes sintered for 10 hours at (a)-(b) 1400 ^oC, (c)-(d) 1500 ^oC hours, (e)-(f) 1600 ^oC and (g)-(h) 1630 ^oC. (a), (c), (e) and (g) show inner surfaces. (b), (d), (f) and (h) show outer surfaces.

6.3.4 Porosity

Apart from mechanical properties, the feasibility of using the $NiAl_2O_4$ hollow fibre membrane prepared in separation process is also determined by fluid flux which is highly dependent on porosity of the membrane. The change in porosity with sintering temperature is shown in Fig. 6.8. Same as results in the previous chapters, porosity decreased with increasing sintering temperature because of shrinkage and pore closure. At 1400 ^oC and 1500 ^oC when sintering was limited, porosity of the $NiAl_2O_4$ membranes were over 60%, despite from the cross-sectional view in Fig. 6.5(b) two-third of the membrane wall had a relatively dense sponge-like structure. Increasing the sintering temperature from 1400 ^oC to 1630 ^oC led to 2.5 times increased in the flexural strength of $NiAl_2O_4$ hollow fibre membrane, with only about 10% trade-off in porosity which was still maintained high at 55.45%. Another reason for this relatively high porosity was the proportion of powder in the slurry for hollow fibre precursor extrusion, which was kept as 50 wt% as the preparation of pure alumina hollow fibre membranes in previous chapters. The average particle size of NiO powder, however, was smaller than that of alumina powder. The total volume of powder in the slurry was therefore lower than pure alumina slurry while keeping the molar ratio of alumina to NiO as 1 : 1. More polymer was in between the alumina and NiO particles when the hollow fibre precursors were formed and resulted in a more porous structure after the polymer was combusted.

Table 6.1 shows a comparison of flexural strengths between all ceramic hollow fibre membranes which have a porosity of 55.45±1% covered in this thesis and other literatures. Among these hollow fibre membranes with similar porosities, the pure $NiAl_2O_4$ sample achieved a flexural strength of 101 MPa which was 1.3 – 1.5 times of that of the other samples presented in this thesis. This flexural strength was also comparable with samples contained yttria-stabilized zirconia (YSZ) reported in other literatures. If sintering temperature could be further increased and lead to more significant shrinkage and pore closure, the flexural strength of $NiAl_2O_4$ hollow fibre membrane could potentially be increased further. An alternate solution to increase flexural strength by lowering porosity was increasing the powder proportion in the slurry for hollow fibre precursory extrusion.

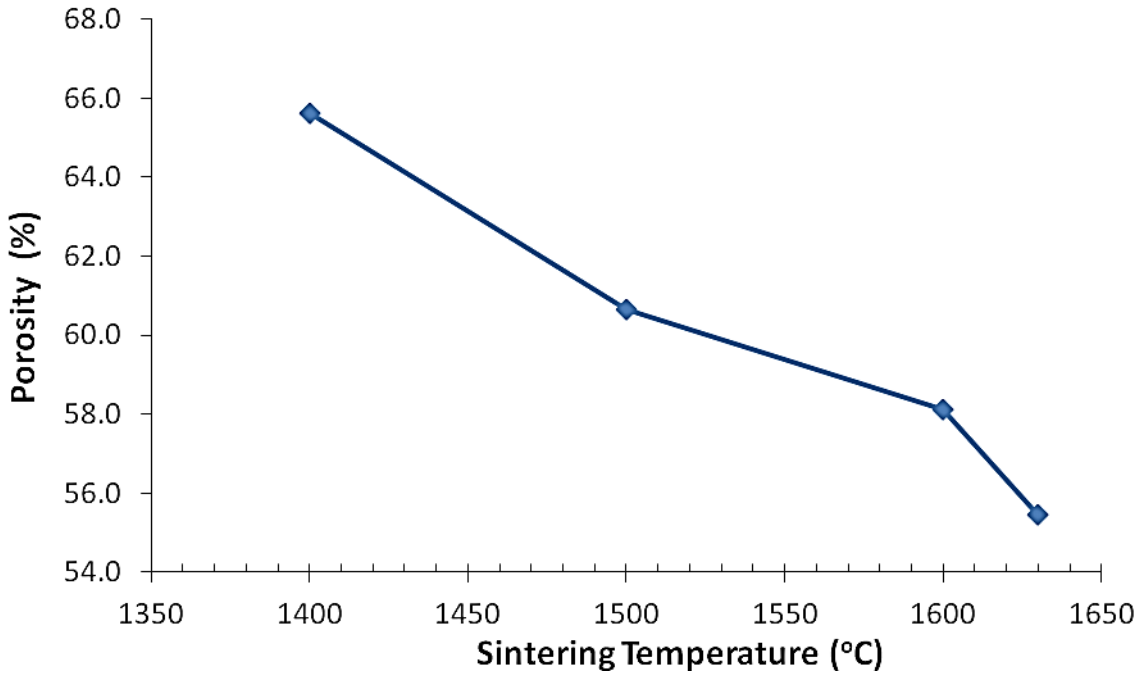

Fig. 6.8 Porosity of $NiAl_2O_4$ hollow fibre membranes sintered at 1400 – 1630 ^oC for 10 hours.

Table 6.1 Comparison of flexural strengths between ceramic hollow fibre membranes with porosity ±1% of that of the $NiAl_2O_4$ hollow fibre membrane sintered at 1630 ^oC.

Sample	**Ref.**	**Porosity**	**Flexural strength (MPa)**
Pure alumina	Ch 4	56.36%	67.7
2.02 wt% $NiAl_2O_4$– NiO powder as starting material	Ch 4	55.16%	76.1
10.0 wt% $NiAl_2O_4$ – NiNW as starting material	Ch 5	55.46%	78.7
15.0 wt% $NiAl_2O_4$– NiNW as starting material	Ch 5	56.16%	72.4
YSZ	[32]	54.5%	114
Ni/YSZ	[114]	56%	59.8
NiO/YSZ	[114]	56%	40.5
Ni/YSZ	[34]	56%	115
NiO/YSZ	[34]	56%	165
Pure $NiAl_2O_4$ sintered at 1630 ^oC	/	55.45%	101

6.3.5 Pure water flux

Pure water flux was an indicator for efficiency of separation processes as it states the rate of fluid passing through the membrane. The effect of sintering temperature on pure water flux of the $NiAl_2O_4$ hollow fibre membranes under a feed pressure of 2 bar is shown in Fig. 6.9. The change in pure water flux of the $NiAl_2O_4$ hollow fibre membranes prepared agreed with their change in porosity with sintering temperature. At 1400 ^oC and 1500 ^oC sintering was limited and hence both centre layers and active layer were highly porous and showed only a minor decrease in pure water flux. When the sintering temperature hit 1600 ^oC and sintering became more significant, a 300 $L/m^2.h.bar$ drop in pure water flux occurred. As the sintering temperature changed from 1400 ^oC to 1630 ^oC, the pure water flux was decreased by 38%. The pure water flux of the sample sintered at 1630 ^oC which achieved the highest flexural strength was 862 $L/m^2.h.bar$. The decrease in pure water flux was a combined effect of drop in overall porosity and pore closure on the active layer, as shown in Fig. 6.6(d) and Fig. 6.7(h).

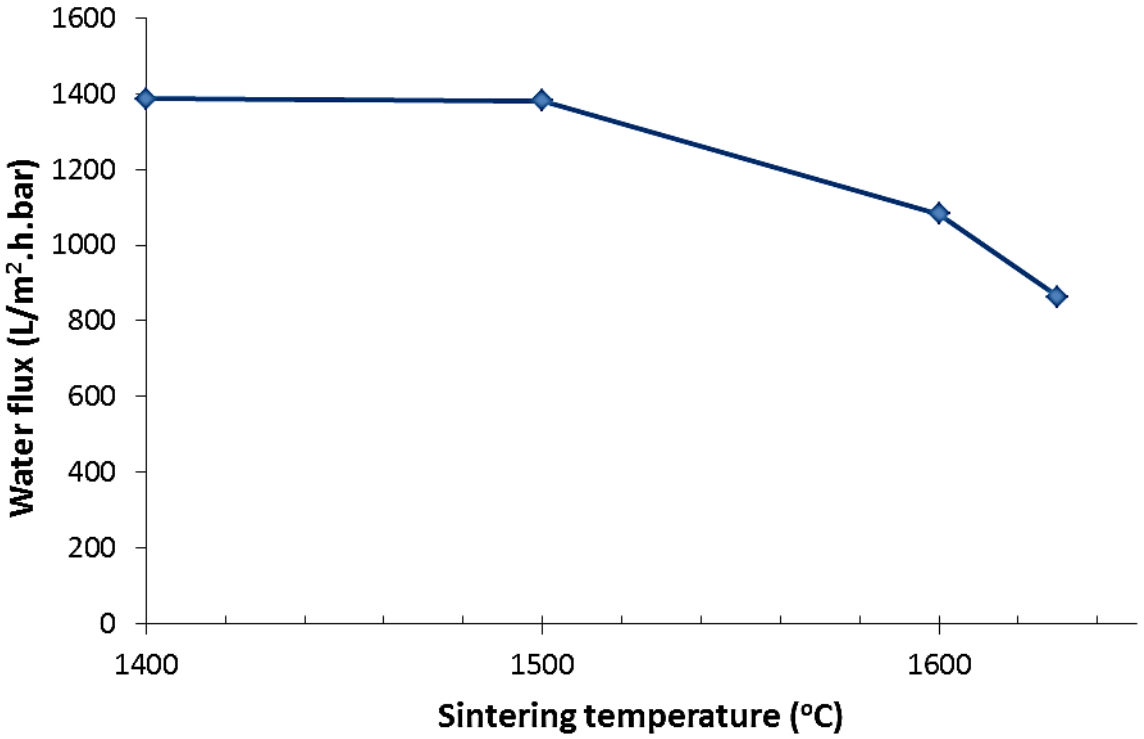

Fig. 6.9 Pure water flux of $NiAl_2O_4$ hollow fibre membranes sintered at 1400 – 1630 ^oC for 10 hours at a feed pressure of 2 bar.

6.3.6 Pore size distribution

Pore size distribution determined the particle size range and effectiveness of a separation process. The pore size distribution curves of $NiAl_2O_4$ hollow fibre membrane sintered at 1400 ^oC and 1630 ^oC obtained by mercury intrusion were shown in Fig. 6.10 and Fig. 6.11. The pore size distribution of these two samples which had the lowest and highest flexural strength were put together for comparison

The overall pore size distribution of the $NiAl_2O_4$ hollow fibre membranes are shown in Fig. 6.10. Each curve shows two major pore size distributions, with one below 1.5 μm and the other over 70 μm of pore size. From visual observation on the SEM images in Fig. 6.5 and Fig. 6.7, the broad binomial distributions of over 70 μm is believed to be representing the finger-like layers and the sharp peaks below 1.5 μm represented the active layer and the sponge-like layer of each sample,. The pore size of finger-like layers was mainly a consequence of the precursor extrusion process and the binomial distributions were a result of inner and outer finger-like layers of each sample, which ranged from approximately 67 – 177 μm at both sintering temperature. The increase in sintering temperature barely changed the pore size distribution in the finger-like layers.

Fig. 6.11 is a magnified view of Fig. 6.10, showing the pore size range of 0 – 1.5 μm which is the sharp peak in Fig. 6.10. A binomial distribution was also shown when the sharp peak was magnified along the x-axis. From the SEM images of the centre and outer surfaces of the $NiAl_2O_4$ hollow fibre membranes in Fig. 6.6 and Fig. 6.7 respectively, the outer surfaces were visually observed to be denser and have smaller pore size than the central sponge-like layer. The left peak of each curve was therefore believed to be the pore size distribution of the active layer and the right one represented that of the sponge-like central layer. This is also supported by the size of the peak which indicated the volume of mercury intruded. The thicker central layer which was more porous and contained larger pores could have more mercury intruded and hence gave a larger peak. Therefore, at 1400 ^oC, the active layer pore size ranged from 0.05 – 0.12 μm. When the sintering temperature was increased to 1630 ^oC, the active layer pore size ranged from 0.05 – 0.14 μm. The active layer pore size of these $NiAl_2O_4$ hollow fibre membranes fell into the microfiltration range. Both the peak representing active layer and the one representing central layer was broadened and shifted slightly towards a larger pore size at a sintering temperature of 1630 ^oC. This was a consequence of grain growth at 1630 ^oC, when larger grains left more void in between and gave larger pores. The change in pore size, however, was very minor with an increase of

sintering temperature as much as 230 °C. More significant effects on flexural strength, porosity and pure water flux were observed with increasing sintering temperature. It was concluded that the increase in sintering temperature contributed more to shrinkage and pore closure than grain growth.

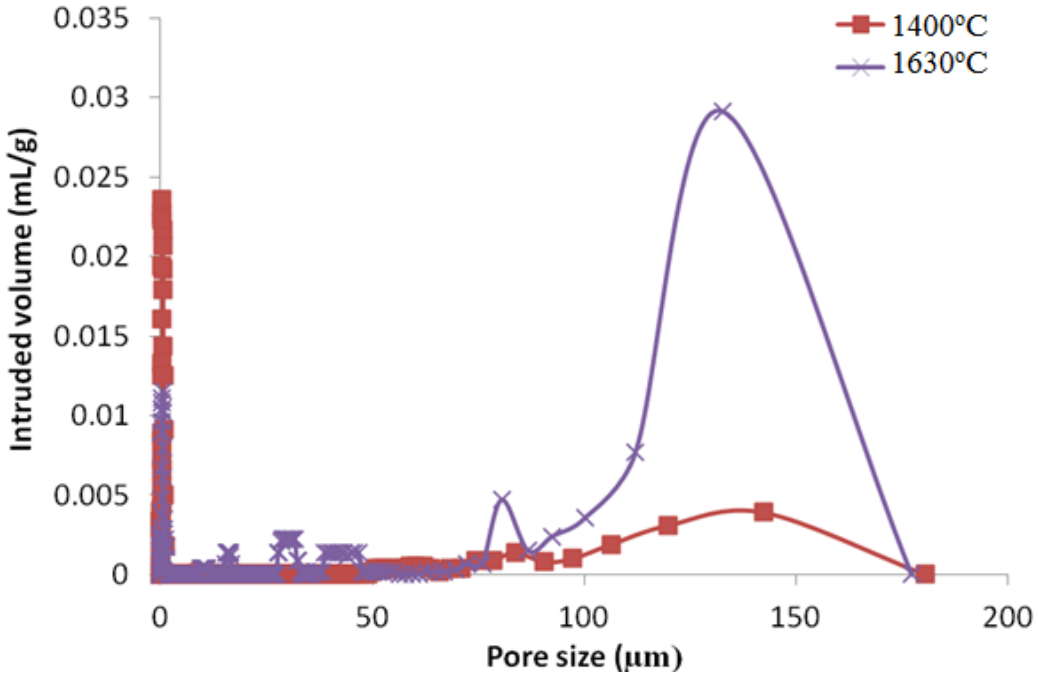

Fig. 6.10 Overall pore size distribution of $NiAl_2O_4$ hollow fibre membrane sintered at 1400 °C and 1630 °C for 10 hours.

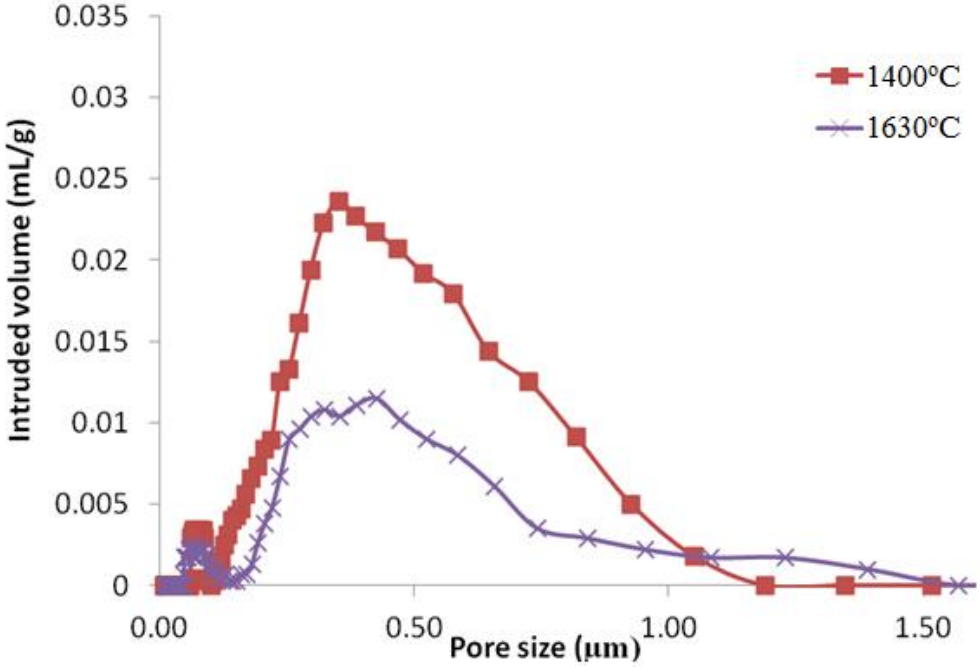

Fig. 6.11 Selective layer and sponge-like layer pore size distribution of $NiAl_2O_4$ hollow fibre membrane sintered at 1400 °C and 1630 °C for 10 hours.

6.3.7 Chemical stability of $NiAl_2O_4$ hollow fibre membrane

The chemical stability of a membrane determined the type of feed it could process, durability, maintenance frequency and hence maintenance cost. A static corrosion test has been carried out on the $NiAl_2O_4$ hollow fibre membrane sintered at 1630 ^oC to investigate its stability in acidic and basic solvents. Hydrochloric acid (HCl) and sodium hydroxide (NaOH) were chosen to be corrosive acid and base respectively. The test was carried out over a period of 72 hours with continuous stirring to minimize the effect of concentration gradient near sample surfaces. The percentage of weight loss of sample in each solvent is shown in Table 6.2.

The $NiAl_2O_4$ hollow fibre membrane showed high stability in HCl. No weight loss was observed for 10 wt% HCl or below and there was only 1.1 % of weight loss in the sample immersed in 20 wt% HCl. The stability of $NiAl_2O_4$ hollow fibre membrane in NaOH, although being lower than in acidic condition, is also appreciable. A weight loss of 2.7% was shown by the sample immersed in 5 wt% NaOH over the 72 hour time period. NaOH solution of below 5 wt% is commonly used as a cleaning detergent for ceramic membrane in the industry to avoid membrane fouling, such as the removal of amaranth starch and whey protein [28, 161]. When the cleaning of fat in ceramic membrane is involved, NaOH is also used for alkaline bath which saponificates fat and increases the pH value in the membrane to provide a better contamination removal environment before the use of sodium hypochlorite (NaOCl) a cleaning detergent that is also a disinfectant and oxidizing agent [44, 138]. The high stability of $NiAl_2O_4$ hollow fibre membrane in both acidic condition and <5 wt% NaOH proved that chemical cleaning is suitable for flux recovery of fouled $NiAl_2O_4$ membrane and would not lead to significant damage or change in characteristics of the membrane.

Table 6.2 Weight loss percentages of $NiAl_2O_4$ hollow fibre membranes in acidic and basic solvent of various concentrations over a time period of 72 hours.

Solvent	Concentration (wt%)	Weight loss (%)
HCl	5	0
	10	0
	20	1.087
NaOH	0.5	0.714
	1	1.205
	5	2.674

The same static corrosion test was also carried out on pure alumina hollow fibre membranes of similar porosity and no observable weight loss was shown. Dong et. al have also reported the chemical stability of porous alumina. Their results showed that porous alumina experienced about 1% of weight loss in 20 wt% boiling acid and 17% weight loss in 5 wt% boiling NaOH solution after 8 hours. [50] This supports the stronger resistance in acid than alkali for both porous alumina and $NiAl_2O_4$. In room temperature, pure alumina hollow fibre membrane showed higher stability in acid and alkali.

6.4 Conclusions

Pure $NiAl_2O_4$ hollow fibre membranes were prepared through the phase-inversion and sintering method. The slurry for membrane precursory extrusion contained homogeneously mixed α-Al_2O_3 and NiO powder in 1 : 1 molar ratio, which underwent solid state reaction and formed $NiAl_2O_4$. A 10 hour sintering period and sintering temperature of 1600 ^oC was found to be sufficient for the both the formation and sintering of $NiAl_2O_4$ to be completed. A flexural strength of 101 MPa was achieved by sintering the $NiAl_2O_4$ hollow fibre membranes at 1630 ^oC, which was the highest among samples tested in this chapter. A high porosity of 55% and pure water flux of 862 $L/m^2.h.bar$ was demonstrated by this $NiAl_2O_4$ hollow fibre membranes. Its active layer pore size ranged from 0.05 – 0.14 μm which fell into the microfiltration range. In comparison with ceramic hollow fibre membranes with similar porosities, $NiAl_2O_4$ hollow fibre membranes showed a flexural strength 1.3-1.5 times higher than other ceramic hollow fibre membranes presented in this thesis and a comparable flexural strength to YSZ samples recorded in other literatures. If higher sintering temperature is achievable, the flexural strength of $NiAl_2O_4$ could be raised further with more completed shrinkage and pore closure. The static corrosion test showed high stability of the $NiAl_2O_4$ hollow fibre membrane under acidic and basic conditions, with a maximum of 2.7% weight loss in 5 wt% NaOH solution, which made chemical cleaning suitable for $NiAl_2O_4$ membranes.

Chapter 7 Conclusions and future recommendations

7.1 Conclusions

To reduce the brittleness of ceramic hollow fibre membrane in general and hence extend its potential application in the industry, this thesis presented the enhancement in flexural strength of the widely used alumina (Al_2O_3) hollow fibre membrane by reinforcement and the use of strong pure ceramic as membrane material.

Reinforcement of alumina hollow fibre membrane was carried out by the formation of nickel aluminate ($NiAl_2O_4$) as discontinuous phase and continuous phase within the alumina matrix. $NiAl_2O_4$ is a ceramic with high thermal stability. In the chemical stability test $NiAl_2O_4$ showed minor weight loss in hydrochloric acid (HCl) and sodium hydroxide (NaOH) as concentrated as 20 wt% and 5 wt% respectively, which were common cleaning detergents for ceramic hollow fibre membranes in the industry. Both approaches involved a solid-solid reaction between nickel (II) oxide (NiO) and Al_2O_3 which formed solid $NiAl_2O_4$ within the ceramic hollow fibre membrane. X-ray diffraction phase identification proved the formation of $NiAl_2O_4$ after heat treatment of Al_2O_3 and NiO mixture at 1400 ^oC or above. The use of nano sized NiO powder and nickel nanowires (Ni NW) as raw materials resulted in discrete and continuous $NiAl_2O_4$ in alumina matrix respectively. NiO and Al_2O_3 powder were also mixed at 1 : 1 molar ratio homogeneously and formed pure $NiAl_2O_4$ hollow fibre membranes. $NiAl_2O_4$ had never been reported as pure membrane material and its hollow fibre membrane was found to have a high flexural strength while maintaining a high porosity. The effects of discrete and continuous $NiAl_2O_4$ on alumina hollow fibre membranes are summarized in Table 7.1. The change in flexural strength, porosity, water flux and mean active layer pore size from the corresponding $NiAl_2O_4$ loadings in Table 7.1 were relative to the pure alumina sample prepared under the same conditions. A comparison between pure $NiAl_2O_4$ and pure alumina hollow fibre membrane of similar porosities presented in this thesis is also shown in Table 7.2.

Table 7.1 Summary of the effects of discrete and continuous $NiAl_2O_4$ reinforcement on alumina hollow fibre membranes.

Reinforcement medium	Discrete $NiAl_2O_4$	$NiAl_2O_4$ chains
Raw materials	Al_2O_3 powder, NiO powder	Al_2O_3 powder, Ni NW
$NiAl_2O_4$ loading at maximum flexural strength	16.4 wt%	2.00 wt%
Change in flexural strength	+131%	+147%
Change in porosity	-9.6%	-9.7%
Change in pure water flux	-72%	-89%
Change in mean active layer pore size	-25%	-7.6%

Reinforcement of alumina hollow fibre membrane by $NiAl_2O_4$ chains gave slightly higher enhancement in flexural strength than discrete $NiAl_2O_4$ with very similar trade off in porosity. Both reinforcement methods led to a significant decrease in pure water flux in comparison with the pure alumina samples, which was a consequence of decrease in porosity, active layer pore size and pore density. The strengthening effect was a consequence of crack growth deflection caused by thermal expansion mismatch between $NiAl_2O_4$ and alumina. In addition to thermal expansion mismatch, crack bridging effect was also present in the formation of $NiAl_2O_4$ chains. In both cases of discrete and continuous $NiAl_2O_4$ reinforcement further increase in the loading of $NiAl_2O_4$ led to uneven grain growth and neck growth in random directions and loose agglomerates, which hindered shrinkage during the sintering process and decreased flexural strength.

Table 7.2 Summary of characteristics of pure $NiAl_2O_4$ and pure alumina hollow fibre membranes with similar porosities in this thesis.

Membrane materials	Pure $NiAl_2O_4$	Pure alumina
Reference	Chapter 6	Chapter 4
Porosity	55.5 %	56.4 %
Flexural strength	101 MPa	67.7 MPa
Pure water flux	863 $L/m^2.h.bar$	2115 $L/m^2.h.bar$
Mean active layer pore size	77.9 nm	420 nm

In comparison with alumina hollow fibre membrane of similar porosity, $NiAl_2O_4$ hollow fibre membrane achieved a flexural strength of 49% higher. This showed that $NiAl_2O_4$ is a mechanically stronger ceramic than alumina and is a suitable material for the fabrication for strong ceramic membranes with high porosities. At similar porosity the larger difference in pure water flux was mainly a consequence of different active layer structure. Apart from smaller mean pore size on its active layer which was the outer surface, $NiAl_2O_4$ hollow fibre membrane also showed lower outer surface porosity than the alumina sample as observed in SEM images.

To conclude, strong ceramic hollow fibre membranes of over 100 MPa have been obtained by all three approaches. The reinforcement and strengthening methods involved have provided solutions for decreasing brittleness of ceramic hollow fibre membranes. Alumina hollow fibre membranes reinforced by $NiAl_2O_4$ showed enhanced flexural strength and pure $NiAl_2O_4$ hollow fibre membranes showed appreciable flexural strength with high porosity. The inclusion of $NiAl_2O_4$ maintained the ceramic nature of alumina hollow fibre membranes and hence kept all the advantages of ceramic as a membrane material including high thermal and chemical stability, ease of cleaning and insensitivity to swelling. The pore size of all ceramic hollow fibre membranes in this thesis falls into the microfiltration range and are suitable for the removal of solid suspensions in liquid. Out of all three types of ceramic hollow fibre membranes investigated, discrete $NiAl_2O_4$ reinforced alumina hollow fibre membrane had the simplest preparation process and phase distribution system in the final product. Reinforcement by $NiAl_2O_4$ chains on the other hand achieved higher increase in

flexural strength with significantly lower $NiAl_2O_4$ content. In these two cases strengthening effect was limited up to a certain $NiAl_2O_4$ loading. Pure $NiAl_2O_4$ hollow fibre membranes showed higher flexural strength than pure alumina and $NiAl_2O_4/Al_2O_3$ hollow fibre membranes of similar porosity. The preparation of pure $NiAl_2O_4$ hollow fibre membrane involved long mixing and sintering time because of the high homogeneity of raw material required and reaction time for the formation of $NiAl_2O_4$ through solid state reaction, which made the fabrication process more complicated, more time and energy consuming than that of pure alumina or $NiAl_2O_4/Al_2O_3$ ceramic hollow fibre membranes.

7.2 Recommendation for future work

In this thesis, flexural strength enhancements were only shown on alumina hollow fibre membranes. A recommendation for future work is to apply these reinforcement methods on other ceramic hollow fibre membranes. $NiAl_2O_4$ the reinforcement medium used in this thesis is a product of solid state reaction between NiO and alumina. In application of the same reinforcement methods in other ceramic hollow fibre membranes, elements which could react with the corresponding ceramic to form a second ceramic phase should be included in the preparation of hollow fibre membrane precursor. The thumb rule is the secondary phase formed must have a higher thermal expansion coefficient. The strengthening effect and suitable loading of the secondary phase depend on the thermal expansion coefficients difference between two ceramic phases, particle sizes and morphologies of raw materials.

Particle size of raw materials for the fabrication of ceramic hollow fibre membranes was a factor that determines reinforcement effect and hence flexural strength, which was not covered in this thesis. Ceramic hollow fibre membranes presented and compared in the previous chapters were prepared by starting materials of the same particle sizes. The ratio of particle size of raw materials could be adjusted and mixed in different proportions to control the size and distribution of the secondary phase, which changed the particle packing of the final product. Particle packing highly affects the mechanical properties and other properties that determine the effectiveness and efficiency of a membrane separation process such as pore size and its distribution, porosity, tortuosity and fluid flux. All the hollow fibre membranes in this thesis have their pore size within the microfiltration range. Adjustment on particle size and packing could potentially extend these ceramic hollow fibre membranes to application of ultrafiltration.

For the application of continuous reinforcement medium as demonstrated by the formation of $NiAl_2O_4$ chains in alumina hollow fibre membrane in Chapter 5, more study on the relationship between flexural strength and characteristics of the reinforcement medium could be carried out in the future. The diameter and length of the continuous reinforcement medium have an effect on the sharing of load within the ceramic matrix. In the case of nickel nanowire as raw material for the preparation of hollow fibre membrane precursor by phase inversion, with the nanowires formed by joined nickel particles, the bond between individual particles within the nanowire is also critical because of the sheering and tearing the nanowires would experience in mixing and extrusion. The surface smoothness of the nickel nanowires which could be easily controlled during the wire formation process as reported in many literatures also deserves some investigation on whether it has an effect on microstructure of the $NiAl_2O_4/Al_2O_3$ hollow fibre membrane.

As mentioned, $NiAl_2O_4$ had not been reported as a membrane material. The change in microstructure and flexural strength of $NiAl_2O_4$ hollow fibre membrane with sintering conditions have been presented in this thesis, while future work is still required to improve the efficiency of its fabrication and determine its suitable applications in the industry. As shown in Chapter 6, the porosities of $NiAl_2O_4$ hollow fibre membranes prepared were significantly higher than that required for sufficient flux in ceramic membranes. This showed that flexural strengths of $NiAl_2O_4$ hollow fibre membranes could be further enhanced by pore closure and shrinkage. Higher degree of shrinkage in the $NiAl_2O_4$ hollow fibre membrane could be attempted by further increasing the sintering temperature. Provided the sintering temperature reported in Chapter 6 was as high as 1630 ^oC, when further increase in sintering temperature is limited by equipment or safety issue, another option was the use of sintering aid which lowers the sintering temperature of ceramics. Further study on microstructure is also needed when further shrinkage and higher flexural strength is achieved.

Testing the strengthened ceramic hollow fibre membranes for real separation processes is a recommended follow up work. Results displayed in this thesis were based on individual ceramic hollow fibre membrane, while in real applications ceramic hollow fibre membranes are bundled up and used as modules. Flexural strength was used as an indicator for brittleness and was obtained by three-point-bending test which a load was applied in the middle of a horizontally placed hollow fibre membrane. In a filtration process, however, pressure is applied over the active layer of the membrane instead of as a point load. The flexural strength of a single ceramic hollow fibre membrane therefore could not fully

represent the performance of a module of the same membrane. As microfiltration membranes, testing on the separation of suspended carbon particles or oil droplets under different pressure with these strengthened ceramic hollow fibre membranes is suggested to demonstrate their efficiency and effectiveness in industrial applications. At the end of a separation process, fouling and cleaning of the ceramic hollow fibre membranes could also be investigated. Before chemical cleaning, blowing of air into the membranes for the removal of accumulated feed on membrane surface is common. Flexural strength of the membrane also determines the pressure of air applied for the most effective cleaning.

List of publication

Journal article

Y.L.E. Fung, H. Wang, Investigation of reinforcement of porous alumina by nickel aluminate spinel for its use as ceramic membrane, Journal of Membrane Science, 444 (2013) 252-258.

Y.L.E. Fung, H. Wang, Nickel aluminate spinel reinforced ceramic hollow fibre membrane, Journal of Membrane Science, 450 (2014) 418-424.

Y.L.E. Fung, H. Wang, Nickel aluminate chains reinforced ceramic hollow fibre membrane (submitted to Journal of Materials Chemistry A).

Conference paper

Y.L.E. Fung, H. Wang, Nickel aluminate spinel reinforced porous ceramic for membrane application, in: 2013 AICHE annual meeting, San Francisco, USA, 2013.

Y.L.E. Fung, H. Wang, Nickel aluminate spinel reinforced ceramic hollow fibre membrane, in: Chemeca 2013 conference, Brisbane, Australia, 2013.

References

[1] E. Drioli, A. Brunetti, G. Barbieri, Ceramic membranes in carbon dioxide capture: applications and potentialities, Advances in Science and Technology, 72 (2010) 14.

[2] S. Luque, D. Gómez, J.R. Álvarez, Industrial applications of porous ceramic membranes (pressure-driven processes), in: M. Reyes, M. Miguel (Eds.) Membrane Science and Technology, Elsevier, 2008, pp. 177-216.

[3] J. Smid, C.G. Avci, V. Günay, R.A. Terpstra, J.P.G.M. Van Eijk, Preparation and characterization of microporous ceramic hollow fibre membranes, Journal of Membrane Science, 112 (1996) 85-90.

[4] A.F. Ismail, K. Li, From polymeric precursors to hollow fiber carbon and ceramic membranes, in: M. Reyes, M. Miguel (Eds.) Membrane Science and Technology, Elsevier, 2008, pp. 81-119.

[5] K. Li, Ceramic hollow fiber membranes and their applications, in: D. Enrico, G. Lidietta (Eds.) Comprehensive Membrane Science and Engineering, Elsevier, Oxford, 2010, pp. 253-273.

[6] R. Weber, H. Chmiel, V. Mavrov, Characteristics and application of new ceramic nanofiltration membranes, Desalination, 157 (2003) 113-125.

[7] F.R. García-García, B.F.K. Kingsbury, M.A. Rahman, K. Li, Asymmetric ceramic hollow fibres applied in heterogeneous catalytic gas phase reactions, Catalysis Today, 193 (2012) 20-30.

[8] E. Gbenedio, Z. Wu, I. Hatim, B.F.K. Kingsbury, K. Li, A multifunctional Pd/alumina hollow fibre membrane reactor for propane dehydrogenation, Catalysis Today, 156 (2010) 93-99.

[9] B.F.K. Kingsbury, Z. Wu, K. Li, Inorganic hollow fibre membranes for chemical reaction, in: Membranes for Membrane Reactors, John Wiley & Sons, Ltd, 2011, pp. 117-153.

[10] L. Liu, S. Liu, X. Tan, Zirconia microbial hollow fibre bioreactor for escherichia coli culture, Ceramics International, 36 (2010) 2087-2093.

[11] A. Srisuwan, D. Wattanasiriwech, S. Wattasiriwech, P. Aungkawattana, Fabrication and microstructure of porous alumina tubular support for SOFC by extrusion, in: TIChE International Conference 2011, Hatyai, Songkhla Thailand, 2011.

[12] C.C. Wei, K. Li, Yttria-stabilized zirconia (YSZ)-based hollow fiber solid oxide fuel cells, Industrial & Engineering Chemistry Research, 47 (2008) 1506-1512.

[13] R.W. Baker, Membranes and Modules, in: Membrane Technology and Applications, John Wiley & Sons, Ltd, 2012, pp. 97-178.
[14] A.G. Fane, S. Chang, E. Chardon, Submerged hollow fibre membrane module — design options and operational considerations, Desalination, 146 (2002) 231-236.
[15] H.K. Lonsdale, Editorial: What is a membrane: Part II, Journal of Membrane Science, 43 (1989) 1-3.
[16] A.S. Grandison, M.J. Lewis, Separation processes in the food and niotechnology industries - principles and applications, in, Woodhead Publishing, 1996.
[17] R.W. Baker, Membrane transport theory, in: Membrane Technology and Applications, John Wiley & Sons, Ltd, 2012, pp. 15-96.
[18] M. Ulbricht, H. Susanto, Porous flat sheet, hollow fibre and capsule membranes by phase separation of polymer solutions, in: Membranes for Membrane Reactors, John Wiley & Sons, Ltd, 2011, pp. 491-510.
[19] K.W. Böddeker, Membrane filtration, in: Liquid Separations with Membranes, Springer Berlin Heidelberg, 2008, pp. 63-80.
[20] K.W. Böddeker, An introduction to barrier separation, in: Liquid Separations with Membranes, Springer Berlin Heidelberg, 2008, pp. 1-16.
[21] H. Fang, J.F. Gao, H.T. Wang, C.S. Chen, Hydrophobic porous alumina hollow fiber for water desalination via membrane distillation process, Journal of Membrane Science, 403–404 (2012) 41-46.
[22] K.H. Lee, M.Y. Youn, B. Sea, Preparation of hydrophilic ceramic membranes for a dehydration membrane reactor, Desalination, 191 (2006) 296-302.
[23] M. Khemakhem, S. Khemakhem, R. Ben Amar, Emulsion separation using hydrophobic grafted ceramic membranes by air gap membrane distillation process, Colloids and Surfaces A: Physicochemical and Engineering Aspects, 436 (2013) 402-407.
[24] C. Picard, A. Larbot, F. Guida-Pietrasanta, B. Boutevin, A. Ratsimihety, Grafting of ceramic membranes by fluorinated silanes: hydrophobic features, Separation and Purification Technology, 25 (2001) 65-69.
[25] S.S. Madaeni, H. Ahmadi Monfared, V. Vatanpour, A. Arabi Shamsabadi, E. Salehi, P. Daraei, S. Laki, S.M. Khatami, Coke removal from petrochemical oily wastewater using γ-Al_2O_3 based ceramic microfiltration membrane, Desalination, 293 (2012) 87-93.
[26] S.R.H. Abadi, M.R. Sebzari, M. Hemati, F. Rekabdar, T. Mohammadi, Ceramic membrane performance in microfiltration of oily wastewater, Desalination, 265 (2011) 222-228.

[27] P.G. Middlewood, J.K. Carson, Extraction of amaranth starch from an aqueous medium using microfiltration: Membrane characterisation, Journal of Membrane Science, 405–406 (2012) 284-290.
[28] P.G. Middlewood, J.K. Carson, Extraction of amaranth starch from an aqueous medium using microfiltration: Membrane fouling and cleaning, Journal of Membrane Science, 411–412 (2012) 22-29.
[29] B.Z. Dong, H.Q. Chu, L. Wang, S.J. Xia, N.Y. Gao, The removal of bisphenol A by hollow fiber microfiltration membrane, Desalination, 250 (2010) 693-697.
[30] M. Hlavacek, Break-up of oil-in-water emulsions induced by permeation through a microfiltration membrane, Journal of Membrane Science, 102 (1995) 1-7.
[31] W. Yin, B. Meng, X. Meng, X. Tan, Highly asymmetric yttria stabilized zirconia hollow fibre membranes, Journal of Alloys and Compounds, 476 (2009) 566-570.
[32] X. Zhang, B. Lin, Y. Ling, Y. Dong, D. Fang, G. Meng, X. Liu, Highly permeable porous YSZ hollow fiber membrane prepared using ethanol as external coagulant, Journal of Alloys and Compounds, 494 (2010) 366-371.
[33] B.F.K. Kingsbury, Z. Wu, K. Li, A morphological study of ceramic hollow fibre membranes: A perspective on multifunctional catalytic membrane reactors, Catalysis Today, 156 (2010) 306-315.
[34] X. Meng, N. Yang, B. Meng, X. Tan, Y. Yin, Z.F. Ma, J. Sunarso, Microstructure tailoring of the nickel–yttria stabilised zirconia (Ni–YSZ) cermet hollow fibres, Ceramics International, 38 (2012) 6327-6334.
[35] S. Liu, K. Li, R. Hughes, Preparation of porous aluminium oxide (Al_2O_3) hollow fibre membranes by a combined phase-inversion and sintering method, Ceramics International, 29 (2003) 875-881.
[36] A.J. Burggraaf, Important characteristics of inorganic membranes, in: A.J. Burggraaf, L. Cot (Eds.) Membrane Science and Technology, Elsevier, 1996, pp. 21-34 (Chapter 22).
[37] R. Wang, T.S. Chung, Determination of pore sizes and surface porosity and the effect of shear stress within a spinneret on asymmetric hollow fiber membranes, Journal of Membrane Science, 188 (2001) 29-37.
[38] F.J. Valdes-Parada, J.A. Ochoa-Tapia, J. Alvarez-Ramirez, Validity of the permeability Carman–Kozeny equation: A volume averaging approach, Physica A: Statistical Mechanics and its Applications, 388 (2009) 789-798.
[39] W. Li, W. Xing, N. Xu, Modeling of relationship between water permeability and microstructure parameters of ceramic membranes, Desalination, 192 (2006) 340-345.

[40] P. Xu, B. Yu, Developing a new form of permeability and Kozeny–Carman constant for homogeneous porous media by means of fractal geometry, Advances in Water Resources, 31 (2008) 74-81.
[41] P. Marchetti, A. Butté, A.G. Livingston, An improved phenomenological model for prediction of solvent permeation through ceramic NF and UF membranes, Journal of Membrane Science, 415–416 (2012) 444-458.
[42] Y. Marselina, P. Le-Clech, R. Stuetz, V. Chen, Detailed characterisation of fouling deposition and removal on a hollow fibre membrane by direct observation technique, Desalination, 231 (2008) 3-11.
[43] A.S. Grandison, M.J. Lewis, Separation processes in the food and biotechnology industries - principles and applications, in, Woodhead Publishing, 1996, pp. 141-153.
[44] P. Le-Clech, V. Chen, T.A.G. Fane, Fouling in membrane bioreactors used in wastewater treatment, Journal of Membrane Science, 284 (2006) 17-53.
[45] V. Gekas, B. Hallström, Microfiltration membranes, cross-flow transport mechanisms and fouling studies, Desalination, 77 (1990) 195-218.
[46] R. Bai, H.F. Leow, Microfiltration of polydispersed suspension by a membrane screen/hollow-fiber composite module, Desalination, 140 (2001) 277-287.
[47] R. Bai, H.F. Leow, Modeling and experimental study of microfiltration using a composite module, Journal of Membrane Science, 204 (2002) 359-377.
[48] G. Azimi, R. Dhiman, H.M. Kwon, A.T. Paxson, K.K. Varanasi, Hydrophobicity of rare-earth oxide ceramics, Nat Mater, 12 (2013) 315-320.
[49] A. Buekenhoudt, Stability of porous ceramic membranes, in: M. Reyes, M. Miguel (Eds.) Membrane Science and Technology, Elsevier, 2008, pp. 1-31.
[50] Y. Dong, B. Lin, J.E. Zhou, X. Zhang, Y. Ling, X. Liu, G. Meng, S. Hampshire, Corrosion resistance characterization of porous alumina membrane supports, Materials Characterization, 62 (2011) 409-418.
[51] B. Krasnyi, V. Tarasovskii, A. Krasnyi, Chemical stability of porous permeable ceramic with aluminosilicate binder in acidic and alkaline reagents, Glass & Ceramics, 68 (2012) 327-329.
[52] T. Van Gestel, C. Vandecasteele, A. Buekenhoudt, C. Dotremont, J. Luyten, R. Leysen, Chemical stability of ceramic multi-layer membranes, Key Engineering Materials, 206-213 (2002) 4.
[53] T. Van Gestel, C. Vandecasteele, A. Buekenhoudt, C. Dotremont, J. Luyten, R. Leysen, B. Van der Bruggen, G. Maes, Alumina and titania multilayer membranes for nanofiltration:

preparation, characterization and chemical stability, Journal of Membrane Science, 207 (2002) 73-89.

[54] S. Jana, M.K. Purkait, K. Mohanty, Preparation and characterizations of ceramic microfiltration membrane: Effect of inorganic precursors on membrane morphology, Separation Science and Technology, 46 (2010) 33-45.

[55] C.T. Lynch, Ceramic materials, in: Practical Handbook of Materials Science, CRC Press, 1989, pp. 281-323.

[56] Y.S. Lin, C.H. Chang, R. Gopalan, Improvement of thermal stability of porous nanostructured ceramic membranes, Industrial & Engineering Chemistry Research, 33 (1994) 860-870.

[57] T. Novaković, N. Radić, B. Grbić, V. Dondur, M. Mitrić, D. Randjelović, D. Stoychev, P. Stefanov, The thermal stability of porous alumina/stainless steel catalyst support obtained by spray pyrolysis, Applied Surface Science, 255 (2008) 3049-3055.

[58] X.H. Wang, C.Y. Li, G. Chen, L. He, H. Cao, Preparation and thermal stability of porous alumina membranes with nano-pore arrays, Appl. Phys. A, 98 (2010) 745-749.

[59] P. Rao, M. Iwasa, I. Kondoh, Properties of low-temperature-sintered high purity α-alumina ceramics, Journal of Materials Science Letters, 19 (2000) 543-545.

[60] A. Balakrishnan, P. Pizette, C.L. Martin, S.V. Joshi, B.P. Saha, Effect of particle size in aggregated and agglomerated ceramic powders, Acta Materialia, 58 (2010) 802-812.

[61] P. Greil, Generic principles of crack-healing ceramics, J Adv Ceram, 1 (2012) 249-267.

[62] J.G.P. Binner, Advanced ceramic processing and technology, in, William Andrew Publishing/Noyes, 1990.

[63] J.S. Reeds, Firing processes, in: Introduction to the principles of ceramic processing, John Wiley & Sons, New York, 1988, pp. 26.

[64] D.W. Richardson, Modern ceramic engineering properties, processing and use in design, 3rd ed., Taylor & Francis Group, Boca Raton, 2006.

[65] M.N. Rahaman, Ceramic processing and sintering, Marcel Dekker, Inc., New York, 1995.

[66] Y.L.E. Fung, H. Wang, Nickel aluminate spinel reinforced ceramic hollow fibre membrane, in: Chemeca 2013 conference, Brisbane, Australia, 2013.

[67] H.M. Bian, Y. Yang, Y. Wang, W. Tian, H.F. Jiang, Z.J. Hu, W.M. Yu, Alumina–titania ceramics prepared by microwave sintering and conventional pressure-less sintering, Journal of Alloys and Compounds, 525 (2012) 63-67.

[68] Z.A. Munir, U. Anselmi-Tamburini, M. Ohyanagi, The effect of electric field and pressure on the synthesis and consolidation of materials: A review of the spark plasma sintering method, Journal of Materials Science, 41 (2006) 763-777.
[69] Z. Shen, H. Peng, M. Nygren, Formidable increase in the superplasticity of ceramics in the presence of an electric field, Advanced Materials, 15 (2003) 1006-1009.
[70] T. Sun, X. Ning, Y. Han, H. Zhou, Study on spark plasma sintering of $NiAl_2O_4$ metal inert anodes, Key Engineering Materials, 280-283 (2005) 4.
[71] Z. Wang, Z. Wu, G. Shi, Effect of annealing treatment on mechanical properties of a ZrB_2–SiC–graphite ceramic, Materials Science and Engineering: A, 528 (2011) 2870-2874.
[72] B. Zou, C. Huang, J. Song, Z. Liu, L. Liu, Y. Zhao, Effects of sintering processes on mechanical properties and microstructure of TiB_2–TiC +8wt% nano-Ni composite ceramic cutting tool material, Materials Science and Engineering: A, 540 (2012) 235-244.
[73] Y. Tao, S. Huiji, Effects of grain size distribution on the creep damage evolution of polycrystalline materials, Journal of Physics D: Applied Physics, 43 (2010) 165401.
[74] R.A. Terpstra, J.P.G.M. van Eijk, J.C.T. van der Heijde, Alternative way of producing porous silicon nitride ceramics for membrane application, Key Engineering Materials 132 - 136 (1997) 4.
[75] X. Tan, S. Liu, K. Li, Preparation and characterization of inorganic hollow fiber membranes, Journal of Membrane Science, 188 (2001) 87-95.
[76] C.C. Wei, O.Y. Chen, Y. Liu, K. Li, Ceramic asymmetric hollow fibre membranes—One step fabrication process, Journal of Membrane Science, 320 (2008) 191-197.
[77] D. Bideau, J.P. Troadec, Compacity and mean coordination number of dense packings of hard discs, Journal of Physics C: Solid State Physics, 17 (1984) L731.
[78] W.M. Visscher, M. Bolsterli, Random packing of equal and unequal spheres in two and three dimensions, Nature, 239 (1972) 504-507.
[79] H.H. Kausch, D.G. Fesko, N.W. Tschoegl, The random packing of circles in a plane, Journal of Colloid and Interface Science, 37 (1971) 603-611.
[80] I.H. Choi, I.C. Kim, B.R. Min, K.H. Lee, Preparation and characterization of ultrathin alumina hollow fiber microfiltration membrane, Desalination, 193 (2006) 256-259.
[81] Y. Liu, O.Y. Chen, C.C. Wei, K. Li, Preparation of yttria-stabilised zirconia (YSZ) hollow fibre membranes, Desalination, 199 (2006) 360-362.
[82] J. Lamon, Ceramic reinforcements for composites, in: P. Boisse (Ed.) Composite reinforcements for optimum performance, Woodhead Publishing Limited, Woodhead Publishing Online, 2011, pp. 51-85.

[83] K. Xia, T. Langdon, The toughening and strengthening of ceramic materials through discontinuous reinforcement, Journal of Materials Science, 29 (1994) 5219-5231.
[84] A.G. Evans, On the formation of a crack tip microcrack zone, Scripta Metallurgica, 10 (1976) 93-97.
[85] W.A. Curtin, Toughening by crack bridging in heterogeneous ceramics, Journal of the American Ceramic Society, 78 (1995) 1313-1323.
[86] R. Paar, J.L. Vallés, R. Danzer, Influence of fibre properties on the mechanical behaviour of unidirectionally-reinforced ceramic matrix composites, Materials Science and Engineering: A, 250 (1998) 209-216.
[87] S. Fünfschilling, T. Fett, M.J. Hoffmann, R. Oberacker, T. Schwind, J. Wippler, T. Böhlke, H. Özcoban, G.A. Schneider, P.F. Becher, J.J. Kruzic, Mechanisms of toughening in silicon nitrides: The roles of crack bridging and microstructure, Acta Materialia, 59 (2011) 3978-3989.
[88] Transformation toughening materials, in: B.L. Karihaloo, J.H. Andreasen (Eds.) North-Holland Series in Applied Mathematics and Mechanics, North-Holland, 1996, pp. 9-33.
[89] Y. Hasegawa, M. Iimura, S. Yajima, Synthesis of continuous silicon carbide fibre, Journal of Materials Science, 15 (1980) 720-728.
[90] S. Yajima, Y. Hasegawa, K. Okamura, T. Matsuzawa, Development of high tensile strength silicon carbide fibre using an organosilicon polymer precursor Nature, 273 (1978) 3.
[91] Y. Yang, X. Liu, Z. Tan, S. Yang, Y. Lu, C. Feng, Synthesis of SiC fibre with low oxygen content and high tensile strength using a polyblend precursor, Journal of Materials Science, 26 (1991) 5167-5170.
[92] X. Shi, Y. Dong, F. Xu, Y. Tan, L. Wang, J.-m. Yang, Preparation and properties of nano-SiC strengthening Al_2O_3 composite ceramics, Materials Science and Engineering: A, 528 (2011) 2246-2249.
[93] M. Lieberthal, W.D. Kaplan, Processing and properties of Al_2O_3 nanocomposites reinforced with sub-micron Ni and $NiAl_2O_4$, Materials Science and Engineering: A, 302 (2001) 83-91.
[94] J.M. Christensen, Human exposure to toxic metals: factors influencing interpretation of biomonitoring results, Science of The Total Environment, 166 (1995) 89-135.
[95] Y. Waku, N. Nakagawa, T. Wakamoto, H. Ohtsubo, K. Shimizu, Y. Kohtoku, A ductile ceramic eutectic composite with high strength at 1,873K, Nature Macmillan Publishers Ltd, 389 (1997) 4.

[96] W. Yi, X. Hu, P. Ichim, X. Sun, Processing and properties of pressable ceramic with non-uniform reinforcement for selective-toughening, Materials Science and Engineering: A, 558 (2012) 543-549.
[97] C.B. Mo, S.I. Cha, K.T. Kim, K.H. Lee, S.H. Hong, Fabrication of carbon nanotube reinforced alumina matrix nanocomposite by sol–gel process, Materials Science and Engineering: A, 395 (2005) 124-128.
[98] A.R. Boccaccini, J. Cho, T. Subhani, C. Kaya, F. Kaya, Electrophoretic deposition of carbon nanotube–ceramic nanocomposites, Journal of the European Ceramic Society, 30 (2010) 1115-1129.
[99] R.N. Singh, M. Sutcu, Determination of fibre-matrix interfacial properties in ceramic-matrix composites by a fibre push-out technique, Journal of Materials Science, 26 (1991) 2547-2556.
[100] M. Du, J.Q. Bi, W.L. Wang, X.L. Sun, N.N. Long, Influence of sintering temperature on microstructure and properties of SiO_2 ceramic incorporated with boron nitride nanotubes, Materials Science and Engineering: A, 543 (2012) 271-276.
[101] G. Shi, Z. Wang, X. Sun, Z. Wu, Effect of the surface oxidation on the flexural strength of the ZrB_2–SiC–ZrC ceramic, Materials Science and Engineering: A, 546 (2012) 162-168.
[102] B.Q. Wang, J.B. Yu, Z.M. Ren, Y.P. Zeng, Fabrication and properties of porous alumina-based ceramic core, Journal of Inorganic Materials, 27 (2012) 239-244.
[103] N. Kayal, A. Dey, O. Chakrabarti, Synthesis of mullite bonded porous SiC ceramics by a liquid precursor infiltration method: Effect of sintering temperature on material and mechanical properties, Materials Science and Engineering: A, 556 (2012) 789-795.
[104] P. Monash, G. Pugazhenthi, Effect of TiO_2 addition on the fabrication of ceramic membrane supports: A study on the separation of oil droplets and bovine serum albumin (BSA) from its solution, Desalination, 279 (2011) 104-114.
[105] A. Kritikaki, A. Tsetsekou, Fabrication of porous alumina ceramics from powder mixtures with sol–gel derived nanometer alumina: Effect of mixing method, Journal of the European Ceramic Society, 29 (2009) 1603-1611.
[106] J.X. Li, T. Narita, J. Ogawa, M. Wadasako, In situ synthesis of porous ceramics with a framework structure of aluminium borate whisker, Journal of Materials Science, 33 (1998) 2601-2605.
[107] X. Li, L. Zhang, X. Yin, Microstructure and mechanical properties of three porous Si3N4 ceramics fabricated by different techniques, Materials Science and Engineering: A, 549 (2012) 43-49.

[108] D.D. Jayaseelan, N. Kondo, M.E. Brito, T. Ohji, High-strength porous alumina ceramics by the pulse electric current sintering technique, Journal of the American Ceramic Society, 85 (2002) 267-269.
[109] C. Wang, J. Chen, L. Fan, Z. Han, H. Wang, Fabrication and properties of supersonic plasma sprayed Al_2O_3 coating on porous Si_3N_4 substrate, Materials Science and Engineering: A, 559 (2013) 725-730.
[110] X. Tan, K. Li, A. Thursfield, I.S. Metcalfe, Oxyfuel combustion using a catalytic ceramic membrane reactor, Catalysis Today, 131 (2008) 292-304.
[111] M. Kilgus, V. Gepert, N. Dinges, C. Merten, G. Eigenberger, T. Schiestel, Palladium coated ceramic hollow fibre membranes for hydrogen separation, Desalination, 200 (2006) 95-96.
[112] H. Liu, X. Tan, Z. Pang, J.C. Diniz da Costa, G.Q. Lu, S. Liu, Novel dual structured mixed conducting ceramic hollow fibre membranes, Separation and Purification Technology, 63 (2008) 243-247.
[113] S. Koonaphapdeelert, K. Li, The development of ceramic hollow fibre membranes for a membrane contactor, Desalination, 200 (2006) 581-583.
[114] N. Yang, X. Tan, Z. Ma, A phase inversion/sintering process to fabricate nickel/yttria-stabilized zirconia hollow fibers as the anode support for micro-tubular solid oxide fuel cells, Journal of Power Sources, 183 (2008) 14-19.
[115] L.F. Han, Z.L. Xu, Y. Cao, Y.M. Wei, H.T. Xu, Preparation, characterization and permeation property of Al_2O_3, Al_2O_3–SiO_2 and Al_2O_3–kaolin hollow fiber membranes, Journal of Membrane Science, 372 (2011) 154-164.
[116] J.W. Zhang, H. Fang, L.Y. Hao, X. Xu, C.S. Chen, Preparation of silicon nitride hollow fibre membrane for desalination, Materials Letters, 68 (2012) 457-459.
[117] X. Dong, W. Jin, N. Xu, K. Li, Dense ceramic catalytic membranes and membrane reactors for energy and environmental applications, Chemical Communications, 47 (2011) 10886-10902.
[118] X. Tan, K. Li, Inorganic hollow fibre membranes in catalytic processing, Current Opinion in Chemical Engineering, 1 (2011) 69-76.
[119] B. Phillips, J.J. Hutta, I. Warshaw, Phase equilibria in the system NiO–Al_2O_3–SiO_2, Journal of the American Ceramic Society, 46 (1963) 579-583.
[120] Y. Cesteros, P. Salagre, F. Medina, J.E. Sueiras, Synthesis and characterization of several Ni/$NiAl_2O_4$ catalysts active for the 1,2,4-trichlorobenzene hydrodechlorination, Applied Catalysis B: Environmental, 25 (2000) 213-227.

[121] P.H.M. De Korte, E.B.M. Doesburg, C.P.J. De Winter, L.L. Van Reijen, Characterization of the interaction between nickel oxide and aluminium oxide in coprecipitated catalysts, Solid State Ionics, 16 (1985) 73-80.
[122] P.G. Kotula, C.B. Carter, Nucleation of solid-state reactions between nickel oxide and aluminium oxide, Journal of the American Ceramic Society, 78 (1995) 248-250.
[123] R.D. Peelamedu, R. Roy, D.K. Agrawal, Microwave-induced reaction sintering of $NiAl_2O_4$, Materials Letters, 55 (2002) 234-240.
[124] E. Loginova, F. Cosandey, T.E. Madey, Nanoscopic nickel aluminate spinel ($NiAl_2O_4$) formation during NiAl(111) oxidation, Surface Science, 6 (2007) 4.
[125] Y.S. Han, J.B. Li, X.S. Ning, X.Z. Yang, B. Chi, Study on NiO excess in preparing $NiAl_2O_4$, Materials Science and Engineering: A, 369 (2004) 241-244.
[126] H. Panitat, K. Nattamon, L. Apirat, Nickel-aluminium complex: a simple and effective precursor for nickel aluminate ($NiAl_2O_4$) spinel, Maejo International Journal of Science and Technology, 2 (2008) 10.
[127] Y.S. Han, J.B. Li, X.S. Ning, B. Chi, Effect of preparation temperature on the lattice parameter of nickel aluminate spinel, Journal of the American Ceramic Society, 87 (2004) 1347-1349.
[128] L. Xiang, X.Y. Deng, Y. Jin, Experimental study on synthesis of NiO nano-particles, Scripta Materialia, 47 (2002) 219-224.
[129] T.L. Lai, Y.Y. Shu, G.L. Huang, C.C. Lee, C.B. Wang, Microwave-assisted and liquid oxidation combination techniques for the preparation of nickel oxide nanoparticles, Journal of Alloys and Compounds, 450 (2008) 318-322.
[130] M. Salavati-Niasari, F. Davar, Z. Fereshteh, Synthesis of nickel and nickel oxide nanoparticles via heat-treatment of simple octanoate precursor, Journal of Alloys and Compounds, 494 (2010) 410-414.
[131] S. Gandhi, N. Nagalakshmi, I. Baskaran, V. Dhanalakshmi, M.R.G. Nair, R. Anbarasan, Synthesis and characterization of nano-sized NiO and its surface catalytic effect on poly(vinyl alcohol), Journal of Applied Polymer Science, 118 (2010) 1666-1674.
[132] Z. Fereshteh, M. Salavati-Niasari, K. Saberyan, S. Mostafa Hosseinpour-Mashkani, F.T. avakoli, Synthesis of Nickel Oxide Nanoparticles from Thermal Decomposition of a New Precursor Journal of Cluster Science, 23 (2012) 7.
[133] K. Shih, Y. Tang, Prolonged toxicity characteristic leaching procedure for nickel and copper aluminates, Journal of Environmental Monitoring, 13 (2011) 829-835.

[134] K. Shih, T. White, J.O. Leckie, Spinel Formation for stabilizing simulated nickel-laden sludge with aluminum-rich ceramic precursors, Environmental Science & Technology, 40 (2006) 5077-5083.
[135] W.J. Koros, R. Mahajan, Pushing the limits on possibilities for large scale gas separation: which strategies?, Journal of Membrane Science, 175 (2000) 181-196.
[136] G. Owen, M. Bandi, J.A. Howell, S.J. Churchouse, Economic assessment of membrane processes for water and waste water treatment, Journal of Membrane Science, 102 (1995) 77-91.
[137] B.K. Nandi, R. Uppaluri, M.K. Purkait, Preparation and characterization of low cost ceramic membranes for micro-filtration applications, Applied Clay Science, 42 (2008) 102-110.
[138] M. Tomaszewska, L. Białończyk, The chemical cleaning of ceramic membrane used in UF, Polish Journal of Chemical Technology., 14 (2012) 5.
[139] Y.L.E. Fung, H. Wang, Nickel aluminate spinel reinforced porous ceramic for membrane application, in: 2013 AICHE annual meeting, San Francisco, USA, 2013.
[140] Alfa Aesar A Johnson Matthey Company, in, 2012.
[141] Sigma Aldrich, in, 2011.
[142] E. Sideridis, G.A. Papadopoulos, Short-beam and three-point-bending tests for the study of shear and flexural properties in unidirectional-fiber-reinforced epoxy composites, Journal of Applied Polymer Science, 93 (2004) 63-74.
[143] Y.H. Zhao, K. Lu, Grain-size dependence of thermal properties of nanocrystalline elemental selenium studied by x-ray diffraction, The American Physical Society, 56 (1997) 8.
[144] Y.L.E. Fung, H. Wang, Investigation of reinforcement of porous alumina by nickel aluminate spinel for its use as ceramic membrane, Journal of Membrane Science, 444 (2013) 252-258.
[145] Y.L.E. Fung, H. Wang, Nickel aluminate spinel reinforced ceramic hollow fibre membrane, Journal of Membrane Science, 450 (2014) 418-424.
[146] K. Shih, T. White, J.O. Leckie, Nickel stabilization efficiency of aluminate and ferrite spinels and their leaching behavior, Environmental Science & Technology, 40 (2006) 5520-5526.
[147] R. Haugsrud, On the high-temperature oxidation of nickel, Corrosion Science, 45 (2003) 211-235.
[148] B. Meng, X. Tan, X. Meng, S. Qiao, S. Liu, Porous and dense Ni hollow fibre membranes, Journal of Alloys and Compounds, 470 (2009) 461-464.

[149] M.J. Graham, M. Cohen, On the mechanism of low-temperature oxidation (23°–450°C) of polycrystalline nickel, Journal of The Electrochemical Society, 119 (1972) 879-882.
[150] C. Peng, Y. Ganesan, Y. Lu, J. Lou, Size dependent mechanical properties of single crystalline nickel nanowires, Journal of Applied Physics, 111 (2012) 063524-063526.
[151] L. Hui, F. Pederiva, B.L. Wang, J.L. Wang, G.H. Wang, How does the nickel nanowire melt, Applied Physics Letters, 86 (2005) 011913-011913.
[152] Y.J. Li, W.H. Qi, B.Y. Huang, M.P. Wang, S.Y. Xiong, Modelling the melting temperature of metallic nanowires, Modern Physics Letters B, 24 (2010) 2345-2356.
[153] Y. Ren, W.K. Chim, S.Y. Chiam, J.Q. Huang, C. Pi, J.S. Pan, Formation of nickel oxide nanotubes with uniform wall thickness by low-temperature thermal oxidation through understanding the limiting effect of vacancy diffusion and the kirkendall phenomenon, Advanced Functional Materials, 20 (2010) 3336-3342.
[154] C. Gong, L. Yu, Y. Duan, J. Tian, Z. Wu, Z. Zhang, The fabrication and magnetic properties of Ni fibers synthesized under external magnetic fields, European Journal of Inorganic Chemistry, 2008 (2008) 2884-2891.
[155] F.L. Jia, L.Z. Zhang, X.Y. Shang, Y. Yang, Non-aqueous sol–gel approach towards the controllable synthesis of nickel nanospheres, nanowires, and nanoflowers, Advanced Materials, 20 (2008) 1050-1054.
[156] S. Tang, Z. Zheng, S. Vongehr, X. Meng, Facile and rapid synthesis of nickel nanowires and their magnetic properties, Journal of Nanoparticle Research, 13 (2011) 7085-7094.
[157] S. Tang, S. Vongehr, H. Ren, X. Meng, Diameter-controlled synthesis of polycrystalline nickel nanowires and their size dependent magnetic properties, CrystEngComm, (2012).
[158] X. Hu, Y.W. Mai, Crack-bridging analysis for alumina ceramics under monotonic and cyclic loading, Journal of the American Ceramic Society, 75 (1992) 848-853.
[159] M. Kawamori, S. Yagi, E. Matsubara, Formation of nickel nanowires via electroless deposition under a magnetic field, Journal of The Electrochemical Society, 158 (2011) E79-E83.
[160] J. Wang, L. Wei, L. Zhang, C. Jiang, E. Siu-Wai Kong, Y. Zhang, Preparation of high aspect ratio nickel oxide nanowires and their gas sensing devices with fast response and high sensitivity, Journal of Materials Chemistry, 22 (2012) 8327-8335.

[161] P. Blanpain-Avet, J.F. Migdal, T. Bénézech, Chemical cleaning of a tubular ceramic microfiltration membrane fouled with a whey protein concentrate suspension—Characterization of hydraulic and chemical cleanliness, Journal of Membrane Science, 337 (2009) 153-174.